The Dissertation Committee for Ryan Lee White
certifies that this is the approved version of the following dissertation:

Resistive Instabilities in Magnetically Confined Fusion Plasmas with Velocity Shear and Rotation

Committee:

Richard Fitzpatrick, Supervisor

Richard Hazeltine

Boris Breizman

Francois Waelbroeck

Oscar Gonzalez

Resistive Instabilities in Magnetically Confined Fusion Plasmas with Velocity Shear and Rotation

by

Ryan Lee White, B.S.; M.A.

DISSERTATION

Presented to the Faculty of the Graduate School of

The University of Texas at Austin

in Partial Fulfillment

of the Requirements

for the Degree of

DOCTOR OF PHILOSOPHY

THE UNIVERSITY OF TEXAS AT AUSTIN

August 2015

To my wife, Leah.

Acknowledgments

First, I wish to thank my supervisor Richard Fitzpatrick, whose continual support during our collaboration has been greatly helpful. His no-frills perspective, vast knowledge, and steadfast work ethic have been a tremendous source of professional inspiration. In our many research-strategy discussions, I have learned a lot about the fundamentals of scientific research, which will continue to serve me well in the future.

I have been fortunate to work alongside, and learn from, several other excellent scientists at IFS: Boris Breizman is a gifted teacher, an excellent plasma physicist, and a great mentor. The course I took from Dr. Breizman changed the way I think about plasma physics, as well as how to effectively communicate technical information. Phil Morrison's door was always open for random research questions, and I received a lot of valuable advice on problem-solving by being a regular guest in the Morrison group. I also had several very useful discussions with Francois Waelbroeck, who helped point me in a fruitful direction with my research.

I have benefitted enormously from my relationship with Richard Hazeltine. Our many scientific discussions were usually productive, and always engaging. When in the midst of a calculational difficulty, his steadfast confidence and enthusiasm were infectious. More importantly, he had confidence in me

after seeing me struggle professionally, and offered essential help in getting me back on my feet. I am very grateful for everything I have learned from him, and for his kindness.

Finally, I am very grateful for the help and support from Cathy Rapinett, and James Halligan. James and Cathy were extremely helpful with a multitude of tasks, and both were always exceptionally friendly, usually while helping me resolve an issue that had nothing to do with their official responsibilities.

Resistive Instabilities in Magnetically Confined Fusion Plasmas with Velocity Shear and Rotation

Publication No. _____

Ryan Lee White, Ph.D.
The University of Texas at Austin, 2015

Supervisor: Richard Fitzpatrick

Using a resistive generalization of the Frieman-Rotenberg formalism for Lagrangian magnetohydrodynamic stability with equilibrium velocity, the leading-order effects of velocity shear and rotation on linear tearing layer stability are studied for tokamak equilibria. The separation-of-time-scales formalism needed for a proper formulation of ideal and resistive stability calculations is presented. Using this formalism, a dispersion relation is first obtained for marginal ideal modes in plane-symmetric equilibria. It is demonstrated how resistive modes arise as a natural continuation of marginal ideal modes. The dispersion relation for resistive modes in slab geometry is derived and used to demonstrate the resistive stability boundary. The widely misrepresented constant-Ψ limit is explained in detail, and used to obtain a dispersion relation for tearing modes. Nyquist techniques are used to compare the Glasser effect in slab and cylindrical models. The resistive layer equations are also

obtained in cylindrical geometry, allowing direct verification of the limited validity of gravity-curvature equivalence heuristic for resistive modes. Numerical complications that arise from velocity shear are discussed. Layer equations are also derived in the constant-Ψ limit. The constant-Ψ dispersion relation is obtained for cylindrical equilibria, and used to study the leading-order effects of rotation and velocity shear on the critical value of Δ' required for tearing instability. It is found that rotation and velocity shear can couple with the parallel current and the current gradient in the layer to reduce $\Delta'_{\rm crit}$. If parallel currents are sufficiently weak to compete with second-order effects, velocity shear can be stabilizing, while rotation is found to have a destabilizing effect. Second-order coupling of velocity shear and rotation can have either sign, and thus can affect stability in either direction.

Table of Contents

Acknowledgments **v**

Abstract **vii**

List of Tables **xii**

List of Figures **xiii**

Chapter 1. Introduction **1**

Chapter 2. Magnetohydrodynamic Stability **8**

2.1 Magnetohydrodynamic Description of Fusion Plasma 8

2.2 Separation of Time Scales 11

2.3 Linear Stability of Slowly-Evolving MHD Profiles 14

2.3.1 Ideal Stability 14

2.3.2 Resistive Instabilities 17

Chapter 3. Localized Instabilities in Slab Geometry **21**

3.1 Gravity-Curvature Analogy 21

3.2 Stability of a Gravitating Slab 22

3.3 Ideal Stability 23

3.3.1 Marginal Ideal-MHD Stability 28

3.3.1.1 Outer Limit 29

3.3.1.2 Inertial Layer 31

3.3.2 Marginal Ideal-MHD Dispersion Relation 34

3.3.2.1 Analysis of Dispersion Relation 36

3.4 Resistive Interchange Modes 37

3.4.1 Outer Limit 39

3.4.2 Resistive Layer Equations 39

3.4.3 Asymptotic Matching 45
3.4.4 Remarks 46
3.4.4.1 Utility of the Asymptotic Approach 46
3.4.4.2 Higher-Order Boundary Layer Theory 47
3.4.5 Dispersion Relation in the Static, Incompressible Limit . 49

Chapter 4. Tearing Modes in Slab Geometry 52
4.1 Boundary Layer Within a Boundary Layer 53
4.1.1 Outer Limit of Resistive Layer Equations 56
4.1.2 Layer Limit of Resistive Layer Equations 57
4.1.3 Remarks 58
4.2 Dispersion Relation in the Incompressible Static Limit 60
4.2.1 Analysis of Dispersion Relation 60

Chapter 5. Localized Instabilities in Straight Tokamak Geometry 66
5.1 Ideal Stability 68
5.1.0.1 Small Velocity Limit 69
5.1.0.2 Nonrotating Limit 70
5.2 Resistive Interchange Ordering 71
5.2.1 Asymptotic Behavior 74
5.2.2 Matching Conditions 74
5.2.2.1 Intermediate Limit 75
5.2.3 Discussion 76

Chapter 6. Tearing Modes in Straight Tokamak Geometry 77
6.0.4 Small Velocity Ordering 81
6.0.4.1 Incompressible Limit 82
6.1 Analysis of Dispersion Relation 84
6.1.1 Plane Incompressible Limit 84
6.1.2 Equilibrium Current-Driven Modes 84
6.1.3 Effect of Rotation and Shear on $\Delta'_{\rm crit}$ 85

Chapter 7. Conclusion 92

Appendices **95**

Appendix A. Eulerian Friemen-Rotenberg Formulation with Dissipation **96**

A.1 Linearized Resistive MHD with Frieman-Rotenberg Displacement Vector 96

A.1.0.1 Continuity Equation 99

A.1.0.2 Induction Equation 100

A.1.0.3 Equation of Motion 101

A.1.0.4 Equation of Heat Transport 101

Appendix B. Calculation of Δ **102**

B.1 Calculation of Δ 102

B.2 Evaluation of Δ 102

B.2.0.5 Zeroth Order 104

Bibliography **110**

Vita **115**

List of Tables

List of Figures

3.1 The outer and layer solutions near z_0. 32

4.1 The contour C_Q in the complex Q plane. 62

4.2 The image of the contour C_Q in the complex Δ' plane, with $D_g = -5$. 63

4.3 The image of the contour C_Q in the complex Δ' plane for cylindrical geometry with $D_s = -5$. 64

6.1 Δ'_{crit} first-order terms versus S for $J = 1$, $J_p = 0$, $D_s = -1$, $\kappa_\alpha = l^3$. The solid, dash, and dash-dotted lines correspond to $\Delta_\theta^{(1)}$, $\Delta_\perp^{(1)}$, and $\Delta_\parallel^{(1)}$, respectively. 89

6.2 Δ'_{crit} second-order positive-definite terms versus S for $J = 1$, $J_p = 0$, $D_s = -1$, $B_\theta/B_z = 0.1$, and $\kappa_\alpha = l^3$. The solid, dash, and dash-dotted lines correspond to $\Delta_{\theta\theta}^{(2)}$, $\Delta_{\perp\perp}^{(2)}$, and $\Delta_{\parallel\parallel}^{(2)}$, respectively. 90

6.3 Δ'_{crit} second-order cross terms versus S for $J = 1$, $J_p = 0$, $D_s = -1$, $B_\theta/B_z = 0.1$, and $\kappa_\alpha = l^3$. The solid, dash, and dash-dotted lines correspond to $\Delta_{\parallel\theta}^{(2)}$, $\Delta_{\perp\theta}^{(2)}$, and $\Delta_{\perp\parallel}^{(2)}$, respectively. 91

A.1 Geometric definition of $\boldsymbol{\xi}$ 97

Chapter 1

Introduction

The fundamental requirement of thermonuclear-fusion-power generation is to develop an apparatus which will reliably confine a high-temperature, high-density Hydrogen plasma for long enough to allow a significant amount of Helium to be produced from the fusion of Hydrogen nuclei. Each atom of Helium produced yields roughly an MeV of excess thermal energy which can be used to power a furnace in an (otherwise) conventional power plant. For a given temperature, the rate of Helium production is proportional to the square of the plasma density. Plasma pressure, and therefore density, is limited by reactor force-balance requirements, leading to an optimal particle density of roughly 10^{14} cm^3, and plasma temperatures approaching 10 keV, or 100 million degrees Kelvin, which is far too hot for direct contact with a solid containment vessel. Magnetic confinement devices address this issue by imposing strong magnetic fields which constrain the motion of the constituent (charged) plasma particles, thus minimizing contact with the terrestrial environment.

A magnetic field $\mathbf{B}$ restricts the motion of the charged plasma particles via the Lorentz force $\mathbf{F} = e\mathbf{v} \times \mathbf{B}$, where $\mathbf{v}$ is the particle's velocity, and e is the charge. This confinement force is perpendicular to $\mathbf{B}$, leading to confined

circular motion perpendicular to the magnetic field, and free translation along the field lines. In tokamak devices, the magnetic field lines are confined within a toroidal chamber, thereby opening up the possibility for confined particle orbits in spite of particles freely streaming along **B**.

Magnetized plasmas exhibit large-scale coherent motion which cannot be reduced to the aggregate effect of individually-confined, free-streaming charged particles in an external magnetic field. Instead, the trajectory of each particle is determined by the self-consistent electromagnetic field produced by every other charged particle in the plasma together with the externally produced magnetic field. These collective effects drive the system to thermal equilibrium, where the temperature and density are constant. In a tokamak, the inner boundary of the toroidal chamber must be well below the material's melting temperature while the peak temperature near the core exceeds 100 million degrees Kelvin. Meanwhile, the plasma density varies by three orders of magnitude as one moves from the edge of the chamber to the core. A tokamak plasma is thus a strongly non-equilibrium system which will naturally act to reduce the externally-imposed temperature and density gradients.

The idealization of an electrically-conducting fluid has been an exceptionally effective continuum model for understanding a wide variety of large-scale coherent dynamics observed in magnetized plasmas. This model is known as magnetohydrodynamics (MHD). In order for a magnetic confinement fusion device to successfully confine a plasma, it is essential that the MHD model predicts that the energy-confining configuration will relax slowly compared to the

Hydrogen burn rate.

A magnetohydrodynamic fluid relaxes to a state of thermal equilibrium via dissipative energy and momentum transport facilitated by resistivity, viscosity, and thermal conductivity. In a high-temperature tokamak plasma, these kinetic coefficients are numerically very small, which means thermal relaxation proceeds slowly. For example, the global resistive-decay time is $\tau_\sigma = L^2\sigma/c^2$ where L is a characteristic gradient length scale, σ is the electrical conductivity of the plasma, and c is the speed of light.[1] The plasma conductivity is given by [4]

$$\sigma = \frac{9 \times 10^{13}}{\Lambda} \text{ sec}^{-1} \approx 10^{18} \text{ sec}^{-1} \tag{1.1}$$

where[2] $\Lambda = 23.4 - 1.15\log(n) + 3.45\log(T_{\text{eV}})$. Inserting the characteristic value $L \approx 100$ cm, we find $\tau_\sigma \approx 100$ seconds. A significant fraction of the Hydrogen nuclei will fuse into Helium within about a minute, so dissipative relaxation of a magnetized plasma is slow enough to generate substantial thermonuclear energy before the confinement profile is significantly degraded.

Unfortunately, plasmas which relax on this slow dissipative time scale are usually unstable with respect to instabilities which grow on a time scale which is more or less independent of the values of the kinetic coefficients. These *ideal* MHD instabilities grow on an Alfven time scale $\tau_A = L/V_A$, where $V_A = B/\sqrt{4\pi\rho}$ is the Alfven velocity, and ρ is the mass density. In tokamak

[1] In this dissertation, Gaussian units will be used throughout.

[2] For reference, the conductivity of Copper at room temperature is 5×10^{17} sec^{-1}.

plasmas, $B \approx 1$ Tesla, $\rho \approx 10^{-10}$ g/cm^3, so that $\tau_A \approx 10^{-6}$ seconds. Clearly, Alfvenic instabilities must be avoided in order for appreciable fusion to occur. Preventing rapidly-growing MHD instabilities is a fundamental challenge in magnetic confinement fusion.

Ideal-MHD instabilities tend to be global and violent, in addition to rapidly-evolving. Fortunately, there has been a great deal of progress made by the fusion research community [2, 12, 25] in understanding ideal-MHD instabilities which can potentially occur in tokamaks. By limiting the plasma pressure and the toroidally-flowing current, ideal instabilities can largely be avoided.

The azimuthally-symmetric tokamak equilibrium profiles which evolve on the slow dissipative time scale have magnetic field lines which ergodically cover two-dimensional toroidal surfaces [21]. These *magnetic surfaces* nest inside one another to foliate the three-dimensional toroidal volume. Because the plasma particles move rapidly along the magnetic field lines but only very slowly across them, the transport of energy and particles across the magnetic surfaces proceeds slowly.

There is a second category of instabilities which affect the confinement of tokamak plasmas by altering the topology of the magnetic field lines to form a chain of magnetic islands embedded in one or more magnetic surfaces. These islands produce a local rapid-transport region within the plasma [20], and thus degrade overall energy and particle confinement. In ideal-MHD instabilities, the magnetic field lines are frozen into the fluid [12], thereby preventing island

formation. One can show [14] that the ideal frozen-in-field-line constraint is removed if electrical resistivity plays a dominant role in the instability. These so-called *resistive instabilities* grow on a hybrid time scale $\tau \sim \tau_\sigma^\alpha \tau_A^{1-\alpha}$ where $0 < \alpha < 1$. In practice, resistive instabilities grow rapidly compared to the burn time. Magnetic islands are regularly observed in tokamak plasmas, but island formation and growth proceeds too quickly to be seen experimentally.

Though resistive instabilities are less catastrophic than ideal modes, they are much more difficult to avoid. It has been shown [16] that resistive stability in tokamaks is largely determined by the average normal curvature of the equilibrium magnetic field lines at so called *rational surfaces*. A rational surface is a magnetic surface for which the magnetic field lines form finite-length closed loops after several toroidal windings, rather than densely filling the surface, which requires an infinitely long surface-filling curve. If the average normal curvature of a rational-surface field line is negative (the sign of the curvature is defined to be positive if it is in the same direction as the pressure gradient), then the forces in the plasma are locally stabilizing with respect to resistive instabilities. This potentially stabilizing influence of rational-surface magnetic curvature is known as the *Glasser effect*. However, forces away from the vicinity of the rational surface may still be sufficiently large to overpower the locally stabilizing rational-surface magnetic curvature, resulting in a resistive instability known as a *tearing mode*. In a tearing mode, the toroidal plasma current sheet at the rational surface tears into helical filaments which eventually become concentrated at the core of the resulting magnetic islands.

Most theoretical results in linear tearing mode theory neglect the equilibrium velocity of the plasma. As a first iteration, this is justified, because the magnetic field dominates the dynamics in tokamak plasmas. However, tokamak plasmas are externally heated by beams of high-energy neutral particles, and this creates a strongly-sheared toroidal velocity profile. There is experimental evidence [7] that these sheared profiles result in reduced occurrence of magnetic islands. This favorable effect is in conflict with the theoretical predictions which exist in the literature [7, 30, 31, 34].

In this dissertation, it will be shown that the main consequence of velocity shear near a rational surface is an amplification of the effect of the surface's field-line curvature. If the magnetic curvature is negative (and thus locally stabilizing against tearing modes), then velocity shear increases the instability threshold; rational surfaces with net positive magnetic curvature are rendered more unstable by velocity shear. This qualitative effect explains the conflict between experimental results and the conclusions based on theoretical predictions in the literature. All of the previous studies were carried out in either slab or cylindrical geometry, which have either no curvature or positive curvature, leading to a destabilizing prediction. In addition, by knowing how the rational-surface velocity profile affects layer stability, neutral beams in future experiments can be directed in a manner which optimizes the stability of the equilibrium profile while heating the plasma.

A careful formulation of the separation of time scales needed for MHD stability analysis is presented in Chapter 2. In Chapter 3, we consider the

stability of a gravitating slab. This geometry simplifies the calculations, and allows explicit demonstration of the gravity-curvature equivalence heuristic. The connections between marginal ideal and resistive modes are also demonstrated. In Chapter 4, we discuss the tearing ordering in detail, and emphasize the relation to localized resistive interchange modes studied in the previous chapter. The *constant*-Ψ dispersion relation is obtained in the incompressible limit without velocity shear. Nyquist techniques are used to explicitly demonstrate the Glasser effect. In Chapter 5, the equations governing the asymptotic behavior of resistive modes in cylindrical geometry are derived. Finally, in Chapter 6, a dispersion relation is derived for a "straight tokamak", with cylindrical geometry, toroidal topology, and toroidal curvature corrections included, along with the effects of velocity shear and rotation. The dispersion relation is used to study the effect of velocity shear and rotation on the tearing stability threshold.

Chapter 2

Magnetohydrodynamic Stability

2.1 Magnetohydrodynamic Description of Fusion Plasma

Magnetically-confined fusion plasmas have large spatial gradients in both energy density and particle density, making them non-equilibrium systems. The constituent electrons, ions, and electromagnetic field collectively conspire to drive the system toward a spatially-homogeneous equilibrium profile with statistical certainty. In a fluid description, the particles and electromagnetic field are spatially and temporally coarse-grained so that the particle, momentum, and energy densities of all species are smooth functions of space and time. Moreover, the velocity profiles are assumed to be locally Maxwellian, i.e. locally in the most probable distribution for given energy and particle densities at each point in the fluid. This makes it possible to define the temperature at each point in space.

The magnetohydrodynamic model treats the plasma as a single quasineutral conducting fluid. The self-consistent equations governing the fluid and the (macroscopic) electromagnetic field [28] are

$$\frac{\partial \rho}{\partial t} + \boldsymbol{\nabla} \cdot \rho \mathbf{V} = 0, \tag{2.1}$$

$$\rho \left[\frac{\partial \mathbf{V}}{\partial t} + (\mathbf{V} \cdot \boldsymbol{\nabla}) \mathbf{V} \right] = -\boldsymbol{\nabla} p + \frac{1}{c} \mathbf{J} \times \mathbf{B} + \rho \nu \nabla^2 \mathbf{V} + \zeta \boldsymbol{\nabla} (\nabla \cdot \mathbf{V}), \tag{2.2}$$

$$\begin{aligned} \rho T \left(\frac{\partial s}{\partial t} + (\mathbf{V} \cdot \nabla) s \right) = & \left[\rho \nu \left(\frac{\partial V_i}{\partial x_k} + \frac{\partial V_k}{\partial x_i} - \frac{2}{3} \delta_{ik} \nabla \cdot \mathbf{V} \right) + \zeta \delta_{ik} \nabla \cdot \mathbf{V} \right] \frac{\partial V_i}{\partial x_k} \\ & + \frac{1}{\sigma} |J|^2 + \kappa \nabla^2 T. \end{aligned} \tag{2.3}$$

$$\boldsymbol{\nabla} \cdot \mathbf{B} = 0, \tag{2.4}$$

$$\boldsymbol{\nabla} \times \mathbf{E} = -\frac{1}{c} \frac{\partial \mathbf{B}}{\partial t}, \tag{2.5}$$

$$\boldsymbol{\nabla} \times \mathbf{B} = \frac{4\pi}{c} \mathbf{J}, \tag{2.6}$$

$$\mathbf{E} + \frac{1}{c} \mathbf{V} \times \mathbf{B} = \sigma \mathbf{J}, \tag{2.7}$$

where ρ is the mass density; $\mathbf{V}$ is the fluid velocity; s is the specific entropy; T is the temperature; p is the pressure; $\mathbf{B}$ is the magnetic field; and $\mathbf{E}$ is the electric field. In addition, ν, ζ, σ, and κ denote the kinematic viscosity, second viscosity, electrical conductivity, and thermal conductivity of the plasma, respectively. In general, a magnetized plasma is an anisotropic medium so the kinetic coefficients are not necessarily scalars, but we neglect this refinement here. Eqs. (2.1)–(2.3) express conservation of mass, momentum, and energy of the plasma, and reduce to the equations of ordinary fluid mechanics when $\mathbf{B} \to 0$. The equations (2.1)–(2.7) also govern the behavior of conducting liquids. A plasma is distinguished from other conducting fluids by its distinct values of σ, κ, ν, and ζ as well as its thermodynamic equation of state. It turns out [33] that tokamak plasma behaves as an ideal gas with constant specific

heats[1] $c_v = 3/2$, $c_p = 5/2$ to a high degree of approximation:

$$p = \rho T/m \tag{2.8}$$

where m is the average particle mass, which is roughly equal to half the average ion mass for tokamak plasma.

By modeling the plasma as a fluid, we neglect the nonlocal effects of Landau damping and (nonthermal) energetic-particle-driven instabilities which arise from deviations from local thermal equilibrium. Including the effects of wave-particle interaction requires abandoning a fluid model in favor of a kinetic description. By beginning from the more fundamental kinetic description, one can obtain fluid equations in the short-mean-free-path limit [4]. In tokamak plasma, the effective mean free path is very long compared to characteristic gradient length scales, so use of a fluid model is difficult to justify theoretically. Nonetheless, the MHD model has historically been an extremely useful framework for understanding a wide variety of instabilities found in tokamak plasmas. One plausible explanation of this fact is that MHD is obtained from kinetic theory in a singular limit, and thus is to be interpreted asymptotically. The leading behavior of an asymptotic series often yields a very accurate approximation far away from the singular limit [1], in contrast to a convergent series. In particular, MHD has been successfully used to understand a wide variety of phenomena associated with the formation and evolution of magnetic islands in tokamaks. In this dissertation, MHD will be

[1]These are specific heats per particle, where both ions and electrons are counted

postulated as an appropriate model to understand the effects of velocity shear on magnetic island formation in tokamak experiments.

The system of equations (2.1)–(2.7) can be simplified by using Eqs. (2.6), (2.7) to eliminate $\mathbf{E}$ and $\mathbf{J}$, and using the local thermodynamic relations to eliminate s. The result is

$$\frac{\partial \rho}{\partial t} + \boldsymbol{\nabla} \cdot \rho \mathbf{V} = 0, \tag{2.9}$$

$$\rho \left[\frac{\partial \mathbf{V}}{\partial t} + (\mathbf{V} \cdot \boldsymbol{\nabla}) \mathbf{V} \right] = - \boldsymbol{\nabla} p + \frac{1}{4\pi} (\nabla \times \mathbf{B}) \times \mathbf{B} + \rho \nu \nabla^2 \mathbf{V} + \zeta \boldsymbol{\nabla} (\nabla \cdot \mathbf{V}), \tag{2.10}$$

$$\frac{\partial p}{\partial t} + (\mathbf{V} \cdot \nabla) p + \Gamma p (\nabla \cdot \mathbf{V}) = (\Gamma - 1) \left(\frac{\eta}{4\pi} |\nabla \times \mathbf{B}|^2 + \kappa \nabla^2 T + \rho \nu \left[\frac{\partial V_i}{\partial x_k} + \frac{\partial V_k}{\partial x_i} \right] \frac{\partial V_i}{\partial x_k} + (\zeta - 2\nu\rho/3)(\nabla \cdot \mathbf{V})^2 \right), \tag{2.11}$$

$$\boldsymbol{\nabla} \cdot \mathbf{B} = 0, \tag{2.12}$$

$$\frac{\partial \mathbf{B}}{\partial t} = \nabla \times (\mathbf{V} \times \mathbf{B}) + \eta \nabla^2 \mathbf{B}, \tag{2.13}$$

where we have defined the resistivity $\eta = c^2/(4\pi\sigma)$, and $\Gamma = c_p/c_v$.

2.2 Separation of Time Scales

A straightforward implementation of the MHD model for studying equilibrium profiles would consist in dropping all time derivatives in the system (2.9)–(2.13). One can readily show that the resulting time-independent equilibria do not have the large gradients in temperature and density required to

produce an appreciable-sized region with fusion conditions. Indeed, large gradients imply the system will evolve in time toward a homogeneous thermal equilibrium profile.

Fortunately, the sufficiently small values of electrical resistivity, thermal conductivity[2], and viscosity lead to profiles which evolve sufficiently slowly to sustain large-gradient confinement profiles for times commensurate with appreciable fusion.

To find the system of equations governing these "dissipative" equilibria, we insert an ordering parameter, ϵ, in front of η, ν, ζ, and κ, and require that all time derivatives be $\mathcal{O}(\epsilon)$ as $\epsilon \to 0+$. This in turn implies $t = t_0/\epsilon$ where t_0

[2]Note that we are considering electrical conductivity to be large, and thermal conductivity to be small. This may not seem reasonable from a physics perspective. However, we are really trying to capture the effects of electrical resistivity apart from the complicating influence of thermal conductivity, so we formally send it to zero. The other option would be to send κ to infinity, but this would not allow for temperature gradients in the equilibrium profiles. Here again, we see the advantage of adding ordering parameters, since it is easy to construct special limits in parameter space which highlight particular phenomena. Moreover, because we are constructing singular limits, there is a good chance that the expansion about $\kappa = 0$ will yield a good approximation for (say) $\kappa \approx 30$, when numerical values are inserted into the appropriate dimensionless parameters.

is independent of ϵ. We thus have

$$\epsilon\frac{\partial\rho_0}{\partial t_0} + \nabla\cdot(\rho_0\mathbf{V_0}) = 0, \tag{2.14}$$

$$\epsilon\frac{\partial\mathbf{V}_0}{\partial t_0} + (\mathbf{V}_0\cdot\nabla)\mathbf{V}_0 = \nabla p_0 + \frac{1}{4\pi}(\nabla\times\mathbf{B}_0)\times\mathbf{B}_0 + \epsilon\rho\nu\nabla^2\mathbf{V}_0 + \epsilon\zeta\boldsymbol{\nabla}(\nabla\cdot\mathbf{V}_0), \tag{2.15}$$

$$\epsilon\frac{\partial\mathbf{B}_0}{\partial t_0} = \nabla\times(\mathbf{V}_0\times\mathbf{B}_0) + \epsilon\eta\nabla^2\mathbf{B}_0, \tag{2.16}$$

$$\epsilon\frac{\partial p_0}{\partial t_0} + (\mathbf{V}_0\cdot\nabla)p_0 + \Gamma p_0(\nabla\cdot\mathbf{V}_0) = \epsilon(\Gamma-1)\left(\frac{\eta}{4\pi}|\nabla\times\mathbf{B}|^2 + \kappa\nabla^2 T + \cdots\right). \tag{2.17}$$

The fields become functions of ϵ, and can be expanded in a series about $\epsilon = 0$. The leading-order behavior will satisfy

$$\nabla\cdot(\rho_0 V_0) \approx 0, \tag{2.18}$$

$$(\mathbf{V}_0\cdot\nabla)\mathbf{V}_0 \approx \nabla p_0 + \frac{1}{4\pi}(\nabla\times\mathbf{B}_0)\times\mathbf{B}_0, \tag{2.19}$$

$$\nabla\times(\mathbf{V}_0\times\mathbf{B}_0) \approx 0, \tag{2.20}$$

$$(\mathbf{V}_0\cdot\nabla)p_0 + \Gamma p_0(\nabla\cdot\mathbf{V}_0) \approx 0. \tag{2.21}$$

as $\epsilon\to 0+$. That is, the dominant behavior of the slowly-evolving confinement profiles must satisfy the equilibrium conditions of ideal MHD, in the small-ϵ limit.

The above procedure of *increasing* the number of parameters in the problem by introducing ϵ is merely a convenient way of expressing an ordering assumption, namely that the terms multiplied by ϵ are relatively small. An alternative approach would be to *reduce* the number of parameters in

the problem by defining dimensionless variables using scales which are intrinsic to the problem, and then considering limiting values of the resulting dimensionless constants. Both approaches are ultimately justified by the self-consistency of the results they lead to—terms which are assumed to be small need to be small. From a formal asymptotic-expansion perspective, the intrinsic dimensionless parameter approach appears to be superior, since it involves physically-meaningful limits, such as the ratio of two length scales. However, in the problems being considered in this dissertation, there are a large number of possible normalizations, leading to an equally large number of possible dimensionless parameters which can be used in an expansion. In this case, dimensional analysis is of little value as a guide for which limits to consider. This dissertation will follow the convention of introducing an extra parameter ϵ, taking the small ϵ limit, setting $\epsilon = 1$ in the final result, and verifying the ordering.

2.3 Linear Stability of Slowly-Evolving MHD Profiles

2.3.1 Ideal Stability

In order for a formal solution of Eqs. (2.18)–(2.21) to have a possibility of being realized in practice, it must be stable with respect to noise-induced infinitesimal disturbances. Recall that the equilibria evolve on a dissipative time scale. A given equilibrium profile is ideal-MHD unstable if an arbitrarily small perturbation can be superposed which causes the system to grow at a rate which is independent of ϵ in the small-ϵ limit. We are thus led to consider

the early-time evolution of the initial configuration

$$\begin{pmatrix} \rho \\ p \\ \mathbf{V} \\ \mathbf{B} \end{pmatrix}(t=0) = \begin{pmatrix} \rho_0 \\ p_0 \\ \mathbf{V}_0 \\ \mathbf{B}_0 \end{pmatrix} + \lambda \begin{pmatrix} \delta\rho \\ \delta p \\ \delta\mathbf{V} \\ \delta\mathbf{B} \end{pmatrix}, \tag{2.22}$$

The governing equations are

$$\frac{\partial \delta\rho}{\partial t} = -\nabla\cdot(\delta\rho\mathbf{V_0} - \rho_0\delta\mathbf{V}) + \mathcal{O}(\lambda,\epsilon), \tag{2.23}$$

$$\frac{\partial \delta\mathbf{V}}{\partial t} = -(\mathbf{V}_0\cdot\nabla)\delta\mathbf{V} - (\delta\mathbf{V}\cdot\nabla)\mathbf{V}_0 - \nabla\delta p + \frac{1}{4\pi}(\nabla\times\delta\mathbf{B})\times\mathbf{B}_0 + \frac{1}{4\pi}(\nabla\times\mathbf{B}_0)\times\delta\mathbf{B} + \mathcal{O}(\lambda,\epsilon), \tag{2.24}$$

$$\frac{\partial \delta\mathbf{B}}{\partial t} = \nabla\times(\delta\mathbf{V}\times\mathbf{B}_0) + \nabla\times(\mathbf{V}_0\times\delta\mathbf{B}) + \mathcal{O}(\lambda,\epsilon), \tag{2.25}$$

$$\frac{\partial \delta p}{\partial t} = -(\mathbf{V}_0\cdot\nabla)\delta p - (\delta\mathbf{V}\cdot\nabla)p_0 - \Gamma\left[\delta p(\nabla\cdot\mathbf{V}_0) - p_0(\nabla\cdot\delta\mathbf{V})\right] + \mathcal{O}(\lambda,\epsilon). \tag{2.26}$$

where λ is a second ordering parameter, and $\rho_0, p_0, \mathbf{V}_0, \mathbf{B}_0$ satisfy Eqs. (2.18)–(2.21). Here we emphasize that we are considering leading-order in both ϵ and λ. In particular, to lowest order in ϵ, the equilibrium quantities do not depend on time.

We can determine the time evolution of an arbitrary perturbation, δf, by considering solutions with exponential time dependence:

$$\delta f \propto \mathrm{e}^{\gamma t}. \tag{2.27}$$

where γ tends to a finite limit as $\epsilon \to 0+$.

This leads to an eigenvalue problem for the normal modes:

$$\gamma\delta\rho \approx -\nabla\cdot(\delta\rho\mathbf{V_0}-\rho_0\delta\mathbf{V}), \tag{2.28}$$

$$\gamma\delta\mathbf{V} \approx -(\mathbf{V}_0\cdot\nabla)\delta\mathbf{V}-(\delta\mathbf{V}\cdot\nabla)\mathbf{V}_0-\nabla\delta p+\frac{1}{4\pi}(\nabla\times\delta\mathbf{B})\times\mathbf{B}_0 + \frac{1}{4\pi}(\nabla\times\mathbf{B}_0)\times\delta\mathbf{B}, \tag{2.29}$$

$$\gamma\delta\mathbf{B} \approx \nabla\times(\delta\mathbf{V}\times\mathbf{B}_0)+\nabla\times(\mathbf{V}_0\times\delta\mathbf{B}), \tag{2.30}$$

$$\gamma\delta p \approx -(\mathbf{V}_0\cdot\nabla)p_0-\Gamma p_0(\nabla\cdot\mathbf{V}_0). \tag{2.31}$$

The eigenfunction

$$\begin{pmatrix}\delta\rho\\ \delta p\\ \delta\mathbf{V}\\ \delta\mathbf{B}\end{pmatrix}(\mathbf{x},\gamma) \tag{2.32}$$

satisfies homogeneous boundary conditions which depend on the geometry of the original problem. The system is ideal-MHD stable if the real part γ is negative for all γ in the spectrum. Note that, just like the equilibrium equations (2.18)–(2.21), the system of equations governing the time-dependence of the perturbation is formally identical to what would be obtained from the ideal-MHD model, where the kinetic coefficients are dropped from the outset.

The ideal-MHD model has several notable features which simplify the analysis of the stability problem. In particular, the magnetic field lines are frozen into the fluid so that time evolution of the fluid induces the evolution of the magnetic field. Thus, when considering stability with respect infinitesimal perturbations, one only needs to consider initial profiles which are *dynamically accessible* from the equilibrium of interest. It turns out that the perturbed fluid

displacement induces the perturbed magnetic field, density, and pressure. This dynamically-constrained motion is most easily formulated using Lagrangian fluid variables. This is done in appendix A. The reduction in the degrees of freedom, due to dynamical constraints, reduces the system of equations (2.28)–(2.31) to a single differential equation called the Frieman-Rotenberg equation [13]:

$$\begin{aligned}\rho_0 \frac{\partial^2 \boldsymbol{\xi}}{\partial t^2} = &- \rho_0 \left[2(\mathbf{V}\cdot\boldsymbol{\nabla})\frac{\partial \boldsymbol{\xi}}{\partial t} + (\mathbf{V}\cdot\boldsymbol{\nabla})[(\mathbf{V}\cdot\boldsymbol{\nabla})\boldsymbol{\xi}] - (\boldsymbol{\xi}\cdot\boldsymbol{\nabla})[(\mathbf{V}\cdot\boldsymbol{\nabla})\mathbf{V}] \right] \\ &- \delta\rho(\mathbf{V}\cdot\boldsymbol{\nabla})\mathbf{V} - \boldsymbol{\nabla}\delta p + \frac{1}{4\pi}(\boldsymbol{\nabla}\times\mathbf{B})\times\delta\mathbf{B} + \frac{1}{4\pi}(\boldsymbol{\nabla}\times\delta\mathbf{B})\times\mathbf{B},\end{aligned} \tag{2.33}$$

where all of the perturbed quantities are expressed in terms of the displacement vector $\boldsymbol{\xi}$:

$$\delta\rho = -\boldsymbol{\nabla}\cdot(\rho\boldsymbol{\xi}), \tag{2.34}$$

$$\delta p = -\boldsymbol{\xi}\cdot\boldsymbol{\nabla}p - \Gamma p\boldsymbol{\nabla}\cdot\boldsymbol{\xi}, \tag{2.35}$$

$$\delta\mathbf{V} = \frac{\partial \boldsymbol{\xi}}{\partial t} + (\mathbf{V}\cdot\boldsymbol{\nabla})\boldsymbol{\xi} - (\boldsymbol{\xi}\cdot\boldsymbol{\nabla})\mathbf{V}, \tag{2.36}$$

$$\delta\mathbf{B} = \boldsymbol{\nabla}\times(\boldsymbol{\xi}\times\mathbf{B}). \tag{2.37}$$

2.3.2 Resistive Instabilities

In the previous section, we assumed that the growth rate tended to a nonzero limit as $\epsilon \to 0$. Even if a given equilibrium is stable with respect to ideal modes, it may still be linearly unstable; we can only conclude that the growth rates of all perturbations vanish in the (ideal) limit $\epsilon \to 0$. Of course, if the growth rate of a perturbation vanishes at a rate proportional to ϵ as

$\epsilon \to 0+$, then it cannot be distinguished from the dissipative time evolution of the equilibrium profile. Hence we must next consider instabilities for which

$$\epsilon \ll \gamma \ll 1, \tag{2.38}$$

as $\epsilon \to 0$. In particular, we consider instabilities which vanish as a fractional power of ϵ:

$$\gamma = \mathcal{O}(\epsilon^\alpha) \tag{2.39}$$

in the small-ϵ limit, where $0 < \alpha < 1$. Note that ideal instabilities correspond to $\alpha = 0$. These instabilities are called dissipation-driven, since they rely on nonzero values of the energy-dissipating kinetic coefficients. In particular, instabilities which vanish as a fractional power of the resistivity are called *resistive instabilities*, and play an important role in magnetically-confined fusion plasmas. Nonzero resistivity breaks the magnetic-flux-freezing constraint of ideal MHD, effectively decoupling the fluid motion from the magnetic field. In this dissertation we will restrict our consideration to dissipation-driven instabilities which depend only on the electrical resistivity, to leading order.

These instabilities are only worth considering for equilibria which are ideal-MHD stable. After all, in our assumed ordering where terms multiplied by ϵ are small, an ideal mode would grow rapidly, altering the background equilibrium profile before the resistive mode has had a chance to develop.

If we no longer drop the resistivity, η, in Eqs. (2.23)–(2.26), they

become

$$\frac{\partial \delta\rho}{\partial t} = -\nabla\cdot(\delta\rho\mathbf{V_0} - \rho_0\delta\mathbf{V}) + \mathcal{O}(\lambda,\epsilon), \tag{2.40}$$

$$\frac{\partial \delta\mathbf{V}}{\partial t} = -(\mathbf{V}_0\cdot\nabla)\delta\mathbf{V} - (\delta\mathbf{V}\cdot\nabla)\mathbf{V}_0 - \nabla\delta p + \frac{1}{4\pi}(\nabla\times\delta\mathbf{B})\times\mathbf{B}_0 + \frac{1}{4\pi}(\nabla\times\mathbf{B}_0)\times\delta\mathbf{B} + \mathcal{O}(\lambda,\epsilon), \tag{2.41}$$

$$\frac{\partial \delta\mathbf{B}}{\partial t} = \nabla\times(\delta\mathbf{V}\times\mathbf{B}_0) + \nabla\times(\mathbf{V}_0\times\delta\mathbf{B}) + \eta\nabla^2\delta\mathbf{B} + \mathcal{O}(\lambda,\epsilon), \tag{2.42}$$

$$\frac{\partial \delta p}{\partial t} = -(\mathbf{V}_0\cdot\nabla)\delta p - (\delta\mathbf{V}\cdot\nabla)p_0 - \Gamma\left[\delta p(\nabla\cdot\mathbf{V}_0) - p_0(\nabla\cdot\delta\mathbf{V})\right] + (\Gamma-1)\frac{\eta}{2\pi}\nabla\times\mathbf{B}\cdot\nabla\times\delta\mathbf{B} + \mathcal{O}(\lambda,\epsilon). \tag{2.43}$$

When dynamical constraints are incorporated, the resulting system of equations is

$$\delta\mathbf{V} = \frac{\partial\boldsymbol{\xi}}{\partial t} + (\mathbf{V}\cdot\nabla)\boldsymbol{\xi} - (\boldsymbol{\xi}\cdot\nabla)\mathbf{V}, \tag{2.44}$$

$$\delta\rho = -\boldsymbol{\nabla}\cdot(\rho\boldsymbol{\xi}), \tag{2.45}$$

$$\delta p = -\boldsymbol{\xi}\cdot\boldsymbol{\nabla}p - \Gamma p\boldsymbol{\nabla}\cdot\boldsymbol{\xi}, \tag{2.46}$$

$$\boldsymbol{\nabla}\cdot\mathbf{b} = 0, \tag{2.47}$$

$$\eta\nabla^2\mathbf{b} = \frac{\partial}{\partial t}[\mathbf{b} - \boldsymbol{\nabla}\times(\boldsymbol{\xi}\times\mathbf{B})] - \boldsymbol{\nabla}\times(\mathbf{V}\times[\mathbf{b} - \boldsymbol{\nabla}\times(\boldsymbol{\xi}\times\mathbf{B})]), \tag{2.48}$$

$$\rho_0\frac{\partial^2\boldsymbol{\xi}}{\partial t^2} = -\rho_0\left[2(\mathbf{V}\cdot\boldsymbol{\nabla})\frac{\partial\boldsymbol{\xi}}{\partial t} + (\mathbf{V}\cdot\boldsymbol{\nabla})[(\mathbf{V}\cdot\boldsymbol{\nabla})\boldsymbol{\xi}] - (\boldsymbol{\xi}\cdot\boldsymbol{\nabla})[(\mathbf{V}\cdot\boldsymbol{\nabla})\mathbf{V}]\right] - \delta\rho(\mathbf{V}\cdot\boldsymbol{\nabla})\mathbf{V} - \boldsymbol{\nabla}\delta p + \frac{1}{4\pi}(\boldsymbol{\nabla}\times\mathbf{B})\times\mathbf{b} + \frac{1}{4\pi}(\boldsymbol{\nabla}\times\mathbf{b})\times\mathbf{B}. \tag{2.49}$$

where we have redefined $\delta\mathbf{B}\to\mathbf{b}$, in order to avoid δ's in the final formulae[3]. The derivation of the linearized equations is provided in Appendix A.1. In the

[3]The fields $\delta\rho$, δp can be eliminated, leaving no δ's in the resulting equations

limit of vanishing resistivity, all perturbed quantities are parameterized by $\boldsymbol{\xi}$, and the ideal Frieman-Rotenberg equation [13] is recovered.

Chapter 3

Localized Instabilities in Slab Geometry

3.1 Gravity-Curvature Analogy

In the limit of arbitrarily large magnetic field strength, a single charged particle executes a circular orbit in the plane perpendicular to $\mathbf{B}$ with (vanishing) radius $\rho = mv_\perp c/(eB)$, where m is the particle's mass, e is the charge, and $v_\perp$ is the magnitude of the velocity perpendicular to the magnetic field. Meanwhile, the particle translates freely along the field lines. The first-order correction in the large-$|B|$ expansion accounts for the finite radius of the circular orbit, which in turn leads to variations in ρ over the orbital period. For example, an external force, $\mathbf{F}$, perpendicular to $\mathbf{B}$ causes $v_\perp$ to increase for one half of the orbit and decrease during the other half. The variation in the radius of curvature causes the particle to execute a drift at constant velocity $\mathbf{v}_d$ perpendicular to $\mathbf{B}$.

A straightforward calculation [23] leads to the following expression for the drift velocity of the *guiding center*:

$$\mathbf{v}_d = -c\frac{\mathbf{F}\times\mathbf{B}}{e|B|^2}. \tag{3.1}$$

Curved magnetic field lines also lead to a drift of the guiding center, and this drift can be understood in terms of Eq. (3.1). To lowest-order, the

particle moves with constant velocity $v_\parallel$ along the curved field lines. The curvature of the field lines

$$\boldsymbol{\kappa}_B = \left(\frac{\mathbf{B}}{|B|}\cdot\nabla\right)\frac{\mathbf{B}}{|B|}, \tag{3.2}$$

implies that the particle's guiding center is accelerating, and this acceleration can be replaced by an inertial force

$$\mathbf{F} = mv_\parallel^2\boldsymbol{\kappa}_B, \tag{3.3}$$

in the particle's frame of reference.

Using this force in Eq. (3.1), we find

$$\mathbf{v}_\kappa = c\frac{mv_\parallel^2}{e}\frac{\boldsymbol{\kappa}_B\times\mathbf{B}}{B^2}, \tag{3.4}$$

which is correct [23].

Thus, as a heuristic principle, viewing field-line curvature and an external gravitational field as equivalent correctly predicts guiding-center drift motion of charged particles in a strong magnetic field. We will directly verify that this principle also holds, to a limited extent, for fluid behavior. This correspondence greatly facilitates the analysis and interpretation of instabilities in toroidal equilibria.

3.2 Stability of a Gravitating Slab

As a first iteration, we consider instabilities in plane geometry with an external gravitational field. According to the previously mentioned heuristic,

this model should be equivalent to studying equilibrium profiles with constant curvature, i.e. cylindrical equilibria. This will be verified below. By first carrying out the analysis in plane geometry, we are able to clearly demonstrate the mathematical structure of resistive instabilities without the additional complications of toroidal coordinates.

We choose the z-axis along the line of the gravitational field so that $\mathbf{g} = -g\mathbf{e}_z$. In order to make the problem more closely correspond to a cylinder, we impose periodicity along the x-axis, with period a. Additionally, we require periodicity in y, with period L, so that our problem is topologically toroidal. Finally, we assume that our fluid is confined by two perfectly conducting walls at $z = \pm Z$. We will find that the particular choice of model boundary conditions is not terribly important in our final result.

3.3 Ideal Stability

Before considering resistive instabilities, we must verify that the profile is ideal-MHD stable. Moreover, the formalism for resistive modes is a straightforward extension of the ideal-stability calculation, so ideal stability is a natural starting point.

From Eqs. (2.18)–(2.21) governing the η-independent component of the equilibrium profile, we find the most general plane-invariant equilibrium has

the form

$$p = p(z), \tag{3.5}$$

$$\rho = \rho(z), \tag{3.6}$$

$$\mathbf{B} = B_x(z)\mathbf{e}_x + B_y(z)\mathbf{e}_y, \tag{3.7}$$

$$\mathbf{V} = V_x(z)\mathbf{e}_x + V_y(z)\mathbf{e}_y, \tag{3.8}$$

with

$$p'(z) + \rho(z)g = -\left(\frac{B^2}{8\pi}\right)'(z). \tag{3.9}$$

Because the background equilibrium profile is independent of x, y, and t, we look for perturbations with *irreducible* dependence [15] in these variables:

$$\delta f(x, y, z, t) \propto f(z)\mathrm{e}^{k_x x + k_y y + \gamma t}. \tag{3.10}$$

where the allowed wavenumbers are constrained to $k_x = m/a$, $k_y = n/L$ by the toroidal topology.

It is convenient to redefine γ at the outset by subtracting off a Doppler-shift-induced real frequency due to the equilibrium velocity at a particular (not yet specified) height z_0. All perturbed quantities, δf, then have the time dependence

$$\delta f \propto \mathrm{e}^{[\gamma - \mathbf{i}\mathbf{k}\cdot\mathbf{V}(z_0)]t}. \tag{3.11}$$

This redefinition is equivalent[1] to computing the growth rate after boosting into the frame moving with the background velocity at $z = z_0$.

[1]Mathematically, we have merely shifted the origin of the complex γ-plane, which implies no loss of generality.

The linearized equations (2.45)–(2.49) for slab equilibria become:

$$\rho\tilde{\gamma}^2\boldsymbol{\xi} = \mathbf{F}(\boldsymbol{\xi},\mathbf{b}) - \mathbf{g}\nabla\cdot(\rho\boldsymbol{\xi}), \tag{3.12}$$

$$\mathbf{b} - \boldsymbol{\nabla}\times(\boldsymbol{\xi}\times\mathbf{B}) = \mathcal{O}(\eta/\tilde{\gamma}), \tag{3.13}$$

$$\boldsymbol{\nabla}\cdot\mathbf{b} = 0, \tag{3.14}$$

with

$$\mathbf{F}(\boldsymbol{\xi},\mathbf{b}) = (1/4\pi)\left[(\boldsymbol{\nabla}\times\mathbf{b})\times\mathbf{B} + (\boldsymbol{\nabla}\times\mathbf{B})\times\mathbf{b}\right] + \boldsymbol{\nabla}(\xi_r p' + \Gamma p\boldsymbol{\nabla}\cdot\boldsymbol{\xi}), \tag{3.15}$$

$$\tilde{\gamma}(z) = \gamma + \mathrm{i}\Omega\,. \tag{3.16}$$

where $\Omega = \mathbf{k}\cdot[\mathbf{V}(z) - \mathbf{V}(z_0)]$.

The boundary conditions are

$$\xi_z(z = \pm Z) = 0. \tag{3.17}$$

It is convenient to expand the perturbed magnetic field and displacement vector field in a field-line projection[2]:

$$\mathbf{b} = b_z\mathbf{e}_z + b_B\frac{\mathbf{B}}{B^2} + b_\perp\frac{\mathbf{e}_z\times\mathbf{B}}{B^2}, \tag{3.18}$$

$$\boldsymbol{\xi} = \xi_z\mathbf{e}_z + \xi_B\frac{\mathbf{B}}{B^2} + \xi_\perp\frac{\mathbf{e}_z\times\mathbf{B}}{B^2}. \tag{3.19}$$

By substituting these expansions into Eqs. (3.12)-(3.14), and projecting these equations along $\mathbf{e}_z$, $\mathbf{B}$, and $\mathbf{e}_z\times\mathbf{B}$, we will obtain a system of equations

[2]This basis makes the comparison with calculations in toroidal geometry more straightforward.

which determine the spectrum of γ's (and the associated eigenfunctions) for the particular equilibrium configuration.

The divergence-free condition on $\mathbf{b}$ gives

$$\frac{\mathrm{d}\, b_z}{\mathrm{d}\, z} + \mathrm{i}F b_B - \mathrm{i}G b_\perp = 0, \tag{3.20}$$

where we have defined $F = \mathbf{k}\cdot\mathbf{B}$, and $G = \mathbf{e}_z \cdot \mathbf{k}\times\mathbf{B}$. Similarly, we have

$$(\nabla\cdot\xi) = \frac{\mathrm{d}\,\xi_z}{\mathrm{d}\, z} + \mathrm{i}F\xi_B - \mathrm{i}G\xi_\perp. \tag{3.21}$$

Dotting Eq. (3.13) with $\mathbf{e}_z$ and $\mathbf{B}$ yields

$$b_z - \mathrm{i}F\xi_z = 0, \tag{3.22}$$

$$b_B - \mathrm{i}F\xi_B + B^2(\nabla\cdot\xi) + \left[4\pi\left(p' + \rho g\right) + (B^2)'\right]\xi_z = 0, \tag{3.23}$$

respectively. Eq. (3.13) implies Eq. (3.14), which is information we have used above. Thus dotting Eq. (3.13) with $\mathbf{e}_z\times\mathbf{B}$ will not yield independent information.

The remaining equations are obtaining by taking scalar products with the perturbed equation of motion. By dotting Eq. (3.12) with $\mathbf{B}$, $\mathbf{e}_z\times\mathbf{B}$, and $\mathbf{e}_z$, we find

$$\rho\tilde{\gamma}^2\xi_B = -b_z\left(p' + \rho g\right) + \mathrm{i}F\left[\xi_z p' + \Gamma p(\nabla\cdot\xi)\right], \tag{3.24}$$

$$\rho\tilde{\gamma}^2\xi_\perp = -b_z\frac{\mathbf{J}\cdot\mathbf{B}}{c} + \frac{\mathrm{i}G}{4\pi}\left[\frac{b_B}{4\pi} - \xi_z p' - \Gamma p(\nabla\cdot\xi)\right] + \frac{\mathrm{i}F}{4\pi}b_\perp, \tag{3.25}$$

$$\begin{aligned}\rho\tilde{\gamma}^2\xi_z =& b_B\left(\frac{p'+\rho g}{B^2}\right) - b_\perp\left(\frac{\mathbf{J}\cdot\mathbf{B}}{cB^2}\right) + \frac{\mathrm{i}F}{4\pi}b_z \\ &- \frac{\mathrm{d}}{\mathrm{d}\, z}\left[\frac{b_B}{4\pi} - \xi_z p' - \Gamma p(\nabla\cdot\xi)\right] - g\rho(\nabla\cdot\xi) - g\xi_z\rho'.\end{aligned} \tag{3.26}$$

Eqs. (3.20)–(3.25) can be used to express the components of $\mathbf{b}$ along with ξ_B, $\xi_\perp$, and $(\nabla \cdot \xi)$ in terms of ξ_z and ξ_z'. After a fair amount of algebra, Eqs. (3.20)–(3.26) can be reduced to a single ordinary differential equation for ξ_z:

$$\frac{\mathrm{d}}{\mathrm{d}\,z}\left(\frac{N}{D}\frac{\mathrm{d}\,\xi_z}{\mathrm{d}\,z}\right) + C(z;\gamma)\xi_z = 0, \tag{3.27}$$

where

$$N = \rho\left(\frac{B^2}{4\pi\rho} + \frac{\Gamma p}{\rho}\right)[\tilde{\gamma}^2 + \omega_A^2(z)][\tilde{\gamma}^2 + \omega_S^2(z)], \tag{3.28}$$

$$D = [\tilde{\gamma}^2 + \omega_{s0}^2(z)][\tilde{\gamma}^2 + \omega_{f0}^2(z)], \tag{3.29}$$

$$C = \rho' g - \rho[\tilde{\gamma}^2 + F^2/(4\pi\rho)] + k^2\rho g^2\frac{\tilde{\gamma}^2 + F^2/(4\pi\rho)}{D} - \left[\rho g\frac{\tilde{\gamma}^2[\tilde{\gamma}^2 + F^2/(4\pi\rho)]}{D}\right]'. \tag{3.30}$$

Here we have defined the Alfven and slow magnetosonic frequencies:

$$\omega_A^2 = F^2/(4\pi\rho), \tag{3.31}$$

$$\omega_S^2 = \frac{\Gamma p}{\Gamma p + B^2/(8\pi)}\omega_A^2, \tag{3.32}$$

as in Ref. [19], and the slow and fast turning point frequencies

$$\omega_{s0,f0}^2 = \frac{1}{2}k^2\left(\frac{F^2}{4\pi\rho} + \frac{\Gamma p}{\rho}\right)\sqrt{1 \pm \frac{F^2 p}{\pi k^2[B^2/(4\pi) + \Gamma p]^2}}. \tag{3.33}$$

In summary, to determine the stability of a particular equilibrium profile–characterized by the five functions $p(z)$, $V_x(z)$, $V_y(z)$, $B_x(z)$, and $B_y(z)$, which are related through Eq. (3.9)–we find the spectrum of eigenvalues of Eq. (3.27), with boundary conditions (3.17). The equilibrium is ideal-MHD unstable if there exists an eigenvalue γ such that $\mathcal{R}\mathrm{e}[\gamma] > 0$.

3.3.1 Marginal Ideal-MHD Stability

In principle, we have outlined a procedure for determining profile stability, but the program is not immediately useful because of the general analytical intractability of the eigenvalue equation (3.27). Moreover, we would like a general criterion, such as[3]

$$V_x''(z) \neq 0 \ \forall z \in (-Z, Z), \tag{3.34}$$

which is independent of any particular functional form one might choose for the equilibrium.

Fortunately, a general stability criterion can be obtained by assuming the equilibrium profile is near a stable-unstable boundary (in equilibrium profile space), and then looking for eigenfunctions with arbitrarily small growth rate. More concretely, consider an N-parameter family of equilibrium profiles, and assume that the parameter space has both a stable and an unstable region. As an arbitrary trajectory in parameter space approaches the stability threshold, the growth rate of the most unstable mode vanishes. To obtain a stability criterion, we therefore consider modes with the smallest growth rates, and look for a property of the equilibrium profile which requires γ to have a definite sign.

We thus adopt the ordering

$$\gamma \to \epsilon\gamma, \tag{3.35}$$

[3]This is Rayleigh's inflection-point criterion [9] for stability of sheared flows.

and study the behavior of the eigenvalues and eigenfunctions in the limit $\epsilon \to 0$.

3.3.1.1 Outer Limit

Making the substitution (3.35) and dropping terms containing ϵ, we have[4]:

$$\frac{\mathrm{d}}{\mathrm{d}\, z}\left(\frac{N}{D}(z;\gamma=0)\frac{\mathrm{d}\,\xi^{(0)}_{z,\mathrm{Out}}}{\mathrm{d}\, z}\right) + C(z;\gamma=0)\xi^{(0)}_{z,\mathrm{Out}} \approx 0, \tag{3.37}$$

Hence, we have assumed

$$\epsilon\gamma^2 {\xi^{(0)}_{z,\mathrm{Out}}}'' \ll C(z,\gamma=0)\xi^{(0)}_{z,\mathrm{Out}}, \tag{3.38}$$

as $\epsilon \to 0+$. Below, we will show that this ordering is valid everywhere *outside* of a thin boundary layer, which forms at a point, z_0, in the domain where

$$\omega_A(z_0) = 0. \tag{3.39}$$

Anticipating the boundary-layer analysis, we follow the convention of Ref. [1] and refer to this ordering of Eq. (3.27) as the *outer limit*.

---

[4]More technically, we assume that the exact solution $\xi_z(z;\epsilon)$ to Eq. (3.27) satisfies the asymptotic relation

$$\frac{\mathrm{d}}{\mathrm{d}\, z}\left(\frac{N}{D}(z;\gamma=0)\frac{\mathrm{d}\,\xi_z}{\mathrm{d}\, z}\right) \sim -C(z;\gamma=0)\xi_z, \tag{3.36}$$

as $\epsilon \to 0+$. If this is the case, then the solution $\xi^{(0)}_{z,\mathrm{Out}}$ of the differential equation obtained by replacing the $'\sim'$ of Eq. (3.36) with an $'='$ will be asymptotic to $\xi_z(z;\epsilon)$ as $\eta \to 0+$. Note, we were careful not to put Eq. (3.36) in the form $F(\xi_z'', \xi_z', \xi_z) \sim 0$, since the only thing asymptotic to zero is zero. In Eq. (3.36), the left and right sides of the relation can differ by (nonzero) subdominant functions. We try to remind the reader of all of these implicit assumptions by using the $'\approx'$ symbol. This technicality in the procedure of generating asymptotic solutions of differential equations, discussed in Ref.[1], will be important in Chapter 4.

Assuming there is a point $z_0 \in (-Z, Z)$ where the Alfven frequency vanishes, one can readily verify that Eq. (3.37) will have a singularity at that point[5].

In addition to Eq. (3.38) becoming singular, the surface $z = z_0$ has the notable property that the equilibrium magnetic field lines return to their original value (i.e. close) after m windings in y, and n windings in x. In fact, if we were to rescale x and y so that the system was periodic in both directions with period one, then the slope of the magnetic field lines at z_0 would be a rational number m/n. These special surfaces are called *rational surfaces*. At $z = z_0$ the field lines have the same periodicity as the perturbation, and $\mathbf{B}(z_0)$ is perpendicular to $\mathbf{k}$, so the field lines at this surface are not bent by the perturbation.

Letting L_{Out} denote the gradient length scale of the equilibrium quantities at z_0, the limiting behavior of Eq. (3.37) as $z \to z_0$ is given by

$$x^2 {\xi^{(0)}_{z,\mathrm{Out}}}''(x) + 2x {\xi^{(0)}_{z,\mathrm{Out}}}'(x) + \frac{1}{1-\kappa_\parallel^2}\left(D_g + \frac{D_\rho}{\beta\Gamma}\left[\frac{1-\kappa_\parallel^{-2}}{1-\kappa_\parallel^{-2}+\frac{2}{\beta\Gamma}}\right]\right)\xi^{(0)}_{z,\mathrm{Out}}(x) \approx 0, \tag{3.40}$$

where we have defined a normalized independent variable $x = (z - z_0)/L_{\mathrm{Out}}$,

[5]Had we not subtracted the Doppler shift due to the velocity at z_0 in Eq. (3.11), we would have had to consider the ordering $\gamma \to \mathrm{i}\mathbf{k}\cdot\mathbf{V}(z_0) + \epsilon\gamma$, instead of Eq. (3.35). This, in turn, is justified by a fairly involved argument, given in [18], which proves that as the most unstable ideal mode transitions to instability, crossing into the unstable half of the γ-plane, it must pass through $\gamma_{\mathrm{crit}} = \mathrm{i}\mathbf{k}\cdot\mathbf{V}(z_0)$.

and dimensionless constants

$$D_g = -\frac{4\pi k^2 g \rho'(z_0)}{F'(z_0)^2}, \tag{3.41}$$

$$\kappa_\parallel = \frac{\sqrt{4\pi\rho}\Omega'(z_0)}{F'(z_0)}, \tag{3.42}$$

$$\beta = 8\pi p(z_0)/B(z_0)^2, \tag{3.43}$$

$$D_\rho = -\frac{16\pi^2 k^2 \rho(z_0)^2 g^2}{F'(z_0)^2}, \tag{3.44}$$

$$D_v = \frac{1}{1-\kappa_\parallel^2}\left(D_s + \frac{D_\rho}{\beta\Gamma}\left[\frac{1-\kappa_\parallel^{-2}}{1-\kappa_\parallel^{-2}+\frac{2}{\beta\Gamma}}\right]\right). \tag{3.45}$$

From Eq. (3.40), we find

$$\xi^{(0)}_{z,\mathrm{Out}} \sim a_1^{(\pm)}|x|^{-\frac{1}{2}+\sqrt{\frac{1}{4}-D_v}} + a_2^{(\pm)}|x|^{-\frac{1}{2}-\sqrt{\frac{1}{4}-D_v}}, \tag{3.46}$$

as $|x| \to 0\pm$. Using Eq. (3.46), it is easy to verify that the outer ordering (3.38) breaks down for $|z - z_0| \approx \epsilon L_{\mathrm{Out}}$. Thus, the mode develops an internal boundary layer at z_0.

3.3.1.2 Inertial Layer

In order to obtain a uniformly valid asymptotic representation of ξ_z, we must find the local behavior for $|z - z_0| \approx \epsilon L_{\mathrm{Out}}$, then asymptotically match the two solutions.

Standard boundary layer theory [1] instructs us to seek a local solution in the form

$$\xi_z(z,\epsilon) \sim \Xi(X = \frac{z-z_0}{\delta(\epsilon)}), \tag{3.47}$$

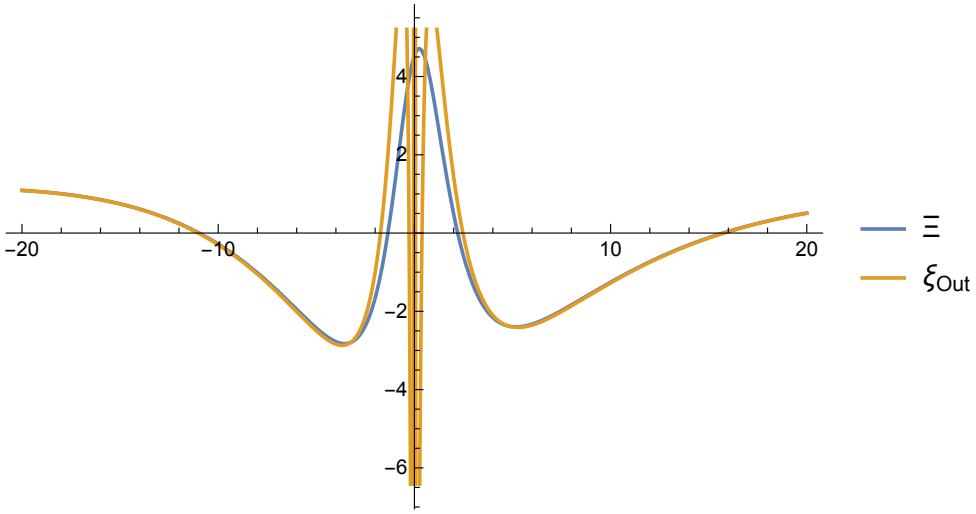

Figure 3.1: The outer and layer solutions near z_0.

as $\epsilon \to 0+$, keeping X fixed, with $\delta(\epsilon)$ chosen to satisfy the regularity condition at z_0. This will come from the highest derivative (locally) contributing to leading order, which implies $\delta = \mathcal{O}(\epsilon)$. By substituting $z - z_0 = \delta X$, the dominant terms in Eq. (3.27) will only depend on the equilibrium values at $z = z_0$.

We find that the local behavior of the eigenfunction satisfies

$$\frac{\mathrm{d}}{\mathrm{d}\,X}\left([X^2 + (1 + \mathrm{i}\kappa_\parallel X)^2]\frac{\mathrm{d}\,\Xi}{\mathrm{d}\,X}\right) + \left(D_g + \frac{D_\rho}{\beta\Gamma}\left[\frac{1 + \frac{X^2}{(1+\mathrm{i}\kappa_\parallel X)^2}}{1 + \frac{X^2}{(1+\mathrm{i}\kappa_\parallel X)^2} + \frac{2}{\beta\Gamma}}\right]\right)\Xi \approx 0. \tag{3.48}$$

as $\epsilon \to 0+$, where $\delta = \epsilon\sqrt{4\pi\rho}\gamma/F'(z_0)$.

The appropriate boundary conditions for Eq. (3.48) are determined by

considering the behavior of ξ_z in an *intermediate limit*:

$$\epsilon \to 0+, \tag{3.49}$$

$$s = (z - z_0)/(\sqrt{\delta L_{\rm Out}}) \text{ fixed.} \tag{3.50}$$

Note

$$X = s/\varepsilon, \tag{3.51}$$

$$x = \varepsilon s. \tag{3.52}$$

where $\varepsilon = \sqrt{\delta/L_{\rm Out}}$. Thus, the intermediate limit is simultaneously the large-$|X|$ limit and the small-$|x|$ limit. We therefore have

$$\xi_z(z = z_0 + s\sqrt{\delta L_{Out}}) \sim \xi^{(0)}_{z,\rm Out}(x = \varepsilon s) \sim \Xi(X = s/\varepsilon), \tag{3.53}$$

for all s as $\epsilon \to 0+$.

The large-$|X|$ asymptotic behavior of Ξ is easily found to be

$$\Xi \sim A_1^{(\pm)}|X|^{-\frac{1}{2}+\sqrt{\frac{1}{4}-D_v}} + A_2^{(\pm)}|X|^{-\frac{1}{2}-\sqrt{\frac{1}{4}-D_v}}, \tag{3.54}$$

as $X \to \pm\infty$. Comparing this to Eq. (3.46), we see that the matching criterion (3.53) can be achieved.

In the intermediate limit,

$$\xi^{(0)}_{z,\rm Out} \sim a_1^{(\pm)}(\varepsilon|s|)^{\nu} + a_2^{(\pm)}(\varepsilon|s|)^{-1-\nu}, \tag{3.55}$$

$$\Xi \sim A_1^{(\pm)}\left(\frac{|s|}{\varepsilon}\right)^{\nu} + A_2^{(\pm)}\left(\frac{|s|}{\varepsilon}\right)^{-1-\nu}. \tag{3.56}$$

as $\varepsilon \to 0+$, with $s = \pm|s|$. We thus find

$$A_1^{(\pm)} = a_1^{(\pm)}(\delta/L_{\rm Out})^{\nu}, \tag{3.57}$$

$$A_2^{(\pm)} = a_2^{(\pm)}(\delta/L_{\rm Out})^{-1-\nu}. \tag{3.58}$$

The constants $a_{1,2}^{(\pm)}$ come from solving Eq. (3.37) outside the inertial layer, subject to the boundary conditions (3.17). An expression for the growth rate is obtained by solving the inertial layer equation (3.48), and imposing the conditions (3.57)–(3.58) at large $|X|$.

The matching conditions (3.57)–(3.58) also relate the arbitrary overall scales of the eigenfunction in the two outer ideal regions. For example, the constants $a_{1,2}^{(+)}$ are obtained by setting

$$\xi_{z,\rm Out}^{(0)}(+Z) = 0, \tag{3.59}$$

$$\xi_{z,\rm Out}^{(0)}{}'(+Z) = \alpha^{(+)}, \tag{3.60}$$

where $\alpha^{(+)}$ is arbitrary, and integrating Eq. (3.37) from $z = Z$ down to the singularity z_0. The asymptotic behavior of $\xi_{z,\rm Out}^{(0)}$ will have the form (3.46), and the constants $a_{1,2}^{(+)}$ will be linear functions of $\alpha^{(+)}$. Similarly, the values $a_{1,2}^{(-)}$ depend linearly on a second arbitrary scale $\alpha^{(-)}$ from the initial condition at $z = -Z$. The constants $\alpha^{(\pm)}$, and the overall scale of the layer eigenfunction, Ξ, are all related through Eqs. (3.57)–(3.58).

3.3.2 Marginal Ideal-MHD Dispersion Relation

We can obtain a closed-form analytic expression for γ in the limit $\beta\Gamma \to \infty$. This limit physically corresponds to incompressibility. In this case, Eq.

(3.48) can be transformed to Legendre's differential equation. The general solution is

$$\Xi(X) = AP_\nu(-\mathrm{i}X[1-\kappa_\parallel^2]) + BQ_\nu(-\mathrm{i}X[1-\kappa_\parallel^2]). \tag{3.61}$$

Using the large-argument asymptotic behavior of the Legendre polynomials [10]

$$P_\nu(z) \sim \frac{1}{\sqrt{\pi}}\frac{\Gamma(\nu+1/2)}{\Gamma(\nu+1)}(2z)^\nu + \frac{1}{\sqrt{\pi}}\frac{\Gamma(-\nu-1/2)}{\Gamma(-\nu)}(2z)^{-1-\nu}, \tag{3.62}$$

$$Q_\nu(z) \sim \sqrt{\pi}\frac{\Gamma(\nu+1)}{\Gamma(\nu+3/2)}(2z)^{-1-\nu}, \tag{3.63}$$

together with the parity-inversion formulae

$$P_\nu(-z) = \mathrm{e}^{\mathrm{i}\nu\pi}P_\nu(z) - \frac{2}{\pi}\sin(\pi\nu)Q_\nu(z), \tag{3.64}$$

$$Q_\nu(-z) = -\mathrm{e}^{-\mathrm{i}\nu\pi}Q_\nu(z), \tag{3.65}$$

the matching conditions (3.57)–(3.58) give

$$a_1^{(+)}\varepsilon^\nu = \frac{A\Gamma(1/2+\nu)}{\sqrt{\pi}\Gamma(1+\nu)}\left(\frac{2(1-\kappa_\parallel^2)}{\mathrm{i}\varepsilon}\right)^\nu, \tag{3.66}$$

$$a_2^{(+)}\varepsilon^{-1-\nu} = \frac{A\Gamma(-1/2-\nu)\Gamma(3/2+\nu) + \pi B\Gamma(-\nu)\Gamma(1+\nu)}{\sqrt{\pi}\Gamma(-\nu)\Gamma(3/2+\nu)}\left(\frac{2(1-\kappa_\parallel^2)}{\mathrm{i}\varepsilon}\right)^{-1-\nu}, \tag{3.67}$$

$$a_1^{(-)}\varepsilon^\nu = \frac{A\mathrm{e}^{\mathrm{i}\pi\nu}\Gamma(1/2+\nu)}{\sqrt{\pi}\Gamma(1+\nu)}\left(\frac{2(1-\kappa_\parallel^2)}{\mathrm{i}\varepsilon}\right)^\nu, \tag{3.68}$$

$$a_2^{(-)}\varepsilon^{-1-\nu} = \left(\frac{2(1-\kappa_\parallel^2)}{\mathrm{i}\varepsilon}\right)^{-1-\nu} \times \frac{A\mathrm{e}^{\mathrm{i}\pi\nu}\Gamma(-1/2-\nu)\Gamma(3/2+\nu) - (2A+\pi\mathrm{e}^{\mathrm{i}\pi\nu}B)\Gamma(-\nu)\Gamma(1+\nu)}{\sqrt{\pi}\Gamma(-\nu)\Gamma(3/2+\nu)}. \tag{3.69}$$

After eliminating A and B from Eqs. (3.66)–(3.69), one finally obtains the *dispersion relation*:

$$\left(\frac{\gamma}{1-\kappa_\parallel^2}\right)^u = \frac{4^{-1/2+u}\Delta' \mathrm{e}^{-\mathrm{i}(1/2+u)\pi}\Gamma(1/2-u)\Gamma(u)}{\Gamma(1/2+u)\left[\mathrm{e}^{\mathrm{i}\pi(u-1/2)}\Gamma(-u)\Gamma(1+u)-\Gamma(1/2-u)\Gamma(1/2+u)\right]}, \tag{3.70}$$

where

$$\Delta' = \frac{a_2^{(+)}}{a_1^{(+)}} + \frac{a_2^{(-)}}{a_1^{(-)}}, \tag{3.71}$$

$$u = \sqrt{\frac{1}{4} - \frac{D_g}{1-\kappa_\parallel^2}}. \tag{3.72}$$

3.3.2.1 Analysis of Dispersion Relation

There is a great deal of information contained in the dispersion relation (3.70). For example, we see by that modifying the equilibrium profile away from z_0, or, by changing the nature of the boundary conditions, the growth rate is only affected through the single parameter Δ'. The quantity Δ' is a linear functional of the profile outside of the layer, and a linear function of the boundary conditions, and thus is insensitive to small changes at any one point. In contrast, we will show that most of the important physics is contained in u, which depends only on the characteristics of the equilibrium at $z = z_0$.

If $4D_g > (1-\kappa_\parallel^2)$, then u is purely imaginary. Substituting $u = \mathrm{i}|u|$ into Eq. (3.70), and solving for γ, we find

$$\gamma_n \propto \exp\left(\frac{2}{u}[\Phi(|u|,\Delta') - n\pi]\right), \tag{3.73}$$

where n is an arbitrary integer, which emerges from taking the logarithm of i, and Φ is an unspecified function. We thus have an infinite sequence of unstable modes, which accumulate at $\gamma_\infty = 0$. The allowed values of n are limited from below by the requirement that γ_n be small, which is our beginning assumption.

For stability, it is clearly necessary that $4D_g < (1 - \kappa_\parallel^2)$. To see what happens near the boundary of this inequality, we look at the small-u limit of Eq. (3.70). Using $\Gamma(u) \sim u^{-1}$, we find

$$\left(\frac{\gamma}{1-\kappa_\parallel^2}\right)^u \approx \frac{-\Gamma(1/2)\Delta'}{2\Gamma(1)}. \tag{3.74}$$

Taking the logarithm of both sides, we get

$$\gamma \approx (1-\kappa_\parallel^2)\mathrm{e}^{-\frac{\sqrt{\pi}\Delta'}{2u}} \tag{3.75}$$

Thus, $u = 0$, or $4D_g = (1 - \kappa_\parallel^2)$, is the ideal stability boundary. We have only considered the analytically-tractable large-$\beta\Gamma$ limit, but we have found a special case of a general result [32]: The equilibrium is stable if and only if the exponents of the asymptotic behavior (3.46) are real.

3.4 Resistive Interchange Modes

In the modes considered in the previous section, the width of the inertial layer is $\delta = \mathcal{O}(\gamma)$. In considering ideal modes, we have neglected the resistivity, η, in the induction equation (2.48), which requires

$$|\eta\nabla^2\mathbf{b}| \ll |\gamma\mathbf{b}|. \tag{3.76}$$

Outside of the inertial layer, this inequality is satisfied. However, within the resistive layer, $|\nabla^2 \mathbf{b}| \approx |\mathbf{b}/\delta^2|$. We showed that $\gamma \to 0$ at the ideal stability boundary, so for sufficiently small γ, it is no longer justified to neglect η within the layer. The two terms in Eq. (3.76) are of the same order of magnitude in the inertial layer when $\gamma \approx \eta^{1/3}$.

These considerations lead us to adopt the ordering

$$\gamma \to \epsilon\gamma, \quad \eta \to \epsilon^3\eta, \quad \delta \to \epsilon\delta. \tag{3.77}$$

The width δ of the boundary layer scales with γ, which is the same as in the ideal modes considered previously. What is new is the resistive diffusion term in Eq. (2.48) will now be competitive with the inertial term within the layer. The equations governing the mode outside the layer are obtained by dropping γ and η, which again leads to Eq. (3.37).

A second way of arriving at the ordering (3.77) is to look for unstable modes whose growth rates vanish in the ideal limit $\eta \to 0$. From Chapter 2, we know that such modes are only interesting if $\eta \ll \gamma$ as $\eta \to 0$, so that one looks for growth rates which vanish as a fractional power of η:

$$\gamma \propto \eta^{\alpha}. \tag{3.78}$$

The width of the inertial layer and the exponent, α, are simultaneously determined [1] in a *distinguished limit*, where the highest derivatives and the inertia are all assumed to contribute to leading order[6]. The ordering (3.77) therefore

[6]This is an example of the heuristic principle of *maximal complication*, which instructs us [26] to keep as many terms as possible when it isn't clear a priori whether they are small.

the natural starting point for studying resistive modes.

3.4.1 Outer Limit

By dropping the resistivity and inertia in each of the component equations, which we have assumed are small in our ordering, we again obtain Eq. (3.37) as our dominant balance in the outer limit. The outer limit breaks down near $z = z_0$, where Eq. (3.37) is singular, and the asymptotic behavior of $\xi^{(0)}_{z,\mathrm{Out}}$ near the singularity is given by Eq. (3.46) as $x \to 0\pm$.

3.4.2 Resistive Layer Equations

To find the behavior of the mode near z_0, we again introduce layer variables:

$$\boldsymbol{\xi}_z(z_0 + \epsilon x) \sim \left(\epsilon \xi_z^{(1)}(x)\mathbf{e}_z + \xi_B^{(0)}(x)\frac{\mathbf{B}}{B^2} + \xi_\perp^{(0)}(x)\frac{\mathbf{e}_z \times \mathbf{B}}{B^2} \right), \tag{3.79}$$

$$\mathbf{b}(z_0 + \epsilon x) \sim \left(\epsilon^2 b_z^{(2)}(x)\mathbf{e}_z + \epsilon b_B^{(1)}(x)\frac{\mathbf{B}}{B^2} + \epsilon b_\perp^{(1)}(x)\frac{\mathbf{e}_z \times \mathbf{B}}{B^2} \right), \tag{3.80}$$

$$(\nabla \cdot \xi)(z_0 + \epsilon x) \sim \epsilon(\nabla \cdot \xi)^{(1)}(x). \tag{3.81}$$

as $\epsilon \to 0+$. The explanation for how we determined the relative ordering of the various components goes as follows: In the outer region, ξ_B, $\xi_\perp$, $(\nabla \cdot \xi)$, b_z, b_B, and $b_\perp$ can all be expressed in terms of ξ_z and ξ_z' through Eqs. (3.20)–(3.25). For example,

$$b_{z,\mathrm{Out}} = \mathrm{i}F(z)\xi_{z,\mathrm{Out}}. \tag{3.82}$$

In an intermediate limit, where the outer and layer solutions should match, the outer-limit relation (3.82) gives

$$b_{z,\mathrm{Out}} \approx \mathrm{i}F'(z_0)(z-z_0)\xi_{z,\mathrm{Out}}, \tag{3.83}$$

which tells us $|b_z| \propto \delta\xi_z$ in the intermediate region. In order to have a match, this ordering must also hold in the intermediate region for the layer variables, which tells us $b_z/\xi_z = \mathcal{O}(\epsilon)$ throughout the layer. Carrying out this reasoning for each of the other components, one finds the ordering (3.79)–(3.81).

The differential equations determining the layer variables are found by projecting the linearized resistive-MHD equations[7]

$$\rho\tilde{\gamma}^2\boldsymbol{\xi} = \mathbf{F}(\boldsymbol{\xi},\mathbf{b}) - \mathbf{g}\nabla\cdot(\rho\boldsymbol{\xi}), \tag{3.84}$$

$$\eta\nabla^2\mathbf{b} = \frac{\partial}{\partial t}[\mathbf{b} - \boldsymbol{\nabla}\times(\boldsymbol{\xi}\times\mathbf{B})] - \boldsymbol{\nabla}\times(\mathbf{V}\times[\mathbf{b} - \boldsymbol{\nabla}\times(\boldsymbol{\xi}\times\mathbf{B})]), \tag{3.85}$$

$$\boldsymbol{\nabla}\cdot\mathbf{b} = 0, \tag{3.86}$$

onto $\mathbf{e}_z$, $\mathbf{B}$, and $\mathbf{e}_z\times\mathbf{B}$, taking the layer limit $\epsilon\to 0+$, $(z-z_0)/\delta = \text{constant}$ and dropping all manifestly subdominant terms.

The $\mathbf{e}_z$ and $\mathbf{B}$ projections of Eq. (3.85) give

$$\eta b_z^{(2)\prime\prime} = \tilde{\gamma}(b_z^{(2)} - \mathrm{i}F'x\xi_z^{(1)}), \tag{3.87}$$

$$\eta b_B^{(1)\prime\prime} = \tilde{\gamma}(b_B^{(1)} - \mathrm{i}F'x\xi_B^{(0)} + B^2(\nabla\cdot\xi)^{(1)} + [4\pi(p'+\rho g) + B^{2\prime}]\xi_z^{(1)}) - (b_z^{(2)} - \mathrm{i}F'x\xi_z^{(1)})M, \tag{3.88}$$

[7] In the ordering (3.77), the resistivity does not contribute to Eq. (2.46) to leading order. The thermal conductivity would if $\kappa = \mathcal{O}(\epsilon)$, but we limit our consideration to resistive modes which are independent of thermal conductivity (and the viscosities) to leading order.

respectively, where $M = \mathbf{e}_z \cdot \mathbf{B} \times (\nabla \times \mathbf{V})$, and all equilibrium quantities are evaluated at z_0.

From Eq. (5.9), we find

$$b_z^{(2)\prime} = \frac{\mathrm{i}G}{B^2} b_\perp^{(1)}. \tag{3.89}$$

Because the zeroth order (in ϵ) component of $(\nabla \cdot \xi)$ vanishes in the layer, we have

$$\xi_z^{(1)\prime} = \frac{\mathrm{i}G}{B^2} \xi_\perp^{(0)}. \tag{3.90}$$

Dotting Eq. (3.84) with $\mathbf{B}$ gives

$$\rho\tilde{\gamma}^2 \xi_B^{(0)} = -(p' + \rho g) b_z^{(1)} + \mathrm{i}F' x [\xi_z^{(1)} p' + \Gamma p (\nabla \cdot \xi)^{(1)}]. \tag{3.91}$$

Finally, the $\mathbf{e}_z$ and $\mathbf{e}_z \times \mathbf{B}$ components of Eq. (3.84) *both* give

$$p' \xi_z^{(1)} + \Gamma p (\nabla \cdot \xi)^{(1)} = \frac{1}{4\pi} b_B^{(1)}, \tag{3.92}$$

to leading order.

Something interesting has happened: we have more unknowns than equations because both of the components of the equation of motion perpendicular to $\mathbf{B}$ give the same information, leading to an underdetermined system. One possible solution would be to keep higher-order terms in the $\mathbf{e}_z$ and $\mathbf{e}_z \times \mathbf{B}$ components of Eq. (3.84), then attempt to algebraically eliminate the dominant information. A second approach, outlined in Ref. [26] is to find a scalar-valued operator which identically annihilates the terms which are dominating in the limit.

Looking at Eq. (3.92), we see that the dominant physics perpendicular to $\mathbf{B}$ is (magnetosonic) force balance. Indeed, if the terms in Eq. (3.92) were competitive with inertia to leading order, then they would dominate the motion, and the resistivity would merely introduce a small correction. To annihilate the magnetosonic forces, we apply the operator $\nabla \cdot (\mathbf{B}/B^2 \times \cdots)$, introduced in Ref [8] to the perturbed equation of motion (3.84). To understand what this annihilator is doing, we apply it to the exact Lorentz force

$$\nabla \cdot \left(\frac{\mathbf{B} \times (\mathbf{J} \times \mathbf{B})}{cB^2} \right) = \mathbf{B} \cdot \nabla \left(\frac{\mathbf{J} \cdot \mathbf{B}}{cB^2} \right) \tag{3.93}$$

where we have used $\nabla \cdot \mathbf{J} = 0$. We see that the annihilator extracts the force density due to parallel currents, i.e. the kink force [12]. In our problem, Eq. (3.92) tells us that, in the plane perpendicular to $\mathbf{B}$, the force due to the current perpendicular to the magnetic field is balanced by the pressure gradient, leaving the kink force to drive the mode.

Applying the annihilator to Eq. (3.84) yields

$$(\tilde{\gamma}^2 \xi_z^{(1)\prime})' = \frac{\mathrm{i}F'x}{4\pi\rho} b_z^{(2)\prime\prime} - \frac{G^2 g}{B^2} \left(\frac{\rho'}{\rho} - \frac{p'}{\Gamma p} \right) \xi_z^{(1)} - \frac{G^2 g}{4\pi\Gamma p B^2} b_B^{(1)}. \tag{3.94}$$

Using Eqs. (3.89)–(3.92) to eliminate $\xi_B^{(0)}$, $\xi_\perp^{(0)}$, $b_\perp^{(1)}$, and $(\nabla \cdot \xi)^{(1)}$, we

obtain

$$\eta b_z^{(2)\prime\prime} = \tilde{\gamma}(b_z^{(2)} - \mathrm{i}F'x\xi_z^{(1)}), \tag{3.95}$$

$$(\tilde{\gamma}^2\xi_z^{(1)\prime})' = \frac{\mathrm{i}F'x}{4\pi\rho}b_z^{(2)\prime\prime} - \frac{G^2 g}{B^2}\left(\frac{1}{\rho}\rho' - \frac{1}{\Gamma p}p'\right)\xi_z^{(1)} - \frac{G^2 g}{4\pi\Gamma p B^2}b_B^{(1)}, \tag{3.96}$$

$$\begin{aligned}\eta b_B^{(1)\prime\prime} = &\left(\tilde{\gamma}\left[1 + \frac{B^2}{4\pi\Gamma p}\right] + \frac{F'^2x^2}{4\pi\rho\tilde{\gamma}}\right)b_B^{(1)} + \left(-M + \frac{\mathrm{i}F'x}{\rho\tilde{\gamma}}(p' + \rho g)\right)b_z^{(2)} \\ &+ \left(\tilde{\gamma}\left[4\pi(p' + \rho g) + B^{2\prime} - \frac{B^2}{\Gamma p}p'\right] + \mathrm{i}MF'x\right)\xi_z^{(1)},\end{aligned} \tag{3.97}$$

where $x = (z - z_0)$, and all equilibrium quantities are evaluated at z_0. Note that if η is dropped from Eqs (3.95), (3.97), then they become algebraic in $b_z^{(2)}$ and $b_B^{(1)}$, yielding the ideal inertial layer equation (3.48) considered previously. In the present case with resistivity included, the variables $b_z^{(2)}$ and $b_B^{(1)}$ can still be eliminated from Eqs. (3.95)–(3.97), but the resulting equation for $\xi_z^{(1)}$ is sixth order. We prefer not to do this since the decoupled equation remains intractable, and the physical meaning of the various terms is less apparent.

Before normalizing these equations, we must incorporate the equilibrium relation (3.9):

$$(B^2)' = -8\pi(p' + \rho g), \tag{3.98}$$

and the Alfven resonance condition (3.39), which gives

$$(m/a)B_x + (n/L)B_y = 0. \tag{3.99}$$

After scaling to reduce the number of apparent parameters, we obtain

$$\Psi'' = \tilde{Q}(\Psi - X\Xi), \tag{3.100}$$

$$\Xi'' = -\frac{2\mathrm{i}\kappa_\parallel}{\tilde{Q}}\Xi' + \left(\frac{X^2}{\tilde{Q}} - \frac{D_g + D_{p'}/(\beta\Gamma)}{\tilde{Q}^2}\right)\Xi - \frac{X}{\tilde{Q}}\Psi + \frac{D_{p'} + D_\rho}{\beta\Gamma}\Upsilon, \tag{3.101}$$

$$\begin{aligned}\Upsilon'' = &\left(\tilde{Q}\left[1 + \frac{2}{\beta\Gamma}\right] + \frac{X^2}{\tilde{Q}}\right)\Upsilon - \left(\frac{X}{\tilde{Q}} + \mathrm{i}\kappa_\perp\right)\Psi \\ &- \left(\left[1 + \frac{D_{p'}}{D_{p'} + D_\rho}\frac{2}{\beta\Gamma}\right]\tilde{Q} - \mathrm{i}\kappa_\perp\right)\Xi.\end{aligned} \tag{3.102}$$

where

$$\begin{aligned} \gamma_\eta &= \eta^{1/3}F'(z_0)^{2/3}/(4\pi\rho)^{1/3}, & \delta_\eta &= \eta^{1/3}(4\pi\rho)^{1/6}/(F'(z_0))^{1/3}, \\ b_z^{(2)} &= \mathrm{i}F'(z_0)^{2/3}\eta^{1/3}(4\pi\rho)^{1/6}\Psi, & \xi_z^{(1)} &= \Xi, \\ b_B^{(1)} &= 4\pi p'(z_0)\Upsilon, & \tilde{Q} &= [\gamma + \mathrm{i}\Omega'(z_0)x]/\gamma_\eta, \\ \beta &= 8\pi p/B^2, & D_{p'} &= \tfrac{16\pi^2k^2\rho g p'}{B^2}. \end{aligned} \tag{3.103}$$

This sixth-order system has six linearly independent solutions which can be characterized by their behavior at large $\pm|X|$. We find

$$\begin{aligned}\Xi \sim &A_1^{(\pm)}|X|^{-\frac{1}{2}+\sqrt{\frac{1}{4}-D_v}} + A_2^{(\pm)}|X|^{-\frac{1}{2}-\sqrt{\frac{1}{4}-D_v}} \\ &+ A_3^{(\pm)}\exp\left[\Lambda_1\left(\mathrm{i}\,|X|\right)^{3/2} - \Pi_1\left(\mathrm{i}\,|X|\right)^{1/2}\right]|X|^{-1/4} \\ &+ A_4^{(\pm)}\exp\left[-\left(\Lambda_1\left(\mathrm{i}\,|X|\right)^{3/2} - \Pi_1\left(\mathrm{i}\,|X|\right)^{1/2}\right)\right]|X|^{-1/4} \\ &+ A_5^{(\pm)}\exp\left[\Lambda_2\left(\mathrm{i}\,|X|\right)^{3/2} - \Pi_2\left(\mathrm{i}\,|X|\right)^{1/2}\right]|X|^{-9/4} \\ &+ A_6^{(\pm)}\exp\left[-\left(\Lambda_2\left(\mathrm{i}\,|X|\right)^{3/2} - \Pi_2\left(\mathrm{i}\,|X|\right)^{1/2}\right)\right]|X|^{-9/4},\end{aligned} \tag{3.104}$$

as $X \to \pm\infty$. Here, we have defined

$$\Lambda_1 = \frac{2}{3}\sqrt{\frac{1-\kappa_\parallel^2}{\kappa_\parallel}}, \tag{3.105}$$

$$\Pi_1 = Q\frac{1+\kappa_\parallel^2}{\kappa_\parallel^{3/2}\sqrt{1-\kappa_\parallel^2}}, \tag{3.106}$$

$$\Lambda_2 = \frac{2}{3}\sqrt{\frac{1-\kappa_\parallel^2-2\kappa_\parallel^2/(\beta\Gamma)}{\kappa_\parallel}}, \tag{3.107}$$

$$\Pi_2 = Q\frac{1+\kappa_\parallel^2+2\kappa_\parallel^2/(\beta\Gamma)}{\kappa_\parallel^{3/2}\sqrt{1-\kappa_\parallel^2-2\kappa_\parallel^2/(\beta\Gamma)}}. \tag{3.108}$$

3.4.3 Asymptotic Matching

The solution of Eqs. (3.100)–(3.102) must be asymptotically matched to $\xi_{z,\mathrm{Out}}^{(0)}$, which implies that the power-law solutions must dominate at large $|X|$. We therefore find

$$A_3^{(+)} = A_4^{(-)} = A_5^{(+)} = A_6^{(-)} = 0. \tag{3.109}$$

In addition, by taking the intermediate limit as in Eqs. (3.55)–(3.56), we obtain

$$A_1^{(\pm)} = a_1^{(\pm)}(\delta_\eta/L)^\nu, \tag{3.110}$$

$$A_2^{(\pm)} = a_2^{(\pm)}(\delta_\eta/L)^{-1-\nu}. \tag{3.111}$$

We can verify that we now have a well-posed problem determining the leading-order asymptotic behavior of γ and ξ_z, inside and outside of the resistive layer, as $\epsilon \to 0+$. There are two arbitrary constants, $\alpha^\pm$, in the solution

$\xi^{(0)}_{z,\mathrm{Out}}$ from the boundary conditions at $z = \pm Z$, and the general solution to the sixth-order system (3.100)–(3.102) contains six arbitrary constants, for a total of eight constants, not including the γ. One of these constants corresponds to an arbitrary overall (nonzero) scale of the eigenfunction. The seven remaining constants, together with γ, are determined by the eight matching conditions (3.109)–(3.111).

3.4.4 Remarks

3.4.4.1 Utility of the Asymptotic Approach

Unfortunately, after all of this work, we still have a system of equations we cannot solve. One may wonder whether all of the approximations which were made in obtaining Eqs. (3.100)–(3.102) were worth the trouble if we have to numerically solve the problem anyway.

For starters, we have already learned that most of the important physics is contained in the resistive layer. Moreover, within the layer, the important dimensionless quantities are D_s, $\kappa_\parallel$, D_ρ, $D_{p'}$, and $\beta\Gamma$. By numerically solving Eqs.(3.100)–(3.102) for various values of these parameters at fixed $a_2^{(\pm)}/a_1^{(\pm)}$, one can quickly map out the stability trends. Without using asymptotics to split the eigenvalue problem into a boundary layer and outer ideal region, one would be forced to numerically solve a rather complicated sixth-order system of ODEs, and try to spot trends while exploring the vast space of arbitrary equilibrium profiles. Our singular limit $\epsilon \to 0+$ highlights–or even exaggerates–contextually relevant features, providing an easily interpretable caricature of

the important physics. In the present case, the context is instabilities which persist within the ideal stability boundary.

There are also practical difficulties associated with direct numerical solution to the general eigenvalue problem when the background profile is close to the stability boundary. In Section 3.2, we saw that the width of the inertial layer is $\mathcal{O}(\gamma)$. Thus a numerical routine will have to self-consistently determine the appropriate highly-nonuniform grid spacing required to capture the salient features of the eigenfunction near $z = z_0$, where the Alfven frequency vanishes.

3.4.4.2 Higher-Order Boundary Layer Theory

Suppose we were able to generate an analytic solution to Eqs. (3.100)–(3.102), and use it to obtain a dispersion relation of the form

$$0 = f(Q, \kappa_\parallel, D_s, a_1^{(\pm)}/a_2^{(\pm)}). \tag{3.112}$$

This would allow us to find the region of parameter space for which the equilibrium is stable with respect to modes whose growth rates vanish like $\gamma = \mathcal{O}(\eta^{1/3})$. This does not mean we have finished with the resistive stability analysis, since we have only computed the leading-order behavior of the growth rate. In general, the growth rate has an asymptotic power series in η. For example, the expansion for γ might be of the form[8]:

$$\gamma \sim \gamma_1 \eta^{1/3} + \gamma_2 \eta^{2/5} \cdots + \gamma_n \eta. \tag{3.113}$$

[8]In this example, we can truncate the expansion at the $n-1$ term, since the correction $\gamma_n \eta$ is indistinguishable from the resistive diffusion of the background.

Of course, we don't know the exponents of the remaining terms a priori, but it is possible that the second term in the series has an exponent less than one, meaning it is still fast compared to the background resistive diffusion. Within the formalism of asymptotics, the second term in the series is infinitesimally small compared to the first. However, we are using an asymptotic *expansion* about $\eta = 0$ to generate a numerical *approximation* for nonzero η. As an approximation, small $|\gamma_1|$ can make the leading behavior competitive with the next term in the series. Similarly, when γ_2 happens to be numerically large, the second term in the series can lead to net instability.

The equations governing the next term in the asymptotic series for γ and ξ_z will have the same form as Eqs. (3.95)–(3.97) within the layer, and Eq. (3.37) in the outer region, only they will have inhomogeneous source terms involving the lowest order quantities, and new constants, involving higher derivatives of the equilibrium quantities at z_0. For example, Eq. (3.92) will become

$$p'\xi_z^{(2)} + \Gamma p(\nabla \cdot \xi)^{(2)} - \frac{1}{4\pi} b_B^{(2)} = \frac{\mathbf{J} \cdot \mathbf{B}}{c} b_z^{(2)} - \rho(\tilde{\gamma}^{(1)})^2 \xi_\perp^{(0)} - \frac{\mathrm{i} F' x}{4\pi} b_\perp^{(1)}, \quad (3.114)$$

where all of the terms on the right-hand side are known from the leading-order solution.

In principle, we would like to have all of the terms in the series which lead to corrections in the growth rate which are $o(\eta)$. In general, the higher-order terms in the asymptotic series for the eigenfunction will also have a boundary layer at z_0, and the width of the width of the layer will tend to

increase.

An alternative approach to carrying out the series to higher order would be to impose an auxiliary ordering from the start. If we had some way of knowing that the series for γ had the form given in Eq. (3.113), and additionally, we are able to arrange the ϵ dependence so that $\gamma_1 = \mathcal{O}(\epsilon^{1/15})$ (perhaps by ordering g), then the first two terms of Eq. (3.113) would both be generated in the leading-order calculation. This approach will be implemented in Chapter 4.

Finally, we note that as we study progressively slower instabilities, the equations which need to be solved tend to get more complicated, because a larger number of terms contribute. In the next section we will find a very interesting exception to this rule.

3.4.5 Dispersion Relation in the Static, Incompressible Limit

It is worthwhile to study the solution to the resistive layer equations in the limit $\kappa_\parallel = 0$, and $\beta\Gamma \to \infty$. In this case, Eqs. (3.100)-(3.101) become a fourth-order autonomous subsystem:

$$\Psi'' = Q(\Psi - X\Xi), \tag{3.115}$$

$$\Xi'' = -\frac{X}{Q}\Psi + \left(\frac{X^2}{Q} - \frac{D_g}{Q^2}\right)\Xi. \tag{3.116}$$

These equations can be solved exactly [24] by Fourier transforming

$$\Xi = \int_{-\infty}^{\infty} \frac{\mathrm{d}\mu}{2\pi} \mathrm{e}^{\mathrm{i}\mu X} \zeta(\mu), \tag{3.117}$$

and assuming a solution of the form

$$\zeta(\mu) = \mu^{\nu} \mathrm{e}^{-Q^{1/2}\mu^2/2} \sum_{j=0}^{n} \alpha_j \mu^{2j}, \tag{3.118}$$

with $\nu = -1/2 + \sqrt{1/4 - D_g}$.

The resulting dispersion relation is

$$Q^{3/2} = \frac{D_g}{\nu + 2n + 1/2 + \sqrt{4\nu n + (2n + 1/2)^2}}. \tag{3.119}$$

Here n is a positive integer, and it has been assumed that $D_g > 0$. This infinite sequence of unstable modes is analogous to behavior of the ideal dispersion relation (3.73) when $D_g > 1/4$. Thus we conclude that the resistive stability boundary is $D_g > 0$.

Examining the small-μ behavior of ζ given in Eq. (3.118), we find

$$\zeta \sim \alpha_0 \mu^{\nu}. \tag{3.120}$$

This corresponds to a large-$|X|$ behavior of Ξ given by

$$\Xi \sim \alpha_0 \sqrt{\frac{2}{\pi}} \Gamma(1 + \nu) \mathrm{e}^{\mathrm{i}\pi/2(\nu+1)} |X|^{-1-\nu}, \tag{3.121}$$

as $X \to \pm\infty$. Comparing with Eq. (3.104), we see that the solutions we have obtained satisfy the special boundary conditions

$$A_1^{(\pm)}/A_2^{(\pm)} = 0, \tag{3.122}$$

$$A_2^{(+)} = A_2^{(-)} = \alpha_0 \sqrt{\frac{2}{\pi}} \Gamma(1 + \nu) \mathrm{e}^{\mathrm{i}\pi(1+\nu)/2}. \tag{3.123}$$

.

For given values of $a_2^{(\pm)}/a_1^{(\pm)}$, which are determined by the equilibrium profile outside of the layer, the solution to Eqs. (3.115)–(3.116) must satisfy

$$\frac{A_1^{(\pm)}}{A_2^{(\pm)}} = \frac{a_1^{(\pm)}}{a_2^{(\pm)}} \left(\frac{\eta^{1/3}(4\pi\rho)^{1/6}}{F'^{1/3} L_{\mathrm{Out}}} \right)^{2\nu+1} . \tag{3.124}$$

In the limit $\eta \to 0$, Eq. (3.124) reduces to Eq. (3.122). Thus, when the resistivity gets very small, the $a_2^{(\pm)}/a_1^{(\pm)}$-dependence vanishes, and the general dispersion relation reduces to Eq. (3.119).

Though we are not able to solve Eqs. (3.115)–(3.116) for arbitrary matching conditions (3.124), the special solutions we have found possess several interesting features. For one thing, the growth rate is completely independent of the equilibrium profile outside of the layer. This is in contrast to the expression (3.70) for the ideal instabilities considered previously, where the growth rates vanish for $a_1^{(\pm)}/a_2^{(\pm)} \to 0$.

Second, the boundary conditions (3.123) are even in Ξ, and the layer equations (3.115)–(3.116) conserve parity, implying the solutions we have found must be even in configuration space. Looking back to Eqs. (3.95)–(3.97), we see that with velocity shear included, the layer equations no longer possess parity-invariant solutions. From an analytical perspective, this loss of parity symmetry makes the layer equations much more difficult to solve. For example, the use of Fourier transform no longer reduces the order of the layer equations.

Chapter 4

Tearing Modes in Slab Geometry

In the last chapter, we were able to find a family of special solutions to the incompressible, static resistive layer equations (3.115)–(3.116) corresponding to the homogeneous boundary conditions

$$A_1^{(\pm)}/A_2^{(\pm)} = 0. \tag{4.1}$$

We showed that this special case of boundary conditions can be interpreted as the limiting behavior[1] $\eta \to 0$, or, for nonzero η, $a_1^{(\pm)}/a_2^{(\pm)} \to 0$. Finally, we noted that these particular solutions were even in Ξ. In this chapter, we will find modes which are driven by $a_1^{(\pm)}/a_2^{(\pm)}$, and we will find that these modes have odd parity in Ξ.

Treating η as a small parameter,

$$\eta \to \epsilon\eta \tag{4.2}$$

[1]We also noted that the ordering leading to Eqs. (3.115)–(3.116) is equivalent to considering the small-η limit of linear resistive instabilities, so taking the small-η limit of the boundary conditions (3.124) is consistent with our practice of only keeping leading-order terms. So, in addition to our inability to calculate the dispersion relation for arbitrary $a_1^{(\pm)}/a_2^{(\pm)} \neq 0$, another good reason for excluding these terms is they are expected to be small in comparison to the D_g-dependent terms given in Eq. (3.116), which produce an instability for $D_g > 0$.

we find that the effects of the equilibrium profile outside the layer produce a higher-order effect on the growth rate than the interchange parameter D_g. Within the domain of self-consistency of our ordering, the influence of nonzero $a_1^{(\pm)}/a_2^{(\pm)}$ is significant only when the destabilizing forces within the layer are small enough to be competitive with the boundary conditions in determining stability.[2] We will thus scale the leading behavior of γ so that the constants $a_1^{(\pm)}/a_2^{(\pm)}$ contribute to leading order.

4.1 Boundary Layer Within a Boundary Layer

We wish to consider the small-D_g limiting behavior of the solution to Eqs. (3.115)–(3.116), with boundary conditions

$$\Xi \sim A_2^{(\pm)} \left(|X|^{-\frac{1}{2}-\sqrt{\frac{1}{4}-D_g}} + \frac{a_1^{(\pm)}}{a_2^{(\pm)}} \left(\frac{\epsilon^{1/3}\delta_\eta}{L_{\rm Out}} \right)^{\sqrt{1-4D_g}} |X|^{-\frac{1}{2}+\sqrt{\frac{1}{4}-D_g}} \right), \tag{4.3}$$

$$\Psi \sim X\Xi, \tag{4.4}$$

as $X \to \pm\infty$. According to Eq. (3.119), we must also take Q to be small so that $D_g \to 0$, $Q \to 0$, while $D_g/Q^{3/2} =$ constant. We thus consider the auxiliary ordering

$$D_g \to \hat{\epsilon}^3 D_g, \quad Q \to \hat{\epsilon}^2 Q. \tag{4.5}$$

[2] In general, it is also possible to be near the stability boundary with $D_g \approx 1$ and $a_1^{(\pm)}/a_2^{(\pm)}$ large–say $\mathcal{O}(\epsilon^{-1/3})$–but this would require a solution to Eqs. (3.115)–(3.116) with inhomogeneous boundary conditions, which does not appear to be analytically tractable.

With the ordering (4.5), Eqs. (3.115)–(3.116) become

$$\Psi'' = \hat{\epsilon}^2 Q(\Psi - X\Xi), \tag{4.6}$$

$$\hat{\epsilon}^2 \Xi'' = -\frac{X}{Q}\Psi + \left(\frac{X^2}{Q} - \frac{D_g}{\hat{\epsilon} Q^2}\right)\Xi. \tag{4.7}$$

The matching solution will have the asymptotic behavior

$$\Xi \sim A_2^{(\pm)} \left(|X|^{-\frac{1}{2}-\sqrt{\frac{1}{4}-\hat{\epsilon}^3 D_g}} + \frac{a_1^{(\pm)}}{a_2^{(\pm)}} \left(\frac{\epsilon^{1/3}\delta_\eta}{L_{\text{Out}}}\right)^{\sqrt{1-4\hat{\epsilon}^3 D_g}} |X|^{-\frac{1}{2}+\sqrt{\frac{1}{4}-\hat{\epsilon}^3 D_g}} \right), \tag{4.8}$$

$$\Psi \sim X\Xi, \tag{4.9}$$

as $X \to \pm\infty$. Thus, the eigenfunctions and growth rates are functions of both ϵ and $\hat{\epsilon}$, and we will look for an asymptotic solution in the limit $\epsilon \to 0+$, $\hat{\epsilon} \to 0+$.

The general solution of Eqs. (4.3)–(4.4) at large $|X|$ is

$$\begin{aligned} \Xi \sim & A_1^{(\pm)} |X|^{-\frac{1}{2}+\sqrt{\frac{1}{4}-\hat{\epsilon}^3 D_g}} + A_2^{(\pm)} |X|^{-\frac{1}{2}-\sqrt{\frac{1}{4}-\hat{\epsilon}^3 D_g}} \\ & + A_3^{(\pm)} \exp\left[|X|^2/(\hat{\epsilon}\sqrt{Q})\right] |X|^{\frac{1}{2}\left(-D_g/Q^{3/2}-1+\hat{\epsilon}^3 Q^{3/2}\right)} \\ & + A_4^{(\pm)} \exp\left[-|X|^2/(\hat{\epsilon}\sqrt{Q})\right] |X|^{\frac{1}{2}\left(D_g/Q^{3/2}-1-\hat{\epsilon}^3 Q^{3/2}\right)}. \end{aligned} \tag{4.10}$$

Comparing this to Eqs. (4.8)–(4.9), we find the matching conditions

$$A_3^{(\pm)} = 0, \tag{4.11}$$

$$\frac{A_1^{(\pm)}}{A_2^{(\pm)}} = \frac{a_1^{(\pm)}}{a_2^{(\pm)}} \left(\frac{\epsilon^{1/3}\delta_\eta}{L_{\text{Out}}}\right)^{\sqrt{1-4\hat{\epsilon}^3 D_g}}. \tag{4.12}$$

By dropping the term $\hat{\epsilon}^2\Xi''$ in Eq. (4.7), the order of the equation is reduced, and we therefore expect a boundary layer to be produced in the limit.

This is analogous to the boundary layer that was produced in Section 3.3.1 by considering the limit of marginal stability. Here we have a boundary-layer structure emerge within a boundary layer. This makes the matching more complicated, while simplifying the equations.

With the auxiliary ordering (4.5), self-consistency requires us to keep an additional term in the annihilated equation of motion. In the incompressible, no shear limit, Eq. (3.94) becomes

$$\hat{\epsilon}^4\gamma^2\xi_z^{(1)\prime\prime} = \frac{\mathrm{i}F'x}{4\pi\rho}b_z^{(2)\prime\prime} - \hat{\epsilon}^3\frac{G^2g}{B^2}\frac{\rho'}{\rho}\xi_z^{(1)} + \epsilon^{1/3}\left(\frac{\mathbf{J}\cdot\mathbf{B}}{cB^2}\right)'b_z^{(2)}. \tag{4.13}$$

This leads to an additional constant in the normalized layer equations:

$$\Psi'' = \hat{\epsilon}^2Q(\Psi - X\Xi), \tag{4.14}$$

$$\hat{\epsilon}^2\Xi'' = -\frac{X}{Q}\Psi + \left(\frac{X^2}{Q} - \hat{\epsilon}\frac{D_g}{Q^2}\right)\Xi + \frac{\epsilon^{1/3}}{\hat{\epsilon}^2}\frac{\delta_\eta}{L_{\mathrm{Out}}}\frac{J_p}{Q^2}\Psi, \tag{4.15}$$

where

$$J_p = \frac{4\pi L_{\mathrm{Out}}G}{F'}\left(\frac{\mathbf{J}\cdot\mathbf{B}}{cB^2}\right)'. \tag{4.16}$$

The limit $\hat{\epsilon} \to 0+$ still produces a boundary layer at $X = 0$, but the ordering is now self-consistent[3].

[3]With the auxiliary ordering, an additional term proportional to J_p must also be kept in the outer equations for $\xi_{z,\mathrm{Out}}^{(0)}$.

4.1.1 Outer Limit of Resistive Layer Equations

The outer limit of Eqs. (4.14)–(4.15) is

$$\Psi''_{\text{Out}} = 0, \tag{4.17}$$

$$\Xi_{\text{Out}} = \Psi_{\text{Out}} \left(\frac{1}{X} + \frac{J_p}{QX^2} \right), \tag{4.18}$$

which contains a one-term dominant balance. This is only self-consistent if Eq. (4.17) is interpreted as an equation, which is more restrictive than an asymptotic relation.[4]

The general solution to Eqs. (4.17)–(4.18) is

$$\Psi_{\text{Out}} = \Psi_0 + \Psi_1 X, \tag{4.19}$$

$$\Xi_{\text{Out}} = (\Psi_0 + \Psi_1 X) \left(\frac{1}{X} + \frac{J_p}{QX^2} \right), \tag{4.20}$$

giving the large-$|X|$ asymptotic behavior

$$\Xi_{\text{Out}} \sim \pm \frac{\Psi_0}{|X|} + \Psi_1. \tag{4.21}$$

From Eq. (4.12), leading-order matching conditions are

$$\frac{A_1^{(\pm)}}{A_2^{(\pm)}} = \frac{a_1^{(\pm)}}{a_2^{(\pm)}} \left(\frac{\epsilon^{1/3} \delta_\eta}{L_{\text{Out}}} \right)^{1+o(\hat{\epsilon}^3 D_s)}, \tag{4.22}$$

where, in the auxiliary limit considered,

$$A_1^{(\pm)} = \Psi_1, \tag{4.23}$$

$$A_2^{(\pm)} = \pm \Psi_0. \tag{4.24}$$

[4]This means that there cannot be Stokes wedges; Ψ must have the same asymptotic behavior as $X \to \infty$ from any direction.

To leading order in $\hat{\epsilon}$, the boundary conditions (4.22) give

$$\Psi_1/\Psi_0 = 0. \tag{4.25}$$

This tells us that to leading order, Ψ is a constant in the outer layer. Since Ψ does not develop a boundary layer in the auxiliary limit, Ψ is a constant across the layer:

$$\Psi = \Psi_0 + o(\hat{\epsilon}^2 D_g) \tag{4.26}$$

With this result, the auxiliary ordering (4.5) is usually referred to as the *constant-Ψ approximation.*

4.1.2 Layer Limit of Resistive Layer Equations

The ordering assumption which led to Eqs. (4.17)–(4.18) is valid as long as

$$\hat{\epsilon^2}\Xi'' \ll X^2\Xi/Q. \tag{4.27}$$

Using the outer solution (4.20), one can verify that this ordering breaks down for $|X|^4 \approx \hat{\epsilon}^2 Q$. We therefore introduce a new stretched variable[5]

$$\xi = \frac{X}{\hat{\epsilon}^{1/2} Q^{1/4}}, \tag{4.28}$$

and define

$$\Phi = \frac{\epsilon^{1/2} Q^{1/4}}{\Psi_0}\Xi. \tag{4.29}$$

[5]The stretched variable ξ is not to be confused with the displacement vector $\boldsymbol{\xi}$.

The layer equations (4.6)–(4.7) become

$$\Psi'' = \hat{\epsilon}^3 Q^{3/2} \Psi_0 (1 - \xi\Phi), \tag{4.30}$$

$$\Phi'' = -\xi + \left(\xi^2 - \frac{D_g}{Q^{3/2}}\right)\Phi + \frac{\epsilon^{1/2} J_p}{\hat{\epsilon}^{5/2} Q^{5/4}}. \tag{4.31}$$

Note that Eq. (4.31) has also become an autonomous subsystem in the limit. We can obtain a dispersion relation by solving Eq. (4.31) for Φ, substituting the solution into Eq. (4.30), and then integrating this equation from $-\infty$ to ∞, which gives

$$\bar{\Delta}' = \Delta, \tag{4.32}$$

where we have defined

$$\Delta = \hat{\epsilon}^3 Q^{3/2} \int_{-\infty}^{\infty} (1 - \xi\Phi)\, \mathrm{d}\xi, \tag{4.33}$$

$$\bar{\Delta}' = \lim_{|\xi|\to\infty} \left[\Psi'(\xi = |\xi|) - \Psi'(\xi = -|\xi|)\right] / \Psi_0. \tag{4.34}$$

From Eqs. (4.3), (4.4), with the ordering (4.5) we find

$$\bar{\Delta}' = \frac{1}{\Psi_0}\left[A_2^{(+)} \frac{a_2^{(+)}}{a_1^{(+)}} - A_2^{(-)} \frac{a_2^{(-)}}{a_1^{(-)}}\right] \left(\epsilon^{1/3} \frac{\delta_\eta}{L_{\mathrm{Out}}}\right) \frac{\mathrm{d}X}{\mathrm{d}\xi} \tag{4.35}$$

$$= \left[\frac{a_2^{(+)}}{a_1^{(+)}} + \frac{a_2^{(-)}}{a_1^{(-)}}\right] \left(\epsilon^{1/3} \frac{\delta_\eta}{L_{\mathrm{Out}}}\right) \hat{\epsilon}^{1/2} Q^{1/4} \tag{4.36}$$

$$= \Delta' \left(\epsilon^{1/3} \frac{\delta_\eta}{L_{\mathrm{Out}}}\right) \hat{\epsilon}^{1/2} Q^{1/4}. \tag{4.37}$$

4.1.3 Remarks

This ordering and subsequent calculation has many interesting features. First, in the outer limit, Eq. (4.17) became a trivial autonomous subsystem.

This allowed us to solve for Ψ, and treat it as a known source in Eq. (4.18). A second interesting feature is the leading order behavior of Ψ does not develop a boundary layer, while, in the auxiliary limit, both Ξ and $\Psi - \Psi_0$ do. Once the known $\Psi = \Psi_0$ is substituted into Eq. (4.18), we can solve for Ξ directly, without having to separately solve inner and outer equations, and asymptotically matching the solutions.

Being able to solve Eq. (4.31) also allowed us to avoid resolving the relative size of $\epsilon^{1/2}\hat{\epsilon}^{-5/2}$; maximal complication instructs us to keep it (if possible), which is equivalent to assuming this term is order unity. In fact, had we assumed $\hat{\epsilon}^5 = \epsilon$ from the start, we would obtain Eqs. (4.30)–(4.31) directly, rather than Eqs. (3.115)–(3.116). We will employ this more complicated ordering in Chapter 6.

In general, analysis of slower fluid motions is more complicated, primarily because more terms in the governing equations contribute substantially. For example, we saw in the previous chapter that the ideal-MHD inertial layer equation was much simpler than the resistive layer equations. By considering even slower motions in this chapter, the limit is complicated but the resulting equations are simple.

4.2 Dispersion Relation in the Incompressible Static Limit

Note that Eq. (4.31) is an inhomogeneous quantum harmonic oscillator equation. This motivates a trial solution of the form

$$\Phi = \mathrm{e}^{-\xi^2/2} \sum_{n=0}^{\infty} a_n H_n(\xi). \tag{4.38}$$

The solution breaks into even and odd parts

$$\Phi = \Phi^{(+)} + \Phi^{(-)}, \tag{4.39}$$

with $\Phi^{(+)} \propto J_p$. However, only $\Phi^{(-)}$ contributes to Δ, so the dispersion relation is independent of J_p. In Chapter 6, we will see that by including velocity shear—which breaks the parity symmetry of the equations—both the even and odd components of Φ will contribute to the dispersion relation. In the present case, J_p alters the shape of the mode without affecting the growth rate.

The details of the calculation follow the same procedure employed in Appendix B to solve a more complicated version of the same equations. The resulting dispersion relation is

$$\Delta' = \left(\frac{\delta_\eta}{L_{\mathrm{Out}}}\right) 2\pi Q^{5/4} \frac{\Gamma\left[\frac{1}{4}(3 - D_g/Q^{3/2})\right]}{\Gamma\left[\frac{1}{4}(1 - D_g/Q^{3/2})\right]}. \tag{4.40}$$

4.2.1 Analysis of Dispersion Relation

Before using Eq. (4.40) to study the effects of Δ', we look at the special case $\Delta' = 0$. The right side of Eq. (4.40) will be zero when the denominator

goes to infinity. The function $\Gamma(z)$ has simple poles at $z = 0, -1, \cdots$, leading to an infinite set of roots

$$\frac{1}{4}(1 - D_g/Q_n^{3/2}) = -n, \tag{4.41}$$

for $n \in \mathbb{N}$. Comparing Eq. (4.41) to the small-D_g limiting behavior of Eq. (3.119), we see that we have recovered the modes considered in Section 3.4.5. Looking back at the integral Δ, we again see that these modes must be even in Ξ.

A second simple case to consider is $D_g = 0$, i.e. no gravity. In this case, the dispersion relation is

$$\Delta' = \left(\frac{\delta_\eta}{L_{\text{Out}}}\right) 2\pi Q^{5/4} \frac{\Gamma(3/4)}{\Gamma(1/4)} \tag{4.42}$$

yielding one root

$$Q = \left(\Delta' \frac{L_{\text{Out}}\Gamma(1/4)}{\delta_\eta 2\pi\Gamma(3/4)}\right)^{4/5}. \tag{4.43}$$

Eq. (4.32) tells us that the associated mode must be odd. This instability is called a *tearing mode*, and was first considered in Ref. [14]. This mode is driven by forces outside of the layer, and we see that, without gravity, the tearing stability criterion is $\Delta' < 0$. For this reason, Δ' is called the *tearing stability index*. Returning to dimensioned variables, Eq. (4.43) implies that $\gamma = \mathcal{O}(\eta^{3/5})$.

A third interesting case to consider is an equilibrium which is locally gravitationally stable with destabilizing forces outside the layer. We follow the approach of Ref. [16] and employ a Nyquist plot, using Eq. (4.40) as a

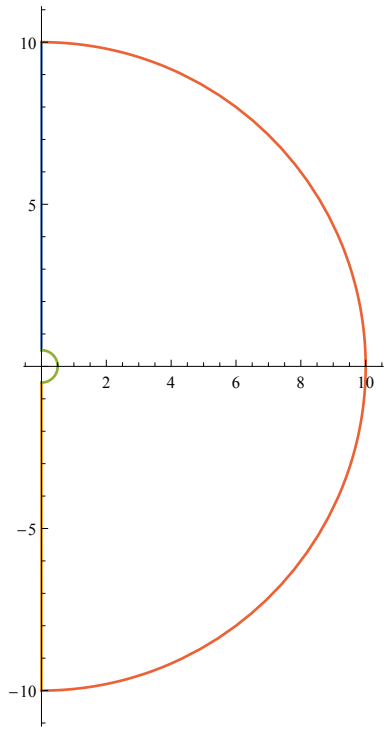

Figure 4.1: The contour C_Q in the complex Q plane.

conformal map from the Q plane to the Δ' plane. In particular, we define the contour C_Q, shown in Figure 4.2.1, which encircles the unstable half of the Q-plane. The image of C_Q under the map (4.40) is shown in Fig. 4.2.1, for the case $D_g < 0$. From Figure 4.2.1, we see that for $D_g < 0$, the critical value $\Delta'_{\text{crit.}} = 0$ is again sufficient for instability.

In contrast, when the analogous interchange parameter is negative in cylindrical geometry, there is a stabilizing effect. Jumping ahead, we show the Nyquist plot for the constant-Ψ dispersion relation in cylindrical geometry in Figure 4.2.1. The analogous interchange parameter, D_s, is negative, meaning

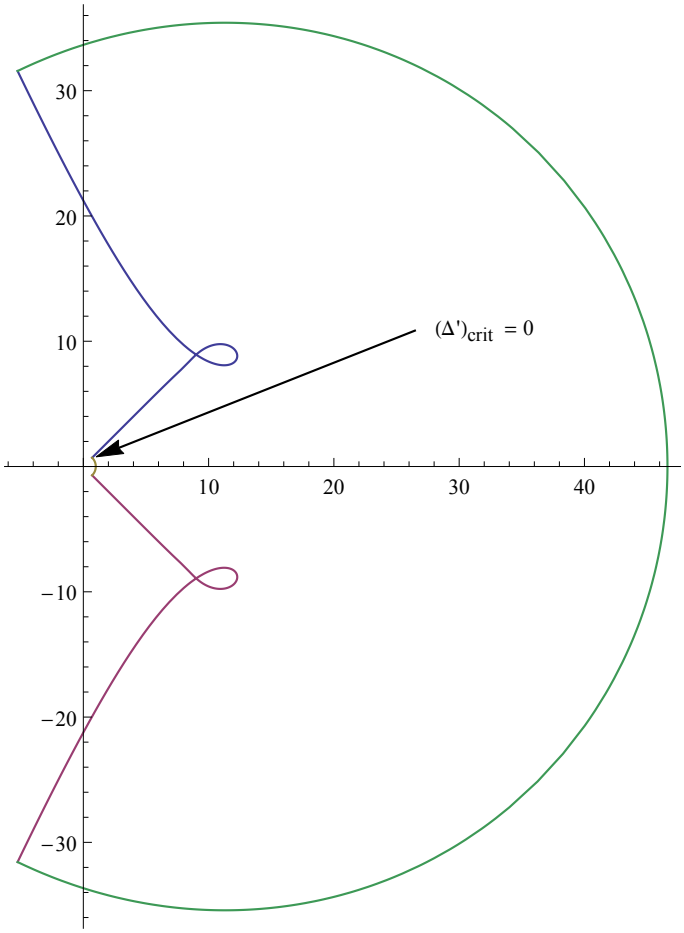

Figure 4.2: The image of the contour C_Q in the complex Δ' plane, with $D_g = -5$.

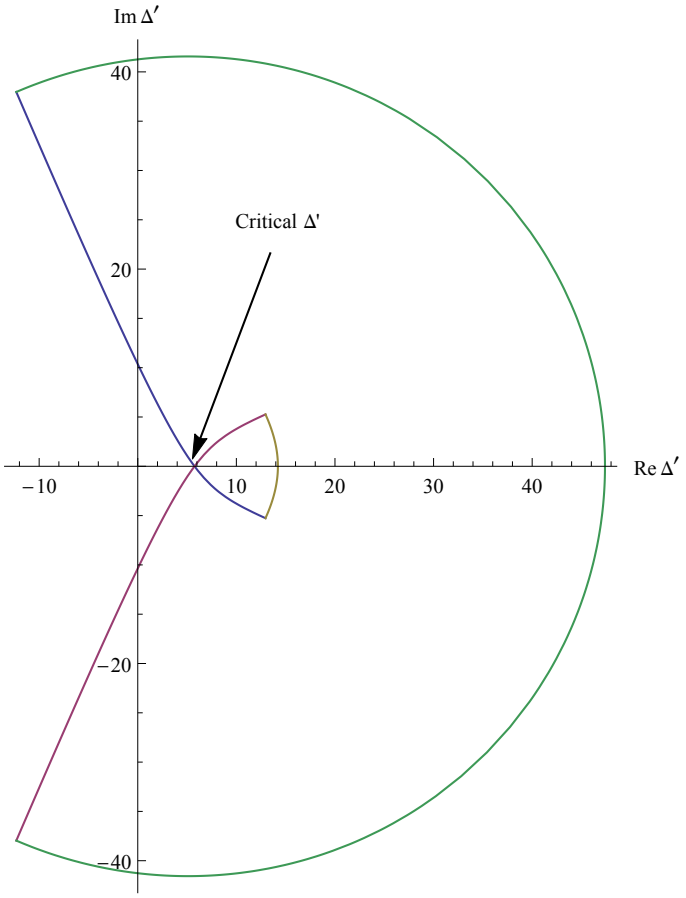

Figure 4.3: The image of the contour C_Q in the complex Δ' plane for cylindrical geometry with $D_s = -5$.

the equilibrium is locally stabilizing with respect to interchange modes. In this case, there is a positive threshold value, Δ'_{crit}, of the tearing stability index required for instability. The stabilizing effect near the rational surface is called the *Glasser effect*. From the Nyquist plot, we see that there are two values $Q_{\text{crit.1,2}}$ on the contour C_Q which cross at $\Delta'_{\text{crit.}}$, and for $D_g < 0$, these growth rates are purely imaginary complex conjugates. We will use this fact in Section 6.1.3 to find an expression for Δ'_{crit}.

Roughly speaking, the Glasser effect expresses the fact that the magnetic curvature is locally stabilizing with respect to the tearing mode, and must be compensated for by a sufficiently large gain in free energy outside of the layer. Interestingly, this effect is not present in the slab model.

Chapter 5

Localized Instabilities in Straight Tokamak Geometry

In the previous chapters, we have demonstrated the techniques used in the analysis of marginal ideal and resistive modes. We now upgrade our model to cylindrical equilibria with periodicity along the axis of symmetry. We will find that gravity plays the same role as curvature in the ideal stability calculation, though as we saw previously, the Glasser effect is not present in the slab model. Our primary objective is to study the effect of velocity shear and rotation on the stability of tearing modes. This will be taken up in the next chapter. Here, we will derive the general resistive layer equations. With shear and rotation included, the resistive interchange layer equations will help us determine the proper auxiliary ordering for the constant-Ψ approximation.

For cylindrical equilibria parameterized with standard (r, θ, z) cylindrical coordinates, the profile is specified by six scalar functions

$$\rho = \rho(r), \tag{5.1}$$

$$p = p(r), \tag{5.2}$$

$$\mathbf{V} = V_\theta(r)\mathbf{e}_\theta + V_z(r)\mathbf{e}_z, \tag{5.3}$$

$$\mathbf{B} = B_\theta(r)\mathbf{e}_\theta + B_z(r)\mathbf{e}_z, \tag{5.4}$$

and the equilibrium equations (2.18)–(2.21) reduce to the single relation

$$\frac{\mathrm{d}\,p}{\mathrm{d}\,r} - \frac{\rho V_\theta^2}{r} = -\frac{B_\theta^2}{4\pi r} - \frac{\mathrm{d}}{\mathrm{d}\,r}\left(\frac{B^2}{8\pi}\right). \tag{5.5}$$

For all perturbations away from equilibrium, we impose periodicity along z with period L, making our model problem topologically toroidal.

With the background equilibrium profile independent of θ, z, and t, we express all perturbed quantities in the form

$$\delta f \propto \exp\left(\mathrm{i}\,\mathbf{k}\cdot\mathbf{r} + [\gamma - \mathrm{i}\,\mathbf{k}\cdot\mathbf{V}(a)]t\right), \tag{5.6}$$

where $\mathbf{k} = (m/r)\mathbf{e}_\theta + (n/L)\mathbf{e}_z$. The integers m and n are the poloidal and toroidal mode numbers, respectively. The linearized equations (2.45)–(2.49) for cylindrical equilibria become:

$$\begin{aligned}
\rho\tilde{\gamma}^2\boldsymbol{\xi} =& F(\boldsymbol{\xi},\mathbf{b}) - 2\mathrm{i}\,\tilde{\gamma}(V_\theta/r)\mathbf{e}_z\times\boldsymbol{\xi} \\
&- \left[(\rho V_\theta^2/r)\boldsymbol{\nabla}\cdot\boldsymbol{\xi} + r\xi_r(\rho V_\theta^2/r^2)'\right]\mathbf{e}_r, && (5.7)\\
\tilde{\gamma}[\mathbf{b} - \boldsymbol{\nabla}\times(\boldsymbol{\xi}\times\mathbf{B})] =& ([\mathbf{b} - \boldsymbol{\nabla}\times(\boldsymbol{\xi}\times\mathbf{B})]\cdot\boldsymbol{\nabla})\mathbf{V} + \eta\nabla^2\mathbf{b}, && (5.8)\\
\boldsymbol{\nabla}\cdot\mathbf{b} =& 0, && (5.9)
\end{aligned}$$

with

$$\begin{aligned}
\mathbf{F}(\boldsymbol{\xi},\mathbf{b}) =& (1/4\pi)\left[(\boldsymbol{\nabla}\times\mathbf{b})\times\mathbf{B} + (\boldsymbol{\nabla}\times\mathbf{B})\times\mathbf{b}\right] + \boldsymbol{\nabla}(\xi_r p' + \Gamma p\boldsymbol{\nabla}\cdot\boldsymbol{\xi}),\\
\tilde{\gamma}(r) =& \gamma + \mathrm{i}\,\Omega(r), && (5.10)\\
\Omega(r) =& \mathbf{k}\cdot[\mathbf{V}(r) - \mathbf{V}(a)]. && (5.11)
\end{aligned}$$

In Eq. (5.7), we have used the simplified form of the inertial terms given in Ref. [3].

5.1 Ideal Stability

Over most of the domain, resistivity and inertia can be neglected, so that the leading-order behavior of a resistive mode satisfies the linearized, marginally-stable, ideal-MHD equations. These equations reduce to a single equation for $\xi_r = \mathbf{e}_r \cdot \boldsymbol{\xi}$, derived in Ref. [3]:

$$\frac{\mathrm{d}}{\mathrm{d}\, r}\left[A(r)\frac{\mathrm{d}(r\xi_r)}{\mathrm{d}\, r}\right] + C(r)(r\xi_r) = 0, \tag{5.12}$$

where

$$A(r) \propto (\mathbf{k}\cdot\mathbf{B})^4. \tag{5.13}$$

This equation has a singularity at $r = a$ where $F = \mathbf{k}\cdot\mathbf{B} = 0$. The assumed ordering of the resistive and inertial terms breaks down in a neighborhood of this point, and an internal boundary layer is formed in the $\eta \to 0$, $\gamma \to 0$ limit.

As $r \to a\pm$, the solution to Eq. (5.12) has the asymptotic behavior

$$\xi_r(r = a(1 \pm |x|)) \sim a_1^{\pm}|x|^h + a_2^{\pm}|x|^{-1-h}, \tag{5.14}$$

with

$$h = \frac{1}{2}\left[\sqrt{1 - 4D_v} - 1\right]. \tag{5.15}$$

The limiting expressions for each component of $\mathbf{b}$ and $\boldsymbol{\xi}$ (in a field-line projection basis) can be expressed in terms of ξ_r:

$$\begin{array}{lll} \mathbf{e}_r\cdot\mathbf{b} \propto (r-a)\xi_r, & \mathbf{B}\cdot\mathbf{b} \propto \xi_r, & (\mathbf{e}_r\times\mathbf{B})\cdot\mathbf{b} \propto [(r-a)\xi_r]', \\ (\boldsymbol{\nabla}\cdot\boldsymbol{\xi}) \propto \xi_r, & \mathbf{B}\cdot\boldsymbol{\xi} \propto \xi_r/(r-a), & (\mathbf{e}_r\times\mathbf{B})\cdot\boldsymbol{\xi} \propto \xi_r'. \end{array} \tag{5.16}$$

as $r \to a\pm$. The relations (5.16) together with Eq. (5.14) can be used to find the relative ordering of the layer variables by demanding consistency in the intermediate region.

The general expression for D_v is

$$D_v = \frac{\kappa_g + D_s\left(1+\frac{\kappa_\theta^2}{\beta\Gamma}+\frac{\kappa_\theta}{\kappa_\parallel}\right) - C_\Upsilon \frac{D_s\kappa_\theta}{\kappa_\parallel}\left(1+\frac{S^2\kappa_\theta^2}{2D_s}\right)}{1-\kappa_\parallel^2}, \tag{5.17}$$

with

$$\begin{aligned}
&\beta = (8\pi p/B^2), && \Omega = \mathbf{k}\cdot\mathbf{V},\\
&\kappa_\parallel = \tfrac{\sqrt{4\pi\rho}\Omega'}{F'}, && D_s = -\tfrac{8\pi n^2 p'}{aL^2F'^2},\\
&\kappa_\perp = \tfrac{4n^2\sqrt{\pi\rho}\left[B_\theta\left(V_\theta'+\frac{V_\theta}{a}\right)+B_zV_z'\right]}{aL^2F'^2}, && \kappa_\theta = \tfrac{\sqrt{4\pi\rho}V_\theta}{B_\theta},\\
&S = \tfrac{2B_\theta n}{LaF'} && C_\Upsilon = \tfrac{(1-\kappa_\parallel^2)\left(1+\frac{S^2\kappa_\theta^2}{2D_s}\right)-\frac{S^2\kappa_\parallel\kappa_\theta}{D_s}+\kappa_\parallel^2\left[S^2/D_s-2/(\beta\Gamma)\right]}{1-\kappa_\parallel^2(1+2/(\beta\Gamma))},\\
&\kappa_s = \tfrac{\rho V_\theta^2}{a}\tfrac{4\pi n^2B^2}{L^2F'^2B_\theta^2}\left(\tfrac{p'}{\Gamma p}-\tfrac{\rho'}{\rho}\right), && \kappa_g = \kappa_s + \kappa_\theta\left(2S^2\kappa_\theta - \kappa_\perp - 2S\kappa_\parallel B_z/B_\theta\right).
\end{aligned} \tag{5.18}$$

As in Section 3.3.2, when the exponents in Eq. (5.14) are complex, there are localized unstable modes.

5.1.0.1 Small Velocity Limit

The parameter D_v depends on V_θ, V_θ', and V_z' through the dimensionless quantities κ_s, κ_θ, $\kappa_\parallel$, and $\kappa_\perp$. These parameters are small when the characteristic velocities are well below the sound speed, which is certainly the case for fusion plasmas. In this limit, the stability parameter simplifies to

$$D_v \approx D_s+\kappa_s+(D_s+S^2)\kappa_\parallel^2+\left(\frac{3S^2}{2}+\frac{D_s}{\beta\Gamma}\right)\kappa_\theta^2-\kappa_\theta\left[\kappa_\perp+2(B_z/B_\theta)\kappa_\parallel\right]. \tag{5.19}$$

We are primarily interested in the case where D_s is negative. In a true cylinder, this only occurs when the pressure increases with r, but when toroidal corrections are taken into account [29], corrections resulting from favorable magnetic curvature can result in negative D_s with radially decreasing pressure.

From Eq. (5.19), we see that the velocity shear perpendicular to the magnetic field, $\kappa_\parallel$, can enhance the stabilizing properties of the magnetic curvature. Conversely, when D_s is positive, $\kappa_\parallel$ enhances the destabilizing effect. At high pressure, rotation always has a destabilizing effect, but at low pressure rotation can also amplify the stabilizing effect of the field line curvature. The κ_s term is associated with equilibrium entropy gradients, and can be stabilizing or destabilizing, depending on the sign. Finally, the last term in Eq. (5.19) arises from κ_g, and is a Coriolis force that can have either sign.

In the following, we find that all of these qualitative effects are the same for resistive instabilities, but there are new destabilizing effects that arise from the parallel current and the current gradient within the layer.

5.1.0.2 Nonrotating Limit

We can verify the gravity-curvature equivalence by looking at the ideal inertial layer equation in the non-rotating, incompressible limit $V_\theta \to 0$, $\beta\Gamma \to \infty$. In this case, we obtain

$$\frac{\mathrm{d}}{\mathrm{d}X}\left(((1+\mathrm{i}\kappa_\parallel X)^2+X^2)\frac{\mathrm{d}\Xi}{\mathrm{d}X}\right)+\left(D_s-\frac{S^2}{1+X^2}\right)\Xi=0. \tag{5.20}$$

where $X=(r-a)\sqrt{4\pi\rho}/\gamma$. This equation has a similar form to Eq. (3.48), and reduces to it in the limit $S \to 0$. The quantity S is a stabilizing parameter which goes to zero in the plane limit. The quantity D_s is proportional to the product $\nabla p \cdot \boldsymbol{\kappa}_B$, so at least in a qualitative sense, magnetic curvature is playing a similar role to gravity.

Another interesting correspondence is the non-rotating, low-pressure limit, $\beta\Gamma \to 0$. Here, Eq. (5.12) becomes

$$\frac{\mathrm{d}}{\mathrm{d}X}\left(([1+\mathrm{i}\kappa_\parallel X]^2+X^2)\frac{\mathrm{d}\Xi}{\mathrm{d}X}\right)+D_s\Xi=0. \tag{5.21}$$

This is exactly the same as Eq. (3.48) with $D_g \to D_s$. Thus we see that, with rotation neglected, gravity can play the same role as magnetic curvature in determining ideal stability.

5.2 Resistive Interchange Ordering

Assuming the equilibrium to be ideally stable, we consider the ordering $\eta \to \epsilon\eta$, and assume $\gamma \to 0$ as $\eta \to 0$. Taking the outer limit, we find that the leading-order behavior of the modes must satisfy Eq. (5.12) everywhere except in the immediate vicinity of $r = a$. To construct a uniformly valid asymptotic expression, we must also find the leading-order solution in the inner limit $\eta \to 0$, $\delta(\eta) \to 0$, with $x = (r-a)/\delta$ held constant.

We can determine $\delta(\epsilon)$ by looking for modes that match the limiting form of Eq. (5.12) in an intermediate region. Using Eqs. (5.14) and (5.16), we find leading-order components in the layer have the relative ordering

$$\boldsymbol{\xi}(r=a+\delta x,\eta) \propto \left[\delta\xi_r^{(1)}(x)\mathbf{e}_r+\xi_B^{(0)}(x)\frac{\mathbf{B}}{B^2}+\xi_\perp^{(0)}(x)\frac{\mathbf{e}_r\times\mathbf{B}}{B^2}\right], \tag{5.22}$$

$$\mathbf{b}(r=a+\delta x,\eta) \propto \left[\delta^2 b_r^{(2)}(x)\mathbf{e}_r+\delta b_B^{(1)}(x)\frac{\mathbf{B}}{B^2}+\delta b_\perp^{(1)}(x)\frac{\mathbf{e}_r\times\mathbf{B}}{B^2}\right], \tag{5.23}$$

$$\boldsymbol{\nabla}\cdot\boldsymbol{\xi}(r=a+\delta x,\eta) \propto \delta(\boldsymbol{\nabla}\cdot\boldsymbol{\xi})^{(1)}(x), \tag{5.24}$$

as $\epsilon \to 0$. In order to retain all of the highest derivatives the layer, the resistivity and growth rate must contribute to leading order, which implies γ and δ vanish like $\eta^{1/3}$.

From (5.22)–(5.24), we see that the leading-order components of both $\boldsymbol{\xi}$ and $\mathbf{b}$ are divergence free:

$$b_\perp^{(1)} = \frac{\mathrm{i}\, B^2}{G} b_r^{(2)\prime}, \tag{5.25}$$

$$\xi_\perp^{(0)} = \frac{\mathrm{i}\, B^2}{G} \xi_r^{(1)\prime}, \tag{5.26}$$

where $G = \mathbf{e}_r \cdot \mathbf{k} \times \mathbf{B}$. The relations (5.25), (5.26) are used to eliminate $\xi_\perp^{(0)}$ and $b_\perp^{(1)}$ in the subsequent equations.

The projection of Eq. (5.7) along $\mathbf{B}$ gives

$$\rho\tilde{\gamma}^2 \xi_B^{(0)} = b_r^{(2)} \left(\frac{\rho V_\theta^2}{a} - p' \right) + \frac{\mathrm{i}\, F'}{4\pi} x b_B^{(1)} - 2\rho\tilde{\gamma} \frac{V_\theta B_\theta}{r} \xi_r^{(1)}, \tag{5.27}$$

while both components of Eq. (5.7) perpendicular to $\mathbf{B}$ give

$$\xi_r^{(1)} p' + \Gamma p (\boldsymbol{\nabla} \cdot \xi)^{(1)} = \frac{b_B^{(1)}}{4\pi}. \tag{5.28}$$

Following Ref. [8], we apply the annihilator $\boldsymbol{\nabla} \cdot \left(\frac{\mathbf{B} \times \cdot}{B^2} \right)$ to Eq. (5.7) to obtain a third independent equation:

$$\begin{aligned} \rho \left(\tilde{\gamma}^2 \xi_r^{(1)\prime} \right)' =& \frac{2G^2}{B^4} \left[\frac{\rho V_\theta^2}{a} - \left(p + \frac{B^2}{8\pi} \right)' \right] b_B^{(1)} + \frac{\mathrm{i}\, F' x}{4\pi} b_r^{(2)\prime\prime} \\ &+ \frac{G^2}{B^2} \left[\frac{\rho V_\theta^2}{a} (\boldsymbol{\nabla} \cdot \xi)^{(1)} + r \xi_r^{(1)} \left(\frac{\rho V_\theta^2}{a^2} \right)' \right] \\ &+ \frac{2\mathrm{i}\, G \rho V_\theta}{a B^2} \left[\mathrm{i}\, (n/L) \tilde{\gamma} \xi_B^{(0)} - B_z \xi_r^{(1)} \tilde{\gamma}' \right]. \end{aligned} \tag{5.29}$$

The projections of Eq. (5.8) along $\mathbf{e}_r$ and $\mathbf{B}$ give

$$\tilde{\gamma}\left(b_r^{(2)} - \mathrm{i}\,F' x \xi_r^{(1)}\right) = \eta b_r^{(2)\prime\prime}, \tag{5.30}$$

and

$$\begin{aligned}\eta b_B^{(1)\prime\prime} =& \tilde{\gamma}\left[b_B^{(1)} - \mathrm{i}\,F' x \xi_B^{(0)} + B^2(\boldsymbol{\nabla}\cdot\xi)^{(1)} + \xi_r^{(1)}\left(\left(B^2+4\pi p\right)' - 4\pi\frac{\rho V_\theta^2}{r}\right)\right] \\ & - \left(b_r^{(2)} - \mathrm{i}\,F' x \xi_r^{(1)}\right)\left[(\mathbf{V}\cdot\mathbf{B})' + \mathbf{e}_r\cdot[(\boldsymbol{\nabla}\times\mathbf{B})\times\mathbf{V}]\right],\end{aligned} \tag{5.31}$$

respectively. Equations (5.31) and (5.28) can be used to eliminate $(\boldsymbol{\nabla}\cdot\boldsymbol{\xi})^{(1)}$ and $\xi_B^{(0)}$. The quantities m and B_z' can be eliminated using the equilibrium relation (5.5) and the resonance condition

$$\frac{n}{L}B_z + \frac{m}{a}B_\theta = 0. \tag{5.32}$$

The resulting system of equations is

$$\Psi'' = \tilde{Q}(\Psi - X\Xi), \tag{5.33}$$

$$\begin{aligned}\Xi'' =& -\frac{2\mathrm{i}\,\kappa_\parallel}{\tilde{Q}}\Xi' + \left(\frac{X^2}{\tilde{Q}} - \frac{\kappa_g}{\tilde{Q}^2}\right)\Xi - \left(\frac{X}{\tilde{Q}} - \frac{\mathrm{i}\,\kappa_\theta D_s}{\tilde{Q}^3}[1+\frac{S^2}{2D_s}\kappa_\theta^2]\right)\Psi \\ & -\frac{D_s}{\tilde{Q}^2}\left(1+\frac{\kappa_\theta^2}{\beta\Gamma}+\frac{\mathrm{i}\,\kappa_\theta X}{\tilde{Q}}\right)\Upsilon,\end{aligned} \tag{5.34}$$

$$\begin{aligned}\Upsilon'' =& \left(\frac{X^2}{\tilde{Q}} + \left[1+\frac{2}{\beta\Gamma}\right]\tilde{Q}\right)\Upsilon - \left(\frac{X}{\tilde{Q}}[1+\frac{S^2}{2D_s}\kappa_\theta^2] + \mathrm{i}\,\frac{\kappa_\psi}{D_s}\right)\Psi \\ & -\left(\tilde{Q}\left[1+\frac{2}{\beta\Gamma}-\frac{S^2}{D_s}(1-\frac{\kappa_\theta^2}{2})\right] + \mathrm{i}\,\frac{\kappa_\perp}{D_s}X\right)\Xi,\end{aligned} \tag{5.35}$$

where we have defined

$$\begin{array}{ll} L_\eta = \left(\frac{4\pi\eta^2\rho}{F'^2}\right)^{1/6}, & \gamma_\eta = \left(\frac{\eta F'^2}{4\pi\rho}\right)^{1/3}, \\ X = x/L_\eta, & Q = \gamma/\gamma_\eta, \\ \kappa_\parallel = \Omega' L_\eta/\gamma_\eta, & \kappa_\psi = \kappa_\perp - S^2\kappa_\theta, \\ \tilde{Q} = Q + \mathrm{i}\,\kappa_\parallel X, & \Xi = \xi_r^{(1)}, \\ \Psi = \frac{b_r^{(2)}}{\mathrm{i}\,(4\pi\rho\eta^2 F'^4)^{1/6}}, & \Upsilon = \frac{b_B^{(1)}}{4\pi p'}a. \end{array} \tag{5.36}$$

5.2.1 Asymptotic Behavior

The appropriate boundary conditions for these equations are determined by matching them to the outer equations, which requires finding the asymptotic behavior of Eqs. (5.33)–(5.35) as $X \to \pm\infty$. The general solution has the leading-order behavior given in Eq. (3.104), where D_v is now given by Eq. (5.17).

5.2.2 Matching Conditions

We define a normalized independent variable for the outer equations:

$$\bar{x} = \frac{r - a}{a}. \tag{5.37}$$

The inner limit of the outer solution has the asymptotic behavior

$$b_r \sim a_1^{(\pm)} |\bar{x}|^{1+h} + a_2^{(\pm)} |\bar{x}|^{-h} \tag{5.38}$$

as $\bar{x} \to 0\pm$.

Once the exponentially growing solutions have been eliminated, the large-$|X|$ asymptotic behavior of the layer equations is

$$\Psi \sim A_1^{(\pm)} |X|^{1+h} + A_2^{(\pm)} |X|^{-h}. \tag{5.39}$$

By taking an intermediate limit, we can determine $A_1^{(\pm)}$ and $A_2^{(\pm)}$ up to an overall multiplicative constant. This will be done in the following subsection. In addition, matching requires the growing exponential solutions to be eliminated. Thus

$$A_3^{(+)} = A_4^{(-)} = A_5^{(+)} = A_6^{(-)} = 0. \tag{5.40}$$

5.2.2.1 Intermediate Limit

Define $s = \frac{r-a}{\sqrt{L_\eta a}}$ and recall $X = \frac{r-a}{L_\eta}$. Then $\bar{x} = \varepsilon s$ and $X = \frac{s}{\varepsilon}$ where $\varepsilon = \left(\frac{L_\eta}{a}\right)^{1/2}$. The limit $\eta \to 0$, with s held constant, is an intermediate limit in which the outer solution and the layer solution should match. The actual matching conditions are obtained by expressing everything in terms of s:

$$\begin{aligned} \Psi &\sim A_1^{(\pm)} \left(\frac{|s|}{\varepsilon}\right)^{1+h} + A_2^{(\pm)} \left(\frac{|s|}{\varepsilon}\right)^{-h}, \\ &\sim \frac{A_1^{(\pm)}}{\varepsilon^{1+h}} \left[|s|^{1+h} + \frac{A_2^{(\pm)}}{A_1^{(\pm)}} \varepsilon^{1+2h} |s|^{-h} \right], \end{aligned} \tag{5.41}$$

$\eta \to 0$, $S = \pm|s|$. In this same intermediate limit,

$$\begin{aligned} b_r &\sim a_1^{(\pm)} (\varepsilon|s|)^{1+h} + a_2^{(\pm)} (\varepsilon|s|)^{-h} \\ &\sim a_1^{(\pm)} \varepsilon^{1+h} \left[|s|^{1+h} + \frac{a_2^{(\pm)}}{a_1^{(\pm)}} \varepsilon^{-1-2h} |s|^{-h} \right]. \end{aligned} \tag{5.42}$$

Because both the outer and layer equations are linear, the overall constants in front of Ψ and b_r are freely chosen. The matching parameter is the ratio of the two power law solutions. Requiring these to be equal, we get

$$\frac{A_1^{(\pm)}}{A_2^{(\pm)}} = \left(\frac{L_\eta}{a}\right)^{1+2h} \frac{a_1^{(\pm)}}{a_2^{(\pm)}}. \tag{5.43}$$

The matching conditions (5.43) imply that to lowest order in resistivity,

$$\frac{A_2^{(\pm)}}{A_1^{(\pm)}} = 0. \tag{5.44}$$

Thus, the leading-order behavior of the growth rate, Q, and the perturbed fields near the rational surface, are determined by finding the solution to the sixth-order system of equations (5.33)–(5.35), with the six homogeneous boundary conditions (5.40) and (5.44).

5.2.3 Discussion

In the static limit, the layer equations (5.33)–(5.35) are invariant under the transformation $X \to -X$, and there is no explicit i-dependence. With equilibrium velocity shear and rotation, the layer equations (5.33)–(5.35) are no longer parity conserving, and now contain both real and imaginary parts. These two facts appear to be related, since an ansatz of the form

$$\Psi = \Psi_r + \mathrm{i}\,\Psi_i, \tag{5.45}$$

$$\Xi = \Xi_r + \mathrm{i}\,\Xi_i, \tag{5.46}$$

$$\Upsilon = \Upsilon_r + \mathrm{i}\,\Upsilon_i, \tag{5.47}$$

leads to a system of six second-order real equations which do happen to conserve parity.

Even when rotation and velocity shear are dropped, finding modes and growth rates requires numerical solution. Many effective routines have been developed [17] for problems of this type, but the implementation is complicated by the fact that the equations (5.33)–(5.35) do not conserve parity. Another difficulty results from the Doppler shift contribution to the growth rate, which turns Q to $\tilde{Q}$. In Fourier space, these terms—which are proportional to X—become derivatives, and the order of the equations is not reduced.

Chapter 6

Tearing Modes in Straight Tokamak Geometry

The boundary conditions for the layer equations (5.33)–(5.35) are homogeneous, so the growth rates can only depend on the characteristics of the equilibrium at the rational surface. The interaction between the layer and the rest of the perturbation is a higher-order effect. If η is treated as the only small parameter, then computing the effect of the equilibrium outside the layer requires solving the problem to *second order* in η.

As discussed in Chapter 4, we really only care about the interaction between the profile outside the layer and the perturbation in the layer when the interaction effects are significant. This occurs when first-order effects are numerically small. Thus we consider a more complicated limit where D_s, κ_s, κ_θ, $\kappa_\perp$, and $\kappa_\parallel$ are all sufficiently small, which in turn implies we are studying the small-$|Q|$ limiting behavior of Eqs. (5.33)–(5.35).

In Chapter4, we had the leading-order dispersion relation (3.119), which instructed us that we must order D_g along with Q. Here, we must use Eqs. (5.33)–(5.35) to determine the ordering. By temporarily dropping the κ's, and taking the large $\beta\Gamma$ limit, we again find $Q \propto D^{2/3}$. This tells us $p, p' = \mathcal{O}(Q^{3/2})$. The velocity shear, $\kappa_\parallel$ will dominate Q for all ξ (in the layer within the layer)

unless $Q \propto \kappa_\parallel^{4/3}$, so that $V, V' = \mathcal{O}(Q^{3/4})$. In dimensioned variables, we have

$$\begin{array}{llll} \eta \to \epsilon^5 \eta, & \gamma \to \epsilon^3 \gamma, & \delta \to \epsilon^2 \delta, & \\ p \to \epsilon^2 p, & p' \to \epsilon^2 p', & V \to \epsilon V, & V' \to \epsilon V'. \end{array} \tag{6.1}$$

Looking at the equilibrium force balance relation (5.5), we see that we are considering the limit of a locally force-free field.

Finally, we note that V, V', and p' must be ordered at least as small as Eq. (6.1). If they are smaller, then they don't contribute to leading order, but they cannot be larger without abandoning self-consistency. So really, we have $p' \leq \mathcal{O}(\epsilon^2)$, $V \leq \mathcal{O}(\epsilon)$, $V' \leq \mathcal{O}(\epsilon)$. On the other hand, p must be at no smaller than $\mathcal{O}(\epsilon^2)$. If we don't order p, then we retain self-consistency, and get the incompressible limit of the maximally ordered equations below. This justifies the incompressible limit for tearing modes.

The lowest-order components of the perturbed fields have the asymptotic behavior

$$\boldsymbol{\xi}(r = a + \epsilon^2 x, \epsilon) \propto \left[\epsilon^2 \xi_r^{(2)}(x) \mathbf{e}_r + \xi_B^{(0)}(x) \frac{\mathbf{B}}{|B|^2} + \xi_\perp^{(0)}(x) \frac{\mathbf{e}_r \times \mathbf{B}}{|B|^2} \right], \tag{6.2}$$

$$\begin{aligned} \mathbf{b}(r = a + \epsilon^2 x, \epsilon) \propto \Bigg[& \left(\epsilon^4 b_{r,0}^{(4)}(x) + \epsilon^6 b_r^{(6)}(x) \right) \mathbf{e}_r + \epsilon^4 b_B^{(4)}(x) \frac{\mathbf{B}}{|B|^2} \\ & + \epsilon^4 b_\perp^{(4)}(x) \frac{\mathbf{e}_r \times \mathbf{B}}{|B|^2} \Bigg], \end{aligned} \tag{6.3}$$

$$(\boldsymbol{\nabla} \cdot \boldsymbol{\xi})(r = a + \epsilon^2 x, \epsilon) \propto \epsilon^2 (\boldsymbol{\nabla} \cdot \boldsymbol{\xi})^{(2)}(x), \tag{6.4}$$

as $\epsilon \to 0$, with $x =$ constant. Following the same procedure used to obtain

Eqs. (5.33)–(5.35), we find

$$\Psi'' = \tilde{Q}(\Psi_0 - X\Xi), \tag{6.5}$$

$$\Xi'' = -\frac{2\mathrm{i}\,\kappa_\parallel}{l^3\tilde{Q}}\Xi' + \left[\frac{X^2}{\tilde{Q}} - \frac{\kappa_g}{l^6\tilde{Q}^2}\right]\Xi - \left[\frac{D_s}{\tilde{Q}^2}\left(1 + \frac{\kappa_\theta^2}{\beta\Gamma} + \mathrm{i}\,\kappa_\theta\frac{X}{l^3\tilde{Q}}\right)\right]\Upsilon + \left[-\frac{X}{\tilde{Q}} + \frac{J_p}{\tilde{Q}^2} - J\frac{\mathrm{i}\,\kappa_\theta}{\tilde{Q}^3}\left(\frac{X}{l^3} - \frac{\mathrm{i}\,\kappa_\theta\tilde{Q}}{\beta\Gamma}\right) + \frac{\mathrm{i}\,\kappa_\theta(2D_s + S^2\kappa_\theta^2)}{2l^9\tilde{Q}^3}\right]\Psi_0, \tag{6.6}$$

$$\Upsilon'' = \left(\frac{X^2}{\tilde{Q}} + \frac{2l^6\tilde{Q}}{\beta\Gamma}\right)\Upsilon + \left(\left[\frac{S^2}{D_s} - \frac{2}{\beta\Gamma}\right]\tilde{Q} - \frac{\mathrm{i}\,\kappa_\perp X}{D_s l^3}\right)\Xi + \left(-\frac{X}{l^6\tilde{Q}} + J\left[\frac{X^2}{D_s\tilde{Q}} + \frac{2l^6\tilde{Q}}{D_s\beta\Gamma}\right] + \mathrm{i}\,\frac{\kappa_\perp - S^2\kappa_\theta}{D_s l^3} - \frac{S^2\kappa_\theta^2 X}{2D_s l^6\tilde{Q}}\right)\Psi_0, \tag{6.7}$$

with

$$\begin{aligned}
&l = \left(\tfrac{L_\eta}{a}\right)^{1/5}, && X = x/(lL_\eta),\\
&Q = \gamma/(l^4\gamma_\eta), && \Xi = \xi_r^{(2)},\\
&\Upsilon = b_B^{(4)}/(4\pi p' l^6), && \Psi_0 = \tfrac{b_r^{(4)}}{\mathrm{i}\,l(4\pi\rho\eta^2F'^4)^{1/6}},\\
&\Psi = \tfrac{b_r^{(6)}}{\mathrm{i}\,l^7(4\pi\rho\eta^2F'^4)^{1/6}}, && \tilde{Q} = Q + \mathrm{i}\,(\kappa_\parallel/l^3)X,\\
&J = \tfrac{4\pi aS}{B^2}\tfrac{\mathbf{J}\cdot\mathbf{B}}{c}, && J_p = \tfrac{2\pi a^2SB^2}{B_\theta^2}\left(\tfrac{\mathbf{J}\cdot\mathbf{B}}{cB^2}\right)'.
\end{aligned} \tag{6.8}$$

The lowest-order radial component of Eq. (5.8) reduces to

$$\frac{\mathrm{d}^2\, b_r^{(4)}}{\mathrm{d}\, x^2} = 0, \tag{6.9}$$

which has the solution

$$b_r^{(4)} = b_{r,0}^{(4)} + Ax. \tag{6.10}$$

By examining the matching conditions (5.43) in the limit (6.1), the constant A is seen to be higher order in ϵ than $b_{r,0}^{(4)}$. It therefore does not affect the leading-order behavior of the tearing layer equations.

Without rotation and shear, the constant-Ψ dispersion relation can be obtained directly from the resistive interchange equations by taking the small-$|Q|$ limit. This limit is singular, and a boundary layer structure is formed within the interchange boundary layer. With rotation or velocity shear, it is necessary to either start from the original equations (5.7)–(5.8), and use the tearing ordering, or keep a few higher-order terms in the resistive interchange ordering, which turn out to contribute to leading order in the more complicated tearing limit. These additional terms give rise to J and J_p.

We can reduce the number of parameters by defining $\xi = \frac{X}{Q^{1/4}}$, $\bar{\Xi} = Q^{1/4}\Xi/\Psi_0$, $\bar{\Upsilon} = l^6 Q^{1/4}\Upsilon/\Psi_0$, $\bar{D}_s = D_s/(l^6 Q^{3/2})$, $\bar{J} = J/Q^{5/4}$, $\bar{J}_p = J_p/Q^{5/4}$, $\bar{\beta} = \beta/(l^6 Q^{3/2})$, $\bar{\kappa}_\parallel = \kappa_\parallel/(l^3 Q^{3/4})$, $\bar{\kappa}_\perp = \kappa_\perp/(l^3 Q^{3/4})$, $\bar{\kappa}_\theta = \kappa_\theta/(l^3 Q^{3/4})$, and $\bar{\kappa}_g = \kappa_g/(l^6 Q^{3/2})$.

In "bar" variables, Eq. (6.5) becomes

$$\frac{\Psi''}{\Psi_0} = Q^{3/2}(1 + \mathrm{i}\,\bar{\kappa}_\parallel \xi)(1 - \xi\,\bar{\Xi}). \tag{6.11}$$

Substituting "bar" variables in Eqs. (6.6), (6.7) is equivalent to setting $\tilde{Q} \to 1 + \mathrm{i}\,\bar{\kappa}_\parallel \xi$ and $l \to 1$.

From the boundary conditions (5.39), taken in the limit (6.1), we obtain

$$\Delta = \lim_{|\xi|\to\infty} \left(\frac{\Psi'(|\xi|) - \Psi'(-|\xi|)}{\Psi_0} \right) = Q^{1/4} \left[\left(\frac{a_2^{(+)}}{a_1^{(+)}} \right) + \left(\frac{a_2^{(-)}}{a_1^{(-)}} \right)^{-} \right]. \tag{6.12}$$

On the other hand, by integrating Eq. (6.11) we find

$$\Delta = Q^{3/2} \int_{-\infty}^{\infty} (1 + \mathrm{i}\,\bar{\kappa}_\parallel \xi)(1 - \xi\,\bar{\Xi}(\xi))\mathrm{d}\,\xi. \tag{6.13}$$

Comparing Eqs. (6.12) and (6.13), we obtain

$$Q^{-5/4}\left[\left(\frac{a_2^{(+)}}{a_1^{(+)}}\right)+\left(\frac{a_2^{(-)}}{a_1^{(-)}}\right)\right]=\int_{-\infty}^{\infty}(1-\xi\,\bar{\Xi}^{(-)})\mathrm{d}\,\xi-\mathrm{i}\,\bar{\kappa}_{\|}\int_{-\infty}^{\infty}\xi^2\,\bar{\Xi}^{(+)}\mathrm{d}\,\xi,\quad(6.14)$$

where $\bar{\Xi}^{(\pm)}$ are the even/odd parts of $\bar{\Xi}$.

The parameter

$$\Delta'=\left[\left(\frac{a_2^{(+)}}{a_1^{(+)}}\right)+\left(\frac{a_2^{(-)}}{a_1^{(-)}}\right)^{-}\right]\quad(6.15)$$

comes from solving the linearized equations outside the layer.

6.0.4 Small Velocity Ordering

By taking the small-$|Q|$ limit of the resistive interchange ordering, the sixth-order system (5.33)–(5.35) has been reduced to the fourth-order autonomous subsystem (6.6)–(6.7). In the small-velocity limit, these equations can be solved exactly. We are unable to solve Eqs. (6.6)–(6.7) for general κ_θ, $\kappa_\|$, $\kappa_\perp$, but as noted previously, these parameters are typically small for magnetically confined fusion plasmas. We therefore calculate leading-order corrections.

Setting

$$\bar{\kappa}_\theta,\bar{\kappa}_\|,\bar{\kappa}_\perp,\bar{J},\bar{J}_p=\mathcal{O}(\lambda),\quad(6.16)$$

we evaluate the dispersion relation to leading order as $\lambda\to 0$. This is done in Appendix B.2. Had we only scaled the $\bar{\kappa}$'s, we would find that the leading-order corrections are proportional to a linear combination of $\bar{J}$ and $\bar{J}_p$, so we have also ordered $\bar{J}$ and $\bar{J}_p$ to pick up the next correction when $\bar{J}$ and $\bar{J}_p$

are small. The calculations can be carried out for arbitrary $\bar{\kappa}_s$, so we do not immediately restrict our calculation to small $\bar{\kappa}_s$.

To leading order in λ, we find

$$\begin{aligned}\frac{\Delta'}{Q^{5/4}} =& a_+ \frac{\Gamma(\frac{1}{4}[3+x_+])}{\Gamma(\frac{1}{4}[5+x_+])} + a_- \frac{\Gamma(\frac{1}{4}[3+x_-])}{\Gamma(\frac{1}{4}[5+x_-])} \\ &+ b_+ \frac{\Gamma(\frac{1}{4}[1+x_+])}{\Gamma(\frac{1}{4}[3+x_+])} + b_- \frac{\Gamma(\frac{1}{4}[1+x_-])}{\Gamma(\frac{1}{4}[3+x_-])},\end{aligned} \tag{6.17}$$

where

$$x_\pm = \frac{1}{\bar{\beta}\Gamma} - \frac{\bar{\kappa}_s}{2} \pm \sqrt{\left(\frac{1}{\bar{\beta}\Gamma} - \frac{\bar{\kappa}_s}{2}\right)^2 + \frac{2\bar{D}_s}{\bar{\beta}\Gamma} - S^2}, \tag{6.18}$$

$$a_+ = \frac{\pi}{2}\frac{(\bar{D}_s + x_+)(1-x_+)}{x_+ - x_-} + \mathcal{O}(\lambda^2), \tag{6.19}$$

$$a_- = \frac{\pi}{2}\frac{(\bar{D}_s + x_-)(x_- - 1)}{x_+ - x_-} + \mathcal{O}(\lambda^2), \tag{6.20}$$

$$b_+ = \mathcal{O}(\lambda^2), \tag{6.21}$$

$$b_- = \mathcal{O}(\lambda^2). \tag{6.22}$$

Eq. (6.18) agrees with the result obtained in Ref. [8] when κ_s is dropped.

6.0.4.1 Incompressible Limit

The general expressions for the perturbation expansions of the a's and b's in Eq. (6.17) are extremely complicated. Here we present the λ expansion in the incompressible limit ($\bar{\beta}\Gamma \to \infty$). The details of the calculation are shown in Appendix B.2. The result is

$$\Delta' = Q^{5/4}\left[\frac{C_0(S)(1+S^2)}{4}\left[S - \bar{D}_s \tanh(\pi S/4)\right] + \Delta^{(1)} + \Delta^{(2)}\right] + \mathcal{O}(\lambda^4). \tag{6.23}$$

We have dropped $\bar{\kappa}_s$, whose effects to all orders with arbitrary pressure can be found from Eq. (6.17).

The first-order term is

$$\Delta^{(1)} = C_0(S)\Big[\mathrm{i}\,(\bar{J}+\bar{J}_p)\bar{\kappa}_\perp F_\perp(S) + \mathrm{i}\,(\bar{J}-\bar{J}_p)\bar{\kappa}_\theta F_\theta(S) + \mathrm{i}\,\bar{J}\bar{\kappa}_\parallel F_J(S) + \mathrm{i}\,\bar{J}_p\bar{\kappa}_\parallel F_p(S)\Big], \tag{6.24}$$

and there are six independent second-order quantities:

$$\Delta^{(2)} = \sum_{\alpha,\beta} \bar{\kappa}_\alpha\bar{\kappa}_\beta C_0(S)\left[F_{\alpha,\beta}(S) + \bar{D}_s H_{\alpha,\beta}(S)\right], \tag{6.25}$$

where α, β run over the indices θ, $\parallel$, and $\perp$. The F's and H's are given in Appendix B.2 along with C_0.

By substituting back the Q and l dependence suppressed in the bar variables, we find the dispersion relation has the form

$$\begin{aligned}\Delta' =& Q^{5/4}\left[f_0(S) + \frac{D_s}{l^6Q^{3/2}}h_0(S)\right] + \mathrm{i}\,\frac{f_1(S,\kappa_\alpha,J_\beta)}{l^3Q^{3/4}} \\ &+ \frac{1}{l^6Q^{1/4}}\left[f_2(S,\kappa_\alpha) + \frac{D_s}{l^6Q^{3/2}}h_2(S,\kappa_\alpha)\right] + \mathcal{O}\Big(\frac{\lambda^4 J}{l^9Q^{9/4}}, \frac{\lambda^4 J_p}{l^9Q^{9/4}}, \frac{\lambda^4}{l^{12}Q^{7/4}}\Big),\end{aligned} \tag{6.26}$$

where, e.g.

$$f_2 = \sum_{\alpha,\beta} \kappa_\alpha\kappa_\beta C_0 F_{\alpha,\beta}. \tag{6.27}$$

6.1 Analysis of Dispersion Relation

6.1.1 Plane Incompressible Limit

In the plane incompressible limit $\kappa_\theta \to 0$, $\kappa_\perp \to 0$, $D_s \to 0$, and $S \to 0$, the expression (6.26) becomes

$$\Delta' = \frac{\pi}{2}\frac{\Gamma(5/4)}{\Gamma(3/4)}\left[Q^{5/4} + \frac{\mathrm{i}\,(J+J_p)\kappa_\parallel}{2l^3Q^{3/4}} - \frac{5\pi}{128}\frac{\kappa_\parallel^2}{l^6Q^{1/4}}\right] + \mathcal{O}(\kappa_\parallel^3), \tag{6.28}$$

which can be solved for Q to second order in $\kappa_\parallel$ to give

$$Q_0 = \left[(2/\pi)\frac{\Gamma(3/4)}{\Gamma(5/4)}\Delta'\right]^{4/5}, \tag{6.29}$$

$$Q = Q_0\left[1 - \frac{2}{5}\mathrm{i}\,(J+J_p)\frac{\kappa_\parallel}{l^3Q_0^2} + \frac{\kappa_\parallel^2}{l^6Q_0^{3/2}}\left(\frac{\pi}{32} + \frac{7}{50}\frac{(J+J_p)^2}{Q_0^{5/2}}\right) + \mathcal{O}(\kappa_\parallel^3)\right]. \tag{6.30}$$

This expression agrees with results found in Refs. [7, 30] using a somewhat different approach.

6.1.2 Equilibrium Current-Driven Modes

In Ref. [8], it was observed that the small-$|Q|$ limit of the resistive interchange dispersion relation is recovered by setting $\Delta' = 0$ in the constant-Ψ dispersion relation, and the same should be true here. The dispersion relation obtained from Eqs. (6.5)–(6.7) can be used to study the limiting behavior of interchange modes with equilibrium flow. Unfortunately, our truncated expansion in λ is not helpful in this respect, since there are no self-consistent roots of (6.26) with the second-order terms dominant. Recovering the limiting behavior of interchange modes driven by rotation or velocity shear appears to require an exact solution of the fourth-order system (6.6), (6.7).

We also find roots which would require extending the calculation in Section 5.2 to the next order in η. By considering the case where the terms in Eq. (6.26) involving Δ', D_s, and f_2 are all relatively small, we find modes driven by the equilibrium current and/or current gradient in the layer:

$$Q^2 \approx \mathrm{i}\,\frac{f_1}{l^3 f_0}. \tag{6.31}$$

These (dimensioned) growth rates scale like $\eta^{1/2}$. In Refs. [7, 30], these modes were obtained using the constant-Ψ approximation and referred to as "large shear" modes. Following our convention where the fundamental small parameter is η, the ordering is "large J_α"; truly large shear would drive an interchange mode with $\gamma \propto \eta^{1/3}$, which is not consistent with the constant-Ψ approximation.

6.1.3 Effect of Rotation and Shear on Δ'_{crit}

For negative D_s, there is a threshold value Δ'_{crit} of the tearing stability index required for instability [8, 16]. Following Ref. [16], we look for roots of (6.26) which correspond to overstable modes at marginal stability:

$$Q = \exp(\pm \mathrm{i}\,\pi/2) Q_0. \tag{6.32}$$

By setting $\mathrm{Im}[\Delta(Q_c)] = 0$, we can solve for Q_c, which is used to compute Δ' at the stability boundary. We find

$$\Delta_{\mathrm{crit}} = \Delta^{(0)}_{\mathrm{crit}} - |f_1| Q_c^{-3/4} N_+ + f_2 Q_c^{-1/4} N_- + |D_s| h_2 Q_c^{-7/4} N_+, \tag{6.33}$$

where

$$Q_c = \left[\frac{-|D_s|h_0\tan(\pi/8)}{l^6 f_0}\right]^{2/3} = \left[\frac{|D_s|}{l^6}\tan(\pi/8)\tanh(\pi S/4)/S\right]^{2/3} \quad (6.34)$$

$$\begin{aligned}\Delta^{(0)}_{\rm crit} &= -f_0 Q_0^{5/4}\sin(\pi/8) - \frac{|D_s|}{l^6}h_0 Q_0^{-1/4}\cos(\pi/8), \\ &= C_0(S)\frac{S}{4}(1+S^2)Q_0^{5/4}\left[\cos^2(\pi/8)-\sin^2(\pi/8)\right]/\sin(\pi/8), \quad (6.35)\end{aligned}$$

and

$$N_\pm = \cos(\pi/8) \pm \frac{5}{6}\sin(\pi/8)[\tan(\pi/8) + (1/5)\cot(\pi/8)]. \quad (6.36)$$

Numerically, $N_+ \approx 1.21$ and $N_- \approx 0.64$, and $C_0(S)$ is defined in Appendix B.2.

From Eq. (6.33) we see that first-order terms are *always destabilizing*. At first glance this is surprising, since the coefficient f_1 is a linear combination of κ's and, thus, can have either sign. It turns out that there are two overstable modes at marginal stability, and the sign of the coefficient f_1 only determines which of the two modes gets destabilized by the κ-J coupling.

It is interesting to compare the effects of J and J_p here versus the static case [8]. In the static limit, the dispersion relation depends only on $\Xi^{(-)}$, and the J's give rise to $\Xi^{(+)}$ without affecting $\Xi^{(-)}$, thus altering the shape of the mode without modifying the growth rate. With velocity shear and rotation, J and J_p contribute to both $\Xi^{(+)}$ and $\Xi^{(-)}$, and moreover, both the even and odd parts of Ξ contribute to the dispersion relation. The J's give rise to layer asymmetry, which can only be seen by going to higher order in the resistive interchange ordering. In the tearing ordering, the layer width is slightly larger

than for resistive interchange, so asymmetry of the equilibrium about $r = a$ affects the physics in the layer.

There are six second-order terms, which we separate into the positive definite κ_α^2 and the cross terms $\kappa_\alpha \kappa_\beta$. The cross terms have a real coefficient, and $\kappa_\alpha \kappa_\beta$ can have either sign, so they can potentially increase or decrease Δ_{crit}. The second-order pure rotation term is negative so in the incompressible limit, pure rotation is always destabilizing. See Fig. 6.1.3.

By evaluating $F_{\alpha\alpha}, H_{\alpha\alpha}$ in Eq. (6.33) with α equal to $\|$ or $\perp$, we find that each of the positive-definite velocity shear terms is stabilizing. This is also seen in Fig. 6.1.3. Thus when velocity shear is sufficiently large that the second-order terms exceed the first-order coupling to the J's, the overall effect of velocity shear can be stabilizing.

For given values of D_s, J, J_p, and S, there is a critical value κ_{crit}, above which shear has a stabilizing effect. From Eq. (6.33), we find

$$\kappa_{\text{crit}} \propto l^5 J_\alpha / |D_s|^{1/3}. \tag{6.37}$$

Thus, as D_s gets small, a larger value of velocity shear is required in order to have a stabilizing effect. This explains the purely destabilizing effect of shear in a slab, where $D_s \to 0$.

Finally we note that effects of $\kappa_\perp$ are numerically small in comparison to $\kappa_\|$ and κ_θ. This can be seen in Figs. 6.1.3–6.1.3. It thus appears that shear of the velocity perpendicular to the field lines is likely to provide the dominant

stabilizing effect. This observation is consistent with the ideal stability criterion (5.19), where $\kappa_\perp$ only enters in the cross terms, and thus has no effect on its own.

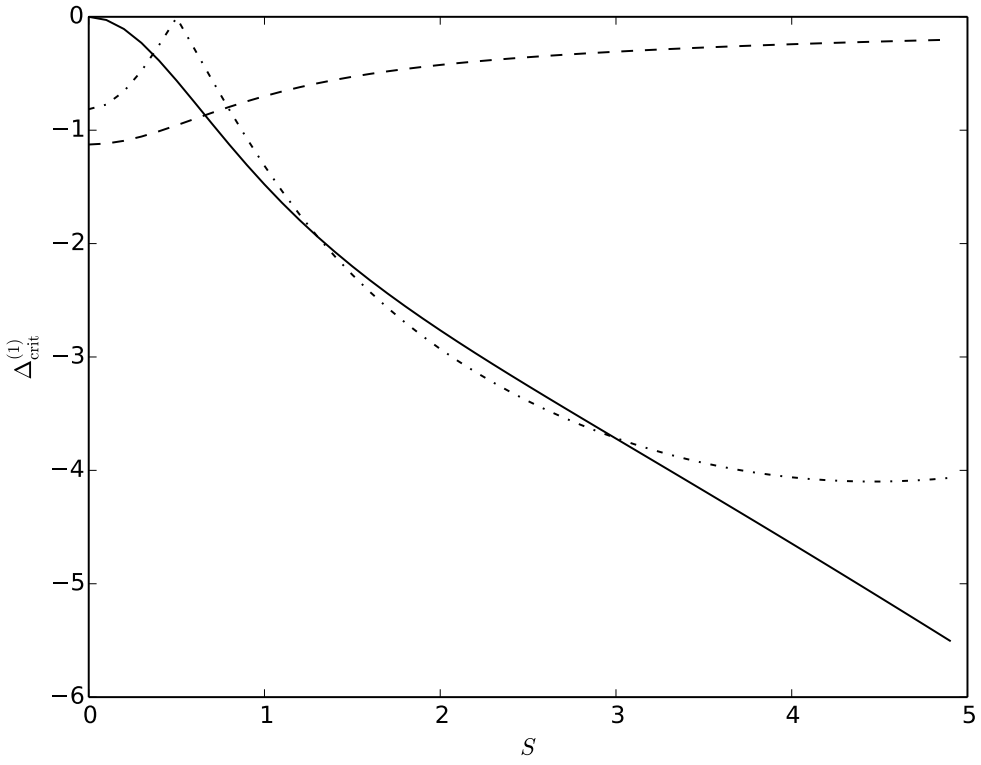

Figure 6.1: Δ'_{crit} first-order terms versus S for $J = 1$, $J_p = 0$, $D_s = -1$, $\kappa_\alpha = l^3$. The solid, dash, and dash-dotted lines correspond to $\Delta^{(1)}_\theta$, $\Delta^{(1)}_\perp$, and $\Delta^{(1)}_\parallel$, respectively.

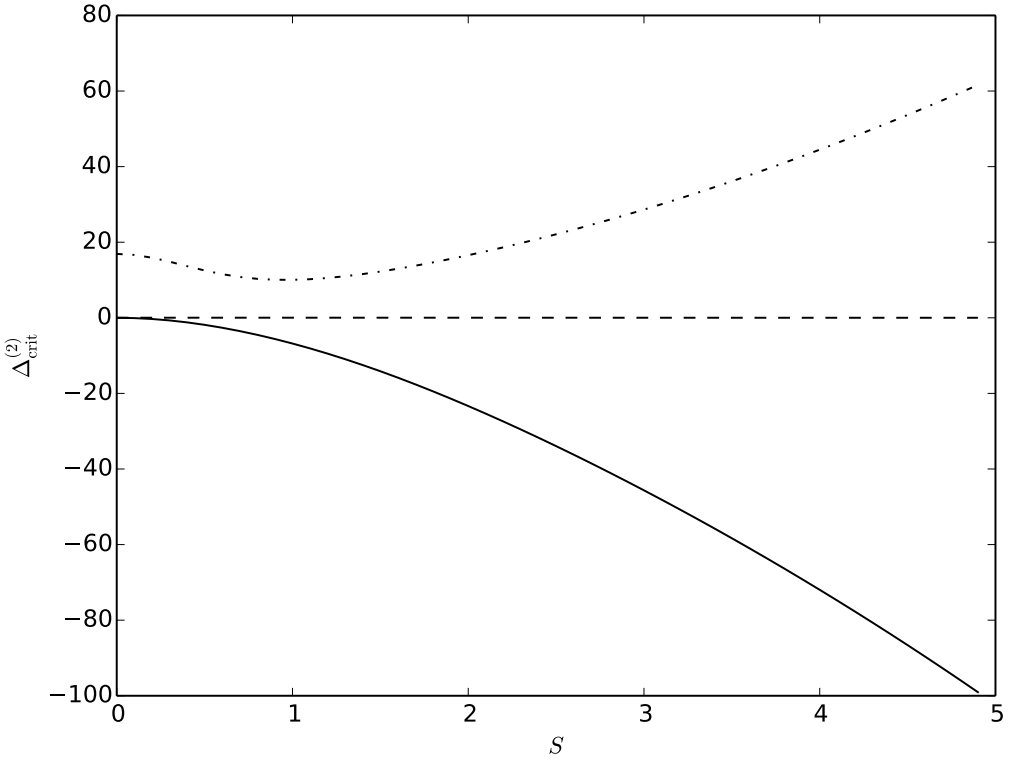

Figure 6.2: Δ'_{crit} second-order positive-definite terms versus S for $J = 1$, $J_p = 0$, $D_s = -1$, $B_\theta/B_z = 0.1$, and $\kappa_\alpha = l^3$. The solid, dash, and dash-dotted lines correspond to $\Delta^{(2)}_{\theta\theta}$, $\Delta^{(2)}_{\perp\perp}$, and $\Delta^{(2)}_{\parallel\parallel}$, respectively.

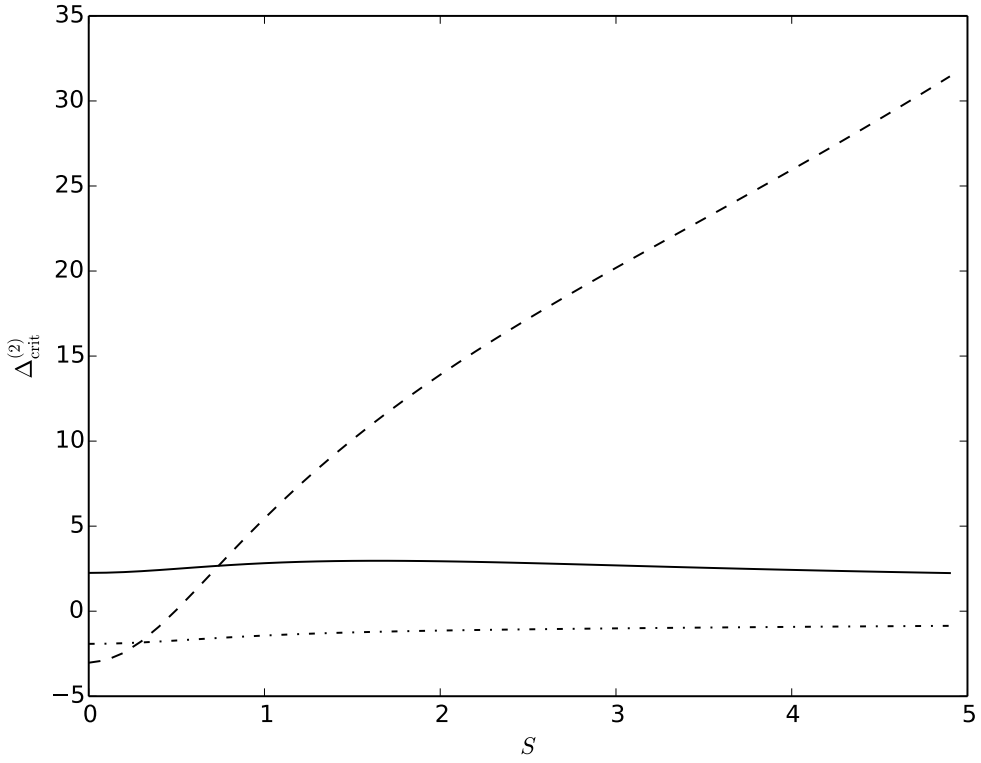

Figure 6.3: Δ'_{crit} second-order cross terms versus S for $J = 1$, $J_p = 0$, $D_s = -1$, $B_\theta/B_z = 0.1$, and $\kappa_\alpha = l^3$. The solid, dash, and dash-dotted lines correspond to $\Delta^{(2)}_{\parallel\theta}$, $\Delta^{(2)}_{\perp\theta}$, and $\Delta^{(2)}_{\perp\parallel}$, respectively.

Chapter 7

Conclusion

We have shown how to introduce a displacement vector for resistive instabilities with flow. Our formulation reduces to the Frieman-Rotenberg equation in the ideal limit, and the matching is therefore straightforward when the Frieman-Rotenberg equation is used in the outer ideal region.

The general resistive layer equations are effectively twelfth order. Calculating growth rates for arbitrary equilibrium parameters requires a numerical solution, just as in the non-rotating case. The numerical problem is similar in character, but the order of the equations is doubled for routines which utilize parity symmety, and the exponentially growing solutions—which need to be eliminated—have an oscillatory behavior.

Analytical results can be obtained in the constant-Ψ limit, with velocity treated as a small parameter. In the incompressible limit, the leading-order effects of rotation and both components of velocity shear reduce the threshold value $\Delta'_{\rm crit}$ required for instability. The first-order coefficients are a linear combination of J and J_p, which both give rise to parity asymmetry of the equilibrium profile in the resistive layer. This effect, like Δ', is not present in the general resistive layer equations unless one is able to carry out the analysis

to the next order in η. Indeed, to leading order in η, the criterion (6.37) becomes $\kappa_\alpha > 0$, where α corresponds to either shear component.

If J and J_p are small, both components of velocity shear are found to be stabilizing. Moreover, the increase in $\Delta'_{\rm crit}$ due to the gradient of the velocity perpendicular to the field lines is several orders of magnitude greater than the increase due to shear of the parallel component. The negligible contribution of $\kappa_\perp$ is also seen in the ideal stability boundary. In the incompressible limit, pure rotation continues to reduce $\Delta'_{\rm crit}$ in second order.

All of the previously mentioned effects on $\Delta'_{\rm crit}$ were found by taking D_s to be negative, which is the case of primary interest. If D_s is positive, then the system is unstable with respect to rapidly growing resistive interchange modes, and $\Delta' \sim 1$ merely introduces a small correction. For cylindrical equilibria, setting $D_s < 0$ means considering profiles with $p' > 0$, and thus is rather artificial–similar to requiring periodicity in z. When toroidal corrections are included, D_s is proportional to the average geodesic curvature of the field lines, and can be negative for systems with $p' < 0$.

If we ignore the coupling to the J's, then all of the qualitative effects of rotation and shear are consistent with the effects on the ideal stability boundary $D_v < 1/4$. In this much simpler analytic expression, one can readily see that velocity shear is stabilizing for $D_s < 0$ and destabilizing for $D_s > 0$. For resistive instabilities, we showed that the second-order stabilizing effects of shear will dominate the first-order coupling to the Js when $|D_s|$ is sufficiently large (and negative.) It thus appears that velocity shear tends to amplify the

stabilizing properties of good magnetic curvature.

Interestingly, while gravity plays the role of magnetic curvature for ideal instabilities, the Glasser effect is not present in the gravitating slab model. Since the Glasser effect amplification leads to the stabilizing effect of velocity shear, we conclude that the slab model lacks the essential physics to understand the role of shear in tearing mode stability.

Appendices

Appendix A

Eulerian Friemen-Rotenberg Formulation with Dissipation

A.1 Linearized Resistive MHD with Frieman-Rotenberg Displacement Vector

Let[1] $\mathbf{V}_0$ be the unperturbed stationary flow, and $\mathbf{V}$ be the exact velocity field which includes the time-dependent perturbation. We define corresponding Lagrangian variables

$$\mathbf{q}(\mathbf{a},t) = \mathbf{q}_0(\mathbf{a},t) + \mathbf{q}_1(\mathbf{a},t), \tag{A.1}$$

via

$$\mathbf{V}_0(\mathbf{q}_0(\mathbf{a},t)) = \dot{\mathbf{q}}_0(\mathbf{a},t), \tag{A.2}$$

$$\mathbf{V}(\mathbf{q}(\mathbf{a},t),t) = \dot{\mathbf{q}}(\mathbf{a},t), \tag{A.3}$$

and

$$\mathbf{q}_0(\mathbf{a},0) = \mathbf{q}(\mathbf{a},0) = \mathbf{a}. \tag{A.4}$$

Geometrically, the vectors $\mathbf{q}(\mathbf{a},t)$ and $\mathbf{q}_0(\mathbf{a},t)$ give the position of a fluid element at time t which was previously located at $\mathbf{a}$ at time $t = 0$ in the exact

[1] In the first part of this section, we explicitly include the subscript zero on equilibrium quantities.

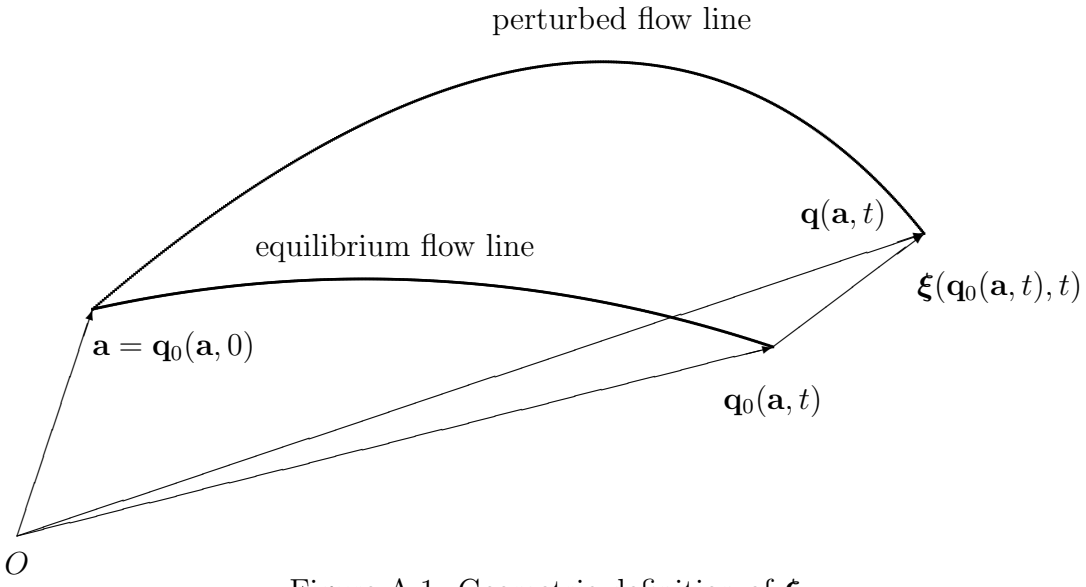

Figure A.1: Geometric definition of $\boldsymbol{\xi}$

and unperturbed flow, respectively. This is consistent with the geometric formulation in Ref. [13], reproduced in Fig. A.1.

Following Ref. [13], we define an Eulerian displacement vector $\boldsymbol{\xi}$ via

$$\boldsymbol{\xi}(\mathbf{q}_0(\mathbf{a},t),t)=\mathbf{q}_1(\mathbf{a},t). \tag{A.5}$$

Taking a time derivative of Eq. (A.1) and using the definitions (A.2), (A.3), and (A.5), we find

$$\dot{\mathbf{q}}(\mathbf{a},t)=\dot{\mathbf{q}}_0(\mathbf{a},t)+\dot{\mathbf{q}}_1(\mathbf{a},t), \tag{A.6}$$

or, using Eqs. (A.2)–(A.3):

$$\mathbf{V}(\mathbf{q}(\mathbf{a},t),t)=\mathbf{V}_0(\mathbf{q}_0(\mathbf{a},t))+\left(\frac{\partial\boldsymbol{\xi}}{\partial t}+(\mathbf{V_0}\cdot\boldsymbol{\nabla})\boldsymbol{\xi}\right)(\mathbf{q}_0(\mathbf{a},t),t). \tag{A.7}$$

In order to re-express the functional relationship (A.7) using a common Eulerian independent variable, let $\mathbf{x}_0=\mathbf{q}_0(\mathbf{a},t)$ and

$$\mathbf{x}=\mathbf{x}_0+\boldsymbol{\xi}(\mathbf{x}_0,t). \tag{A.8}$$

Equation (A.8) determines $\mathbf{x}_0$ implicitly in terms of $\mathbf{x}$ and $\boldsymbol{\xi}$. This relationship can be put in recursive form:

$$\mathbf{x}_0 = \mathbf{x} - \boldsymbol{\xi}(\mathbf{x} - \boldsymbol{\xi}(\cdots), t). \tag{A.9}$$

From Eqs. (A.7) and (A.9) we obtain

$$\begin{aligned}\mathbf{V}(\mathbf{x}, t) =& \left(\mathbf{V}_0 + \frac{\partial \boldsymbol{\xi}}{\partial t} + (\mathbf{V}_0 \cdot \boldsymbol{\nabla})\boldsymbol{\xi}\right)(\mathbf{x}_0 = \mathbf{x} - \boldsymbol{\xi}(\mathbf{x} - \boldsymbol{\xi}(\cdots), t)), t) \\ =& \mathbf{V}_0(\mathbf{x}, t) - (\boldsymbol{\xi} \cdot \boldsymbol{\nabla})\mathbf{V}_0(\mathbf{x}, t) + \frac{\partial \boldsymbol{\xi}}{\partial t}(\mathbf{x}, t) + (\mathbf{V}_0 \cdot \boldsymbol{\nabla})\boldsymbol{\xi}(\mathbf{x}, t) + \mathcal{O}(\xi^2) \\ =& \mathbf{V}_0(\mathbf{x}, t) + [\mathbf{V}_0, \boldsymbol{\xi}](\mathbf{x}, t) + \frac{\partial \boldsymbol{\xi}}{\partial t}(\mathbf{x}, t) + \mathcal{O}(\xi^2),\end{aligned} \tag{A.10}$$

where $[\mathbf{A}, \mathbf{B}] = (\mathbf{A} \cdot \nabla)\mathbf{B} - (\mathbf{B} \cdot \nabla)\mathbf{A}$. It follows that

$$\mathbf{v} = [\mathbf{V}_0, \boldsymbol{\xi}] + \frac{\partial \boldsymbol{\xi}}{\partial t}. \tag{A.11}$$

We can follow the same procedure used in the derivation of Eq. (A.10) to obtain the first-order expression for the acceleration in terms of $\boldsymbol{\xi}$. We begin with the acceleration in the Lagrangian description:

$$\ddot{\mathbf{q}} = \ddot{\mathbf{q}}_0 + \ddot{\mathbf{q}}_1. \tag{A.12}$$

Taking a time derivatives of Eqs. (A.2)–(A.5) and substituting the expressions into Eq. (A.12), we find

$$\begin{aligned}\left(\frac{\partial \mathbf{V}}{\partial t} + (\mathbf{V} \cdot \boldsymbol{\nabla})\mathbf{V}\right)(\mathbf{q}(\mathbf{a}, t), t) =& \Bigg[(\mathbf{V}_0 \cdot \boldsymbol{\nabla})\mathbf{V}_0 + \frac{\partial^2 \boldsymbol{\xi}}{\partial t^2} \\ &+ (\mathbf{V}_0 \cdot \boldsymbol{\nabla})\left(2\frac{\partial \boldsymbol{\xi}}{\partial t} + (\mathbf{V}_0 \cdot \boldsymbol{\nabla})\boldsymbol{\xi}\right)\Bigg](\mathbf{q}_0(\mathbf{a}, t), t) \\ &+ \mathcal{O}(\xi^2).\end{aligned} \tag{A.13}$$

Finally, changing to a common Eulerian independent variable $\mathbf{x}$ using Eq. (A.9), we have

$$\left(\frac{\partial \mathbf{V}}{\partial t} + (\mathbf{V}\cdot\boldsymbol{\nabla})\mathbf{V}\right)(\mathbf{x},t) = \Bigg[(\mathbf{V}_0\cdot\boldsymbol{\nabla})\mathbf{V}_0 + \frac{\partial^2\boldsymbol{\xi}}{\partial t^2} + (\mathbf{V}_0\cdot\boldsymbol{\nabla})\left(2\frac{\partial\boldsymbol{\xi}}{\partial t} + (\mathbf{V}_0\cdot\boldsymbol{\nabla})\boldsymbol{\xi}\right) - (\boldsymbol{\xi}\cdot\boldsymbol{\nabla})\left[(\mathbf{V}_0\cdot\boldsymbol{\nabla})\mathbf{V}_0\right]\Bigg](\mathbf{x},t) + \mathcal{O}(\xi^2). \tag{A.14}$$

Taking the first-order components of both sides of Eq. (A.14) gives

$$\frac{\partial \mathbf{v}}{\partial t} + (\mathbf{V}_0\cdot\boldsymbol{\nabla})\mathbf{v} + (\mathbf{v}\cdot\boldsymbol{\nabla})\mathbf{V}_0 = \frac{\partial^2\boldsymbol{\xi}}{\partial t^2} + (\mathbf{V}_0\cdot\boldsymbol{\nabla})\left(2\frac{\partial\boldsymbol{\xi}}{\partial t} + (\mathbf{V}_0\cdot\boldsymbol{\nabla})\boldsymbol{\xi}\right) - (\boldsymbol{\xi}\cdot\boldsymbol{\nabla})\left[(\mathbf{V}_0\cdot\boldsymbol{\nabla})\mathbf{V}_0\right]. \tag{A.15}$$

We now substitute the expressions (A.11) and (A.14) into the linearized equations (2.40)–(2.43) to obtain the resistive Frieman-Rotenberg equations. The subscript zero will be suppressed for subsequent calculations.

A.1.0.1 Continuity Equation

By substituting Eq. (A.11) into Eq. (2.40), we find

$$\frac{\partial}{\partial t}(\delta\rho + \boldsymbol{\nabla}\cdot(\rho\boldsymbol{\xi})) + \boldsymbol{\nabla}\cdot(\delta\rho\mathbf{V} + \rho[\mathbf{V},\boldsymbol{\xi}]) = 0. \tag{A.16}$$

Note

$$\begin{aligned}\boldsymbol{\nabla}\cdot(\rho[\mathbf{V},\boldsymbol{\xi}]) =&\boldsymbol{\nabla}\cdot(\rho(\mathbf{V}\cdot\boldsymbol{\nabla})\boldsymbol{\xi}-\rho(\boldsymbol{\xi}\cdot\boldsymbol{\nabla})\mathbf{V})\\ =&(\partial_j(\rho V_i\partial_i\xi_j))+(\partial_j(\rho\xi_i\partial_i V_j))\\ =&(\partial_j\partial_i(\rho V_i\xi_j)-\partial_j(\xi_j\boldsymbol{\nabla}\cdot(\rho\mathbf{V})))+(\partial_j(\partial_i(\rho\xi_i V_j))-V_j\partial_i\rho\xi_i)\\ =&\partial_i\partial_j(\rho V_i\xi_j-\rho V_j\xi_i)+\partial_j(V_j\partial_i(\rho\xi_i))\\ =&-\boldsymbol{\nabla}\cdot(\mathbf{V}(\boldsymbol{\nabla}\cdot\rho\mathbf{V})),\end{aligned}\tag{A.17}$$

where we have used Eq. (2.18). Using this result in Eq. (2.40), we find

$$\frac{\partial}{\partial t}[\delta\rho+\boldsymbol{\nabla}\cdot(\rho\boldsymbol{\xi})]+\boldsymbol{\nabla}\cdot([\delta\rho+\boldsymbol{\nabla}\cdot(\rho\boldsymbol{\xi})]\mathbf{V})=0,\tag{A.18}$$

which implies

$$\delta\rho=-\boldsymbol{\nabla}\cdot\rho\boldsymbol{\xi},\tag{A.19}$$

as long as we choose Eq. (A.19) to hold at $t=0$.

A.1.0.2 Induction Equation

In order to express the induction equation in terms of $\boldsymbol{\xi}$, we substitute Eq. (A.11) into Eq. (2.42), yielding

$$\frac{\partial\mathbf{b}}{\partial t}=\boldsymbol{\nabla}\times\left(\mathbf{V}\times\mathbf{b}+\left[[\mathbf{V},\boldsymbol{\xi}]+\frac{\partial\boldsymbol{\xi}}{\partial t}\right]\times\mathbf{B}\right)+\eta\nabla^2\mathbf{B}.\tag{A.20}$$

After a considerable amount of algebra, this equation can be put in the form

$$\frac{\partial}{\partial t}\left[\mathbf{b}-\boldsymbol{\nabla}\times\boldsymbol{\xi}\times\mathbf{B}\right]-\boldsymbol{\nabla}\times(\mathbf{V}\times[\mathbf{b}-\boldsymbol{\nabla}\times\boldsymbol{\xi}\times\mathbf{B}])=\eta\nabla^2\mathbf{B}.\tag{A.21}$$

In obtaining Eq. (A.21), we have made use of the Jacobi identity

$$[\mathbf{B}_0,[\mathbf{V}_0,\boldsymbol{\xi}]]+[\boldsymbol{\xi},[\mathbf{B}_0,\mathbf{V}_0]]+[\mathbf{V}_0,[\boldsymbol{\xi},\mathbf{B}_0]]=0.\tag{A.22}$$

and the equilibrium relation (2.20).

In the ideal limit, Eq. (A.21) implies

$$\mathbf{b} = \boldsymbol{\nabla} \times (\boldsymbol{\xi} \times \mathbf{B}), \tag{A.23}$$

which is the expression used in Ref. [13].

A.1.0.3 Equation of Motion

The expression for the perturbed equation of motion follows directly from the expression (A.15), which upon substitution into Eq. (**??**) yields:

$$\rho \left[\frac{\partial^2 \boldsymbol{\xi}}{\partial t^2} + 2(\mathbf{V}\cdot\boldsymbol{\nabla})\frac{\partial \boldsymbol{\xi}}{\partial t} + (\mathbf{V}\cdot\boldsymbol{\nabla})[(\mathbf{V}\cdot\boldsymbol{\nabla})\boldsymbol{\xi}] - (\boldsymbol{\xi}\cdot\boldsymbol{\nabla})[(\mathbf{V}\cdot\boldsymbol{\nabla})\mathbf{V}] \right] = -\delta\rho(\mathbf{V}\cdot\boldsymbol{\nabla})\mathbf{V} - \boldsymbol{\nabla}\delta p + \frac{1}{4\pi}\left[(\boldsymbol{\nabla}\times\mathbf{B})\times\mathbf{b} + (\boldsymbol{\nabla}\times\mathbf{b})\times\mathbf{B}\right]. \tag{A.24}$$

This expression reduces to the *Frieman-Rotenberg equation* when the ideal-MHD relations for $\delta\rho$, δp, and $\mathbf{b}$ are used.

A.1.0.4 Equation of Heat Transport

The heat transport equation (2.43) becomes

$$\left(\frac{\partial}{\partial t} + \mathbf{V}\cdot\boldsymbol{\nabla}\right)\left(\delta p + \boldsymbol{\xi}\cdot\boldsymbol{\nabla}p + \Gamma p\boldsymbol{\nabla}\cdot\boldsymbol{\xi}\right) = (\Gamma-1)\frac{\eta}{2\pi}\boldsymbol{\nabla}\times\mathbf{B}_0\cdot\boldsymbol{\nabla}\times\mathbf{b}. \tag{A.25}$$

Just as in the case without equilibrium flow [8], the Ohmic heating term can be neglected for the instabilities with boundary-layer thickness $\delta \ll \eta/\gamma$ as $\eta \to 0$. Thus the ideal-MHD relation

$$\delta p = -\boldsymbol{\xi}\cdot\boldsymbol{\nabla}p - \Gamma p\boldsymbol{\nabla}\cdot\boldsymbol{\xi}, \tag{A.26}$$

can be used for the instabilities of interest here.

Appendix B

Calculation of Δ

B.1 Calculation of Δ

B.2 Evaluation of Δ

With the ordering (6.16), our solution becomes a function of λ and we can expand Ξ and Υ in powers of λ.

$$\Xi(\xi;\lambda) = \frac{\Psi_0}{Q^{1/4}}\exp\left[-\frac{\xi^2}{2}\right]\sum_k \lambda^k \phi^{(k)}(\xi), \tag{B.1}$$

$$\Upsilon(\xi;\lambda) = \frac{\Psi_0}{Q^{1/4}}\exp\left[-\frac{\xi^2}{2}\right]\sum_k \lambda^k \upsilon^{(k)}(\xi). \tag{B.2}$$

The functions $\phi^{(k)}$, $\upsilon^{(k)}$ satisfy aligns of the form

$$\phi^{(k)\prime\prime} - 2\xi\phi^{(k)\prime} - (1-\bar{\kappa}_s)\phi^{(k)} + \bar{D}_s\upsilon^{(k)} = \mathcal{S}_1^{(k)} e^{\xi^2/2}, \tag{B.3}$$

$$\upsilon^{(k)\prime\prime} - 2\xi\upsilon^{(k)\prime} - \left(1+\frac{2}{\bar{\beta}\Gamma}\right)\upsilon^{(k)} + \left(\frac{2}{\bar{\beta}\Gamma} - \frac{S^2}{\bar{D}_s}\right)\phi^{(k)} = \mathcal{S}_2^{(k)} e^{\xi^2/2}. \tag{B.4}$$

By expanding $\phi^{(n)}$, $\upsilon^{(n)}$ in Hermite polynomials

$$\phi^{(n)}(\xi) = \sqrt{2}\exp\left(\frac{-\xi^2}{2}\right)\sum_m \frac{1}{4^m m!}\left[A_m^{(k)}(+)H_{2m}(\xi) + A_m^{(k)}(-)H_{2m+1}(\xi)\right], \tag{B.5}$$

$$\upsilon^{(n)}(\xi) = \sqrt{2}\exp\left(\frac{-\xi^2}{2}\right)\sum_m \frac{1}{4^m m!}\left[B_m^{(k)}(+)H_{2m}(\xi) + B_m^{(k)}(-)H_{2m+1}(\xi)\right], \tag{B.6}$$

solving Eqs. (B.3)–(B.4) reduces to expanding $\mathcal{S}_i^{(k)}$ in Hermite polynomials. This task is facilitated by the formulae

$$1 = \sqrt{2}\exp\left(\frac{-\xi^2}{2}\right)\sum_{m=0}^{\infty}\frac{H_{2m}(\xi)}{4^m m!}, \tag{B.7}$$

$$\xi = \sqrt{2}\exp\left(\frac{-\xi^2}{2}\right)\sum_{m=0}^{\infty}\frac{H_{2m+1}(\xi)}{4^m m!}, \tag{B.8}$$

$$\xi^2 = \sqrt{2}\exp\left(\frac{-\xi^2}{2}\right)\sum_{m=0}^{\infty}\frac{(4m+1)H_{2m}(\xi)}{4^m m!}, \tag{B.9}$$

$$\xi^3 = \sqrt{2}\exp\left(\frac{-\xi^2}{2}\right)\sum_{m=0}^{\infty}\frac{(4m+3)H_{2m+1}(\xi)}{4^m m!}, \tag{B.10}$$

$$\xi^4 = \sqrt{2}\exp\left(\frac{-\xi^2}{2}\right)\sum_{m=0}^{\infty}\frac{(16m^2+8m+3)H_{2m}(\xi)}{4^m m!}. \tag{B.11}$$

The expansions (B.7), (B.8) are derived in Ref. [24], and the rest can be obtained using recursion relations for the H_m's.

The inhomogeneous terms $\mathcal{S}_i^{(k)}$ also involve linear combinations of terms of the form

$$\frac{\mathrm{d}^m}{\mathrm{d}\,\xi^m}\left(\xi^n\phi^{(l)}\right). \tag{B.12}$$

These can be expanded in H_m's using

$$\sum_{n=0}^{\infty}a_n^{(k)}H_n(\xi) = \sum_{m=0}^{\infty}\frac{1}{4^m m!}\left[A_m^{(k)}(+)H_{2m}(\xi) + A_m^{(k)}(-)H_{2m+1}(\xi)\right], \tag{B.13}$$

$$\frac{\mathrm{d}}{\mathrm{d}\,\xi}\sum_{n=0}^{\infty}a_n^{(k)}H_n(\xi) = \sum_{m=0}^{\infty}\frac{1}{4^m m!}\left[(2+4m)A_m^{(k)}(-)H_{2m}(\xi) + A_{m+1}^{(k)}(+)H_{2m+1}(\xi)\right], \tag{B.14}$$

$$\xi \sum_{n=0}^{\infty} a_n^{(k)} H_n(\xi) = \sum_{m=0}^{\infty} \frac{1}{4^m m!} \Bigg[\Big(2(m+1/2) A_m^{(k)}(-) + 2m A_{m-1}^{(k)}(-) \Big) H_{2m}(\xi) + \frac{1}{2} \Big(A_m^{(k)}(+) + A_{m+1}^{(k)}(+) \Big) H_{2m+1}(\xi) \Bigg], \tag{B.15}$$

which are derived using the recursion relations

$$\xi H_n(\xi) = n H_{n-1}(\xi) + \frac{1}{2} H_{n+1}(\xi), \tag{B.16}$$

$$H_n'(\xi) = 2n H_n(\xi). \tag{B.17}$$

Finally, the formulae (B.13)–(B.14) can be viewed as operators acting on the sequences of coefficients $\{A_m^{(k)}(\pm)\}$. Using this perspective, we apply the operator $\hat{\xi}$ twice to find

$$\begin{aligned} \xi^2 \sum_{n=0}^{\infty} a_n^{(k)} H_n(\xi) = \sum_{m=0}^{\infty} \frac{1}{4^m m!} \Bigg[\Big(& (m+2/4) A_{m+1}^{(k)}(+) \\ & + 2(m+1/4) A_m^{(k)}(+) + m A_{m-1}^{(k)}(+) \Big) H_{2m}(\xi) \\ & + \Big((m+6/4) A_{m+1}^{(k)}(-) + 2(m+3/4) A_m^{(k)}(-) \\ & + m A_{m-1}^{(k)}(-) \Big) H_{2m+1}(\xi) \Bigg]. \end{aligned} \tag{B.18}$$

The Hermite coefficients of all inhomogeneous terms are readily computed using a combination of the "operators" provided.

B.2.0.5 Zeroth Order

Using Eqs. (6.16) and (B.1), the Eqs. (B.3)–(B.4) give

$$\phi^{(0)\prime\prime} - 2\xi\phi^{(0)\prime} - (1-\kappa_s)\phi^{(0)} + D_s v^{(0)} = -\xi e^{\xi^2/2}, \tag{B.19}$$

$$v^{(0)\prime\prime} - 2\xi v^{(0)\prime} - \left(1 + \frac{2}{\beta\Gamma}\right) v^{(0)} + \left(\frac{2}{\beta\Gamma} - \frac{S^2}{D_s}\right) \phi^{(0)} = -\xi e^{\xi^2/2}. \tag{B.20}$$

By expanding the right sides using Eq. (B.8), we find

$$A_m^{(0)}(-) = \left(\frac{\left(4m + 3 + \frac{2}{\beta\Gamma}\right) + \bar{D}_s}{(4m + 3 - \bar{\kappa}_s)\left(4m + 3 + \frac{2}{\beta\Gamma}\right) + S^2 - \bar{D}_s\left(\frac{2}{\beta\Gamma} - \frac{S^2}{\bar{D}_s}\right)} \right), \tag{B.21}$$

$$B_m^{(0)}(-) = \left(\frac{(4m + 3 - \bar{\kappa}_s) + \left(\frac{2}{\beta\Gamma} - \frac{S^2}{\bar{D}_s}\right)}{(4m + 3 - \bar{\kappa}_s)\left(4m + 3 + \frac{2}{\beta\Gamma}\right) + S^2 - \bar{D}_s\left(\frac{2}{\beta\Gamma} - \frac{S^2}{\bar{D}_s}\right)} \right), \tag{B.22}$$

$$A_m^{(0)}(+) = B_m^{(0)}(+) = 0. \tag{B.23}$$

Now that we have the Hermite coefficients, the integrals needed in Eq. (6.14) are

$$I(-) = \int_\infty^\infty \left(1 - \xi\phi^{(-)}\right) \mathrm{d}\,\xi, \tag{B.24}$$

$$I(+) = \int_\infty^\infty \xi^2 \phi^{(+)} \mathrm{d}\,\xi. \tag{B.25}$$

Evaluating the dispersion relation to kth order in λ requires $I^{(-)}$ to kth order and $I^{(+)}$ to order $k-1$, since it is multiplied by $\kappa_\parallel$. Using Eq. (B.8), and

$$\int_{-\infty}^\infty \mathrm{e}^{-\xi^2/2} H_{2m}(\xi) \mathrm{d}\,\xi = \sqrt{2\pi}\frac{2m!}{m!}, \tag{B.26}$$

from Ref. [11], we obtain

$$I(-) = \int_{\infty}^{\infty} \sum_{m=0}^{\infty} e^{-\xi^2/2} \left[\frac{\sqrt{2}}{4^m m!} H_{2m}(\xi) - a_{2m+1} \xi H_{2m+1}(\xi) \right] \mathrm{d}\,\xi$$
$$= \sum_{m=0}^{\infty} \left[\frac{1}{4^m m!} \sqrt{2\pi} \frac{2m!}{m!} \left(\sqrt{2} - [(2m+1)A_m(-) + 2mA_{m-1}(-)] \right) \right]. \tag{B.27}$$

Similarly, using Eq. (B.9) we find

$$I(+) = \sqrt{2\pi} \sum_{m=0}^{\infty} \left(\frac{\Gamma(m+\frac{1}{2})}{\Gamma(m+1)} \Big[\left(m + \frac{1}{2} \right) A_{m+1}(+) \right.$$
$$\left. + \left(2m + \frac{1}{2} \right) A_m(+) + m A_{m-1}(+) \Big] \right). \tag{B.28}$$

Using the previous formulae in Eq. (6.14), we get

$$\Delta/Q^{5/4} = \frac{4}{\pi} \sum_{m=0}^{\infty} \frac{\Gamma(m+\frac{1}{2})}{\Gamma(m+1)} \left[\frac{a_+}{4m+3-x_+} \right] + \frac{4}{\pi} \sum_{m=0}^{\infty} \frac{\Gamma(m+\frac{1}{2})}{\Gamma(m+1)} \left[\frac{a_-}{4m+3-x_-} \right]$$
$$+ \frac{4}{\pi} \sum_{m=0}^{\infty} \frac{\Gamma(m+\frac{1}{2})}{\Gamma(m+1)} \left[\frac{b_+}{4m+1-x_+} \right] + \frac{4}{\pi} \sum_{m=0}^{\infty} \frac{\Gamma(m+\frac{1}{2})}{\Gamma(m+1)} \left[\frac{b_-}{4m+1-x_-} \right], \tag{B.29}$$

with $x_\pm$ defined in Eq. (6.18).

Each of these series is in the form of a hypergeometric series summed in Ref. [14]. The result is Eq. (6.17).

As in previous work [8], the Gamma functions in the dispersion relation can be expressed in terms of hyperbolic functions in the incompressible limit. This simplifies the calculation of Δ'_{crit}, where the real and imaginary parts need to be separated. To second order in λ, the dispersion relation is given by Eq. (6.23), where

$$C_0 = \frac{\pi^2 \mathrm{sech}(\pi S/2)\cosh(\pi S/4)}{\sqrt{2}\left|\Gamma\left(\frac{5+iS}{4}\right)\right|^2}, \tag{B.30}$$

$$r = \frac{\left|\Gamma\left(\frac{5+iS}{4}\right)\right|^2}{\left|\Gamma\left(\frac{3+iS}{4}\right)\right|^2}, \tag{B.31}$$

$$f = 2\,\mathrm{Re}[G(3/2 - \mathrm{i}\,S/2)] \tag{B.32}$$

$$g = 2\,\mathrm{Im}[G(3/2 - \mathrm{i}\,S/2)], \tag{B.33}$$

$$C_\alpha = C_0[F_\alpha(S) + \bar{D}_s H_\alpha(S)], \tag{B.34}$$

$$F_\perp = 1/16, \tag{B.35}$$

$$F_\theta = (S/16)[S - 8r\tanh(\pi S/4)], \tag{B.36}$$

$$F_J = \frac{1}{48}\left[6 - 7r + (3+2r)S^2 - 30rS\tanh(\pi S/4)\right], \tag{B.37}$$

$$F_p = \frac{1}{48(9+S^2)}\left[3(9+S^2)(2+5S^2) - 24rS(37+4S^2)\tanh(\pi S/4)\right], \tag{B.38}$$

for the first-order coefficients, and

$$F_{\perp,\perp} = -\frac{5\tanh(\pi S/4)}{128S}, \tag{B.39}$$

$$H_{\perp,\perp} = \frac{3}{128(4+S^2)}, \tag{B.40}$$

$$\begin{aligned} F_{\theta,\theta} =& \frac{S}{128}\big[64rS - 8\pi S(1+S^2)\mathrm{sech}(\pi S/2) \\ & - (48+75S^2-4g(S+S^3))\tanh(\pi S/4)\big], \end{aligned} \tag{B.41}$$

$$\begin{aligned} H_{\theta,\theta} =& \frac{S}{128}\big[4g(1+S^2) - 3S[9+4/(4+S^2)] \\ & + 8[\pi(1+S^2)\mathrm{sech}(\pi S/2) - 4r]\tanh(\pi S/4)\big], \end{aligned} \tag{B.42}$$

$$\begin{aligned} F_{\parallel,\parallel} =& \frac{-1}{8}\Bigg[\frac{rS^2(604+130S^2+7S^4)}{(9+S^2)^2} \\ & + \frac{S(128+1007S^2+165S^4+6S^6)\tanh(\pi S/4)}{32(9+S^2)(16+S^2)} \\ & + \frac{(4S^2-5)[g(1+S^2)\tanh(\pi S/4) + f(1+S^2) - 8]}{8(1+S^2)}\Bigg], \end{aligned} \tag{B.43}$$

$$\begin{aligned} H_{\parallel,\parallel} =& \frac{1}{8}\Bigg[\frac{29808+39192S^2+8257S^4+563S^6+10S^8}{32(4+S^2)(9+S^2)(36+S^2)} \\ & + \frac{rS(442+94S^2+5S^4)\tanh(\pi S/4)}{(9+S^2)^2} \\ & + \frac{(5-4S^2)(g(1+S^2) + [f(1+S^2)-8]\tanh(\pi S/4))}{8S(1+S^2)}\Bigg], \end{aligned} \tag{B.44}$$

$$\begin{aligned} F_{\parallel,\theta} =& \frac{1}{4}\Bigg[rS^2\left(1+\frac{1}{9+S^2}\right) + \frac{[32R+2(5+32R)S^2+11S^4]\tanh(\pi S/4)}{32S} \\ & - \frac{1}{128}(16R+S^2)\left[(1+S^2)(f+g\tanh(\pi S/4)) - 8\right]\Bigg], \end{aligned} \tag{B.45}$$

$$H_{\parallel,\theta} = \frac{-1}{4}\Bigg[\frac{48+74S^2+29S^4-32R(4+S^2)}{32(4+S^2)} + \frac{(16R+S^2)[(1+S^2)(g-f\tanh(\pi S/4))-8]}{128S} - 4rS\tanh(\pi S/4)\Bigg], \tag{B.46}$$

$$F_{\perp,\parallel} = \frac{1}{256}\left[(1+S^2)(f+g\tanh(\pi S/4)) + 4\tanh(\pi S/4)/S - 72\right], \tag{B.47}$$

$$H_{\perp,\parallel} = \frac{1}{256}\Big[\frac{g(1+S^2)+-f\tanh(\pi S/4)+8\tanh(\pi S/4)}{S} + 36/(4+S^2) - 16\Big], \tag{B.48}$$

$$F_{\perp,\theta} = \frac{1}{128S}\big(16+46S^2-3gS(1+S^2))\tanh(\pi S/4) - S(3f(1+S^2)+8(4r-3))\big], \tag{B.49}$$

$$H_{\perp,\theta} = \frac{1}{128S}\left[22S+3(1+S^2)(f\tanh(\pi S/4)-g)-24\right]. \tag{B.50}$$

The function $G(z)$ is defined in Ref. [10].

Bibliography

[1] C. M. Bender and S. A. Orszag. *Advanced Mathematical Methods for Scientists and Engineers I.* McGraw-Hill, New York NY, 1978.

[2] I. B. Bernstein, E. A. Frieman, M. D. Kruskal, and R. M. Kulsrud. An Energy Principle for Hydromagnetic Stability Problems. *Proc. Roy. Soc. (London) A*, 244:17, 1958.

[3] A Bondeson, R Iacono, and A Bhattacharjee. Local magnetohydrodynamic instabilities of cylindrical plasma with sheared equilibrium flows. *Phys. Fluids*, 30:2167, 1987.

[4] S. I. Braginskii. Transport processes in a plasma. In M. A. Leontovich, editor, *Reviews of Plasma Physics*, volume 1. Consultants Bureau, 1965.

[5] D. Chandra, A. Sen, and P. Kaw. Dynamical origin of shear flow induced modifications of magnetic islands. *Nucl. Fusion*, 47:1238, 2007.

[6] D. Chandra, A. Thyagaraja, A. Sen, C. J. Ham, T. C. Hender, R. J. Hastie, J. W. Connor, P. Kaw, and J. Mendonca. Modelling and analytic studies of sheared flow effects on tearing modes. *Nucl. Fusion*, 55:053016, 2015.

[7] X. L. Chen and P. J. Morrison. Resistive tearing instability with equilibrium shear flow. *Phys. Fluids B*, 2:495, 1990.

[8] B. Coppi, J. M. Greene, and J. L. Johnson. Resistive instabilities in a diffuse linear pinch. *Nucl. Fusion*, 6:101, 1966.

[9] P. G. Drazin and W. H. Reid. *Hydrodynamic Stability.* Cambridge University Press, Cambridge UK, 2004.

[10] A Erdélyi, editor. *Higher Transcendental Functions*, volume 1. McGraw Hill, New York NY, 1953.

[11] A Erdélyi, editor. *Higher Transcendental Functions*, volume 2. McGraw Hill, New York NY, 1953.

[12] J. P. Freidberg. Ideal magnetohydrodynamic theory of magnetic fusion systems. *Rev. Mod. Phys.*, 54:801, 1982.

[13] E. A. Frieman and M. Rotenberg. On hydromagnetic stability of stationary equilibria. *Rev. Mod. Phys.*, 32:898, 1960.

[14] H. P. Furth, John Killeen, and M. N. Rosenbluth. Finite-resistivity instabilities of a sheet pinch. *Phys. Fluids*, 6:459, 1963.

[15] H. Georgi. *The Physics of Waves.* Prentice-Hall, Englewood Cliffs NJ, 1993.

[16] A. H. Glasser, J. M. Greene, and J. L. Johnson. Resistive instabilities in general toroidal plasma configurations. *Phys. Fluids*, 18:875, 1975.

[17] A. H. Glasser, S. C. Jardin, and G. Tesauro. Numerical solution of the resistive magnetohydrodynamic boundary layer equations. *Phys. Fluids*, 27:1225, 1984.

[18] J. P. Goedbloed, R. Keppens, and S. Poedts. *Advanced Magnetohydrodynamics*. Cambridge University Press, Cambridge, UK, 2010.

[19] J. P. Goedbloed and Stefaan Poedts. *Principles of Magnetohydrodynamics: with Applications to Laboratory and Astrophysical Plasmas*. Cambridge University Press, Cambridge UK, 2004.

[20] R. D. Hazeltine, P. Helander, and P. J. Catto. Plasma transport near the separatrix of a magnetic island. *Phys. Plasmas*, 4:2920, 1997.

[21] R. D. Hazeltine and J. D. Meiss. *Plasma Confinement*. Dover Publications, Mineola, NY, 2004.

[22] A Ishida, H Momota, and L. C. Steinhauer. Variational formulation for a multifluid flowing plasma with application to the internal tilt mode of a field-reversed configuration. *Phys. Fluids*, 31:3024, 1988.

[23] J. D. Jackson. *Classical Electrodynamics*. Wiley, Hoboken NJ, 1998.

[24] J. L. Johnson, J. M. Greene, and B. Coppi. Effect of resistivity on hydromagnetic instabilities in multipolar systems. *Phys. Fluids*, 6:1169, 1963.

[25] B. B. Kadomtsev. Hydromagnetic stability of a plasma. In M. A. Leontovich, editor, *Reviews of Plasma Physics*, volume 2. Consultants Bureau, 1966.

[26] M. D. Kruskal. Asymptotology. In S. Drobot and P. A. Viebrock, editors, *Mathematical Models in Physical Sciences*. Prentice-Hall, Englewood Cliffs NJ, 1963.

[27] R. J. La Haye, D. P. Brennan, R. J. Buttery, and S. P. Gerhardt. Islands in the stream: The effect of plasma flow on tearing stability). *Phys. Plasmas*, 17:056110, 2010.

[28] L. D. Landau, E. M. Lifshitz, and L. P. Pitaevskii. *Electrodynamics of Continuous Media*. Butterworth Heinemann, Oxford UK, 2099.

[29] Y. P. Pao. Instabilities in toroidal plasmas. *Phys. Fluids*, 18:1192, 1975.

[30] R. B. Paris and W. N. Sy. Influence of equilibrium shear flow along the magnetic field on the resistive tearing instability. *Phys. Fluids*, 26:2966, 1983.

[31] A. Sen, D. Chandra, and P. Kaw. Tearing mode stability in a toroidally flowing plasma. *Nucl. Fusion*, 53:053006, 2013.

[32] B. R. Suydam. Stability of a linear pinch. *Jou. Nucl. Energy*, 7:275, 1958.

[33] A. A. Vedenov. Thermodynamics of a plasma. In M. A. Leontovich, editor, *Reviews of Plasma Physics*, volume 1. Consultants Bureau, 1965.

[34] K. P. Wessen and M Persson. Tearing-mode stability in a cylindrical plasma with equilibrium flows. *J. Plasma Phys.*, 45:267, 1991.

Vita

Ryan Lee White was born June 13, 1982 in Reno, Nevada to parents Lee and Eileen. He attended the University of Nevada, Reno where he earned his Bachelor of Science degree in Physics in 2006. He enrolled in the Physics graduate program at the University of Texas at Austin. In the fall semester of 2009, he earned his Master of Arts degree in Physics in 2009, working with Dr. Richard Hazeltine. After working as a Systems Engineer at AT&T Labs in San Ramon, California, he returned to University of Texas at Austin to complete his graduate work as a Ph.D. student. He completed his doctoral work under the supervision of Dr. Richard Fitzpatrick in the summer of 2015.

Permanent address: 507 East 49th Street
Austin, Texas 78751

This dissertation was typeset with LaTeX[†] by the author.

[†]LaTeX is a document preparation system developed by Leslie Lamport as a special version of Donald Knuth's TeX Program.